Biochemical and structural studies of the interaction between ARNO and the Epidermal Growth Factor Receptor

Dissertation

zur
Erlangung des Doktorgrades (Dr. rer. nat.)
der Mathematisch-Naturwissenschaftlichen Fakultät
der Rheinischen Friedrich-Wilhelms-Universität Bonn

Vorgelegt von:

Benjamin Felix Crispin Weiche

ausCottbus

Bonn, 2014

Angefertigt mit Genehmigung der Mathematisch-Naturwissenschaftlichen Fakultät der Rheinischen Friedrich-Wilhelms-Universität Bonn.

1. Gutachter:	Prof. Dr. Michael Famulok
2. Gutachter:	PD Dr. Anton Schmitz
Tag der Promotion:	10. Juli 2014
Erscheinungsjahr:	2014

Parts of this thesis were published in:

Niebel B., Weiche B., Mueller A.L., Li D.Y., Karnowski N., Famulok M. (2011). A luminescent oxygen channeling biosensor that measures small GTPase activation. Chem. Commun. (Camb). **47**(26):7521-23

Danksagung

Prof. Dr. Michael Famulok

Für die Möglichkeit ein sehr vielschichtiges Projekt mit deiner Unterstützung durchzuführen und dabei menschlich wie wissenschaftlich zu reifen.

PD Dr. Anton Schmitz

Für ein sehr gutes persönliches und wissenschaftliches Miteinander. Ich konnte viel von dir lernen und habe immer gern mit dir zusammen gearbeitet. Außerdem natürlich ein großer Dank für die Übernahme des Zweitgutachtens.

Prof. Dr. Michael Hoch

Ein großer Dank für die Übernahme des Drittgutachtens und die unkomplizierte und schnelle Zusage dafür.

Prof. Dr. Aymelt Itzen

Sowohl während als auch nach meiner Doktorarbeit hast du mich immer ohne zu zögern unterstützt. Vielen Dank für deine Betreuung am MPI Dortmund und die Begutachtung meiner Doktorarbeit.

Den Arbeitsgruppen Famulok und Mayer gebührt mein Dank für die tolle Zeit, die ich mit euch allen verbringen durfte, für viele Arbeitstage, Feierabendbiere, Frittebud-Burger, Spielabende und sportliche Erfolge.

Björn Niebel

Du warst mir besonders am Anfang meiner Arbeit ein hervorragender Betreuer. Ohne dich wäre ich nicht soweit gekommen.

AG Goody (MPI Dortmund)

Für die freundliche Aufnahme in die Arbeitsgruppe und den hervorragenden wissenschaftlichen Austausch. Insbesondere danke ich **Dr. Matthias Müller** für die methodische Betreuung und die fruchtbaren Diskussionen rund um die Inhalte meiner Arbeit und **Prof. Roger Goody** für die Möglichkeit wesentliche Teile meiner Arbeit in seiner Arbeitsgruppe durchführen zu dürfen.

Meine „alten“ Freunde

Viele aufbauende Worte, schöne Erinnerungen und Ratschläge in allen Lebenslagen sind euch zu verdanken.

Meinen Eltern und meiner Schwester möchte ich für die Unterstützung jeglicher Art und zu allen Zeiten vor und während meiner Doktorarbeit danken.

Anna-Lena

Vielen Dank dafür, dass du die guten Zeiten mit mir zusammen verbringst und mich in den schlechten Zeiten erträgst.

TABLE OF CONTENTS

1 Abstract

Receptor tyrosine kinases (RTKs) and small GTP binding proteins (GTPases) are essential regulators of multiple cellular processes, making a tight control of their activity crucial for cellular homeostasis. Recently, it was shown that members of a class of guanine nucleotide exchange factors (GEFs), the cytohesin family, influence not only their canonical target proteins (small GTPases) but also the signaling of RTKs. Most prominently, they increase epidermal growth factor receptor (EGFR) activity by directly interacting with its intracellular domain. This mechanism is of pathophysiological relevance as demonstrated by *in vivo* studies in animal models and analysis of human tumor samples. In this study, I applied a combination of biochemical assays to further characterize the interaction between cytohesins and the EGFR.

Using chemical crosslinking studies supplemented with microscale thermophoresis and fluorescence polarization experiments, I provide evidence for the direct interaction of the Sec7 domain of cytohesin 2 (ARNO) with the juxtamembrane (JM) domain of EGFR. Furthermore, the binding site was found to involve the C-terminus of ARNO Sec7 and the N-terminal region of EGFR JM. Together with functional data investigating the nucleotide exchange activity of ARNO, these results suggest a model in which the JM domain contacts the hydrophobic grove formed by helix F, G and H of ARNO Sec7. This interaction provides possible explanations for the positive regulation of EGFR kinase activity by ARNO.

The discovery of non-canonical functions of cytohesins raises concerns about the use of GEF inhibitors like SecinH3 as specific inhibitors for Arf GTPases. Therefore, a high throughput screening (HTS) assay was established to identify small molecules that disrupt the interaction of active Arf6 with its specific effector protein JIP4. Due to very similar binding sites for different effector proteins on Arf6, molecules found in this assay are likely to exhibit a general inhibitory potential on GTPase signaling. The assay is based on fluorescence polarization (FP) and accurately tracks complex formation between Arf6 and the leucine zipper II (LZII) domain of JIP4. Tolerance towards detergents and organic solvents and an excellent Z' value observed throughout the screening process indicate that the assay is suitable for future HTS applications using small molecule libraries optimized towards inhibitors for protein-protein-interactions.

2 Introduction

2.1 Cell homeostasis

The interplay and communication of eukaryotic cells depends on the transfer of information across and between different membranes. It is of vital importance for cells to maintain their physiological balance while still being able to recognize and integrate changes in their environment. This requires a highly regulated exchange of information and contents between different separated compartments inside and the outside of a cell. Intercompartment exchange inside the cell is mainly facilitated by vesicle transport, a process governed by small GTPases. In contrast, the integration of signals from the outside requires specialized proteins that can cross the plasma membrane barrier: transmembrane proteins known as receptors.
Thus, small GTPases and membrane receptors are critical to maintain the cellular homeostasis and are of special interest to this study. Therefore, a detailed description of their biochemistry follows.

2.2 Communication with the extracellular space – transmembrane receptors

2.2.1 Transmembrane proteins translate extracellular signals into intracellular responses

The intricate balance maintained in all cells, from single cell organisms to the building blocks of complex tissues, needs to be regulated with regard to the environment. Therefore, extracellular signals (e.g. growth factors) are recognized at the outside of the plasma membrane and transmitted to the interior of the cell. For this purpose an array of transmembrane proteins exist that all share a similar organization: They contain an extracellular domain for the recognition of signals and binding of signaling molecules, a transmembrane domain that anchors the protein in the lipid bilayer, and an intracellular domain which is responsible for the initiation of a cellular response. Those proteins act as receptors and can, with some exceptions (e.g. receptors that depend on regulated proteolysis like Notch-Delta or Wnt, (*1, 2*)), be grouped into 3 major classes according to

their mode of action: G protein coupled receptors, ion channel coupled receptors and enzyme linked receptors.

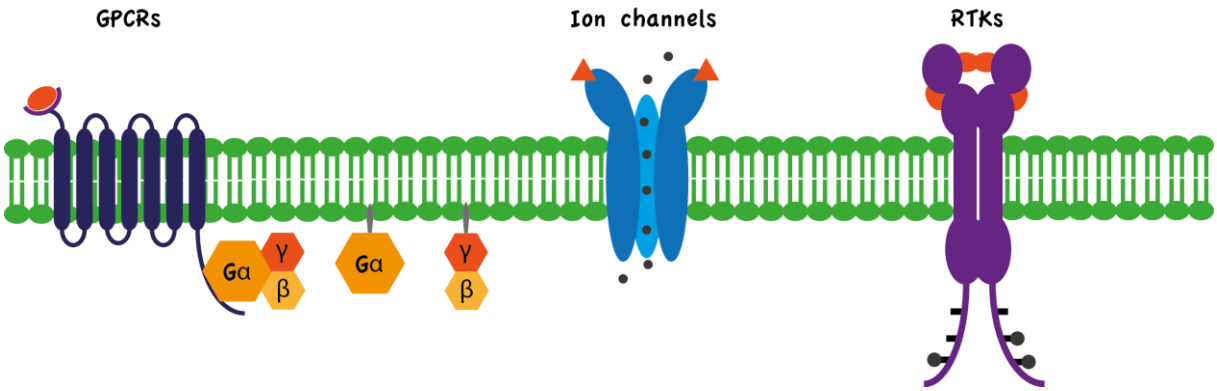

Fig. 2.1 The three major classes of transmembrane receptors.G-protein coupled receptors (GPCRs) transmit their signal via associated trimeric G-proteins. Ion channels are gates through the membrane that allow hydrophilic molecules to pass when appropriately stimulated. Receptor tyrosine kinases (RTKs) translate an extracellular signal into intracellular enzymatic activity to promote signal transduction.

G-protein coupled receptors

G-protein coupled receptors are seven span transmembrane proteins that interact with a trimeric G-protein (GTPase protein) at the intracellular side of the membrane. Upon activation, they promote the exchange of a guanine di-phosphate (GDP) for a guanine tri-phosphate (GTP) in the α subunit of the G-protein. This activation leads to dissociation of the Gα subunit from the βγ complex. Both molecules are membrane attached via lipid modifications on α and γ subunit and initiate signaling cascades governed by adenylate cyclase and phospholipase C and their respective second messengers cyclic AMP and inositol 1,4,5 trisphosphate/diacylglycerol (*3*). Gα has an intrinsic catalytic activity and is stimulated to hydrolyze GTP to GDP and inorganic phosphate by associated proteins. The following re-association of all three subunits terminates the signal. Hence, the default state of the receptors is inactive, ensuring that no unintended activation with potentially severe consequences can occur. Specialized members of G-protein coupled receptors are the rhodopsin photoreceptors in cells of the vertebrate retina (*4*) and olfactory receptors that integrate taste and smell (*5*) illustrating the widespread importance and diversity of this receptor class.

Ion channels

Some receptor molecules respond to the encounter of extracellular ligands by selectively disturbing the barrier formed by the plasma membrane. Usually this lipid bilayer separates the aqueous solutions on the outside and inside of the cell and allows both compartments to have a very distinct composition of molecules. Especially charged molecules (ions) can not simple diffuse through the hydrophobic environment and need specialized proteins to allow for exchange between outside and inside of a cell. Ion concentration changes are of special importance in the nervous system and at the neuromuscular junction where the influx of ions results in depolarization and is responsible for signal transmission between cells (*6*). Ion channels are the key players mediating this behavior. These channels consist of several subunits that form a pore across the membrane that is closed in the inactive conformation. Upon binding of an extracellular ligand (e.g. a neurotransmitter like Acetyl-Choline) the receptor undergoes a conformational change that opens the pore for specific ions (*7, 8*). Due to a concentration gradient across the membrane this leads to a flow of ions and a change in charge and ion concentration close to the membrane. Subsequently, this signal is either transported along the cell for signal transmission (e.g. long axons in the nervous system) or integrated into a cellular response (e.g. the contraction of muscle cells). Active processes are necessary to re-establish the original ion composition inside the cell and terminate the signal.

The third class of receptors consists of transmembrane proteins with enzymatic activity and is discussed in detail in the following paragraphs.

2.3 Receptors with enzymatic activity – receptor tyrosine kinases (RTKs)

Binding of an extracellular ligand leads to conformational changes in GPCRs and ion channels that result in the above described responses. However, proteins of the receptor tyrosine kinase (RTK) family are single span transmembrane proteins and communication of the signal to the inside via a single helical structureis difficult.
Therefore, an appropriate ligand is recognized by the extracellular domain and induces either the dimerization of two RTK molecules or a conformational change in preformed

inactive dimers. This process is essential for signal transmission across the membrane and initiation of the kinase activity in the intracellular domain of the proteins.
Once activated, the dimerized receptor phosphorylates tyrosine residues, either at its own C-terminus - a process known as autophosphorylation - or on other target proteins, in order to further increase its catalytic activity and to initiatedownstream signal transduction (*9*).

2.3.1 RTKs are vital for physiological processes

Receptor tyrosine kinases (RTKs) are key players in both physiological and pathophysiological cell biology. They are known to control cell proliferation, differentiation, survival and general metabolism, thereby determining the fate of cells in development and homeostasis. The human genome contains 58 RTK family members that can be separated into 20 subfamilies with structural differences predominately localized to the extracellular domain (*10*). Despite the diversity observed in the RTK family, their general topology as well as the mechanism behind their activation remained highly conserved during evolution (*10*). Fig. 2.2 shows a simplified scheme of RTK topology indicating all common structural features shared by the family members. The extracellular domain (ECD) is responsible for ligand recognition and initiates the conformational rearrangements required for receptor activity. Kinase activity takes place inside the cell. A tyrosine kinase domain (TKD) is the common feature of RTKs and is divided into a N-lobe and a C-lobe whose relative orientation is crucial for catalytic activity. Furthermore, the intracellular part of the receptor has a C-terminal part that harbors tyrosine residues as targets for autophosphorylation and serves as a regulatory element (*11-13*). Another crucial regulatory part is the juxtamembrane domain (JMD) that spans the region between the kinase domain and the membrane. JM domains can have both inhibitory (e.g. Ephrin) (*14*) and activating function (e.g. EGFR) (*13, 15*). The final common element in the receptors is the transmembrane domain (TMD). It is a single α helix that spans the plasmamembrane and connects the ECD on the outside with the intracellular parts of RTKs. Besides anchoring of the protein in the membrane the TMD is described to be involved in dimerization and transmission of conformational changes across the membrane (*16-18*). The presented topology showcases all common features of RTKs

required for efficient signaling. Tight control of the interplay between the structural elements is necessary to avoid undesired activation with disastrous consequences.

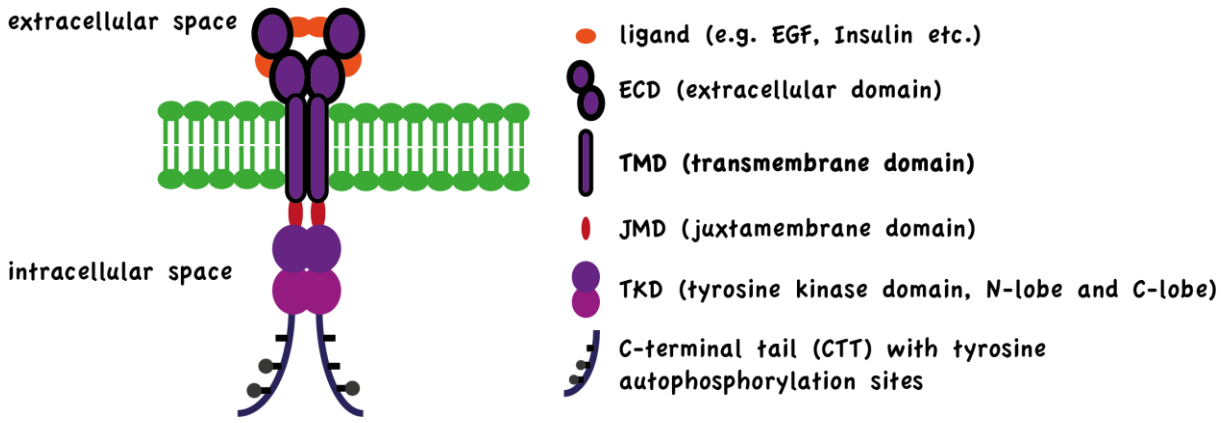

Fig. 2.2 A simplified scheme of Receptor tyrosine kinase topology. Shown are all features shared by different members of the RTK family.

2.3.2 Mutations in RTKs are the cause for severe pathological phenotypes

The importance of RTKs and associated signaling processes is illustrated by the prevalence of pathologies caused by either mutations or inappropriate expression levels of the proteins. Indeed, the role of several RTKs in cancer was discovered due to oncogenic products of viral origin that could induce transformation of cells via activation of RTK pathways (*19-21*). Later it was discovered that mutations or amplifications in the EGFR gene are responsible for brain tumor formation (*22*). Many receptor family members promote cell proliferation or survival and are therefore prone to induce malignant transformation of cells when not appropriately controlled.

In contrast, reduced or abolished signaling activity also has severe consequences. A hallmark of Diabetes mellitus type II is insulin resistance caused by a decrease in insulin receptor (IR) signaling. Several genetic disorders lead to extreme forms of insulin resistance connected to low expression levels of IR protein (*23*). Furthermore, inactivating mutations in the gene for fibroblast growth factor receptor 2 (FGFR2) or its ligand FGF10 lead to the developmental pathology known as LADD (lacrimo-auriculo-dento-digital) syndrome characterized by dysplasias of the anatomical structures eye, ear, teeth and digits (*24*).

All given examples emphasize the importance of a tightly regulated activation of RTKs to ensure physiological signaling. Control elements on different levels of receptor biochemistry evolved for this purpose.

2.3.3 Ligand binding and dimerization are the initial steps in RTK activation

Binding of an extracellular ligand to RTKs is essential for their canonical activation. In some cases, ligand binding induces association of two molecules forming an active dimer. This is either achieved by bivalent ligands that connect two receptors with symmetrical binding sites (e.g. Kit and its ligand stem cell factors (SCF) or members of the VEGFR family (*25, 26*)), or ligand binding exposes dimerization motifs on the proteins that in turn allow association of two molecules. Different modes of ligand and receptor contribution to the dimerization interface are known. One extreme is observed for RTKs that are preassembled as dimers or oligomers even in the absence of ligand (*27, 28*). Thus, these receptor molecules are sufficient to multimerize independently of other binding partners. A prominent example is the insulin receptor (IR). Here, one receptor monomer consists of an α and a β-subunit that are covalently connected via a disulfide bridge (*29*). Two αβ subunits are further disulfide-linked to each other to form the mature receptor. Insulin binding results in a complex structural rearrangement causing receptor activation (*30*).
These examples show that dimer formation is required but not always sufficient for receptor activation and that other conformational responses are induced to translate ligand binding into an intracellular response.

2.3.4 Structural features of tyrosine kinase domains in active and inactive states

The intracellular tyrosine kinase domain (TKD) of RTKs consists of an N-lobe and a C-lobe forming the active site for substrate phosphorylation in a cleft between them (Fig. 2.3). All TKDs of RTKs exhibit a very similar conformation when activated (*31*). This is due to the conservation of the phosphotransfer reaction catalyzed by the receptors (*32*). Two of the most prominent structural features determining activity are the “activation loop” that serves as the substrate docking site in the active conformation and the αC helix in the TKD N lobe (Fig. 2.3). Both elements contribute to the transition between active and inactive TKD by structurally affecting the binding of substrate and ATP (*32, 33*). In the active conformation the αC helix is closely packed to the N-lobe. A crucial glutamate (Glu, E) makes contact with a lysine (Lys, K) residue in the N-lobe. This interaction is essential for the coordination of the α and β phosphate of ATP, and

mutations affecting these residues abolish kinase activity (*34*). In the N-terminal part of the "activation loop" is a conserved DFG (aspartate, phenylalanine, glycine) motif. The aspartate is engaged in coordinating an Mg^{2+} ion that is crucial for ATP binding, while the C-terminal part of the activation loop serves as a docking site for the substrate that is exposed in the active structure of a kinase (*32*). The actual catalytic loop precedes the activation loop and contains a conserved HRD (histidine, arginine, aspartate) motif with the aspartate residue serving as the catalytic base and proton acceptor from the substrate's hydroxy group. All mentioned elements have to be aligned in precise spatial order to facilitate the phosphotransfer from ATP to a substrate.

An inactive conformation is structurally defined by a swung-out αC helix and a small helix formed by the part of the activation loop directly adjacent to the DFG motif (*35, 36*). This conformation is known as the CDK/Src-like inactive conformation since it was first observed in crystal structures of these kinases. Src kinases are kept inactive via intramolecular contacts involving their Src homology 2 and 3 domains (*37, 38*) and loss of contact sites results in constitutively active kinases (*39*). In contrast, cyclin dependent kinases (CDKs) are inactive and become activated only when specific cyclins are expressed during the cell cycle (*40*). A different inactive kinase structure is characterized by the DFG-out conformation in which aspartate and phenylalanine have switched positions, disturbing Mg^{2+} binding (*41, 42*). Although both activation loop and αC helix are positioned correctly in these receptor molecules, this is not sufficient for kinase activity.

This list of examples illustrates that active conformations are well defined and both inactive structures and modes of activity control can vary in different kinases.

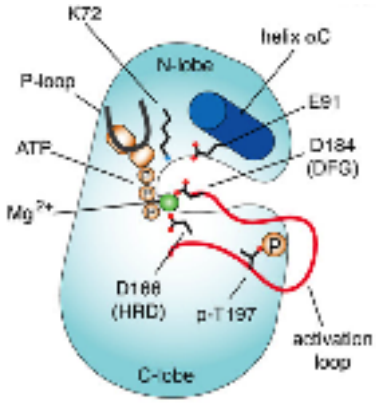

Fig. 2.3 Important structural features of an active kinase. This schematic representation shows how the activation loop adopts an extended conformation while the helix αC is "swung in" and allows for ion bridge formation between a glutamate (E91) and a lysine (K72) in the N-lobe. Additional features not discussed in the text are the P-loop that is important for ATP binding and a threonine in the activation loop (T197) that is phosphorylated to fully activate the kinase. All amino acid positions refer to protein kinase A (PKA). Figure from Jura et. al (*32*).

2.3.5 Intrinsic autoinhibition of RTKs

Structural differences among RTKs are mainly observed in their inactive state, which allows selective interaction with specific binding partners (*32*). This is also reflected in the different modes of kinase-activity regulation. A single RTK molecule is intrinsically autoinhibited to avoid unintended activation of the receptor and downstream signaling. Different mechanisms are known that control this cis-autoinhibition, which is crucial for the physiological activity of RTKs. The insulin receptor (IR) represents an example for autoinhibition via the "activation loop". A critical tyrosine at position 1162 (Y1162) occludes the active site and prevents substrate and ATP binding. Phosphorylation of Y1162 in trans after initial receptor activation displaces the "activation loop" and allows for a reorientation of the αC helix (Fig. 2.3). This dramatically increases kinase activity by allowing for optimal positioning of both substrate and ATP at the active site (*33*). Other examples include the fibroblast growth factor receptor (FGFR). The autoinhibition is also released via trans phosphorylation of the "activation loop". However, no direct occlusion of the active site via a tyrosine is observed but an inactive conformation is favored before phosphorylation (*43*).

A second structural element often involved in autoinhibition is the juxtamembrane domain (JMD). By making contact to structural elements that are functionally important for TKD activity, such as the "activation loop" or the αC helix, the JMD promotes an inactive conformation that is released by trans phosphorylation of specific tyrosines (*44*). Examples for the JMD mediated activity control are found in the stem cell factor receptor KIT and the family of Ephrins (*14, 41*).

Less well characterized is the influence of the C-terminal tail on autoinhibition. It is suggested that this region can block the binding of substrate to the active site in certain RTKs, thereby inhibiting catalytic activity even in otherwise structurally "active" kinases (*45*).

Autophosphorylation in trans is the common feature in releasing autoinhibition (with the exception of EGFR, see below) to fully activate the TKD of RTKs. Basal kinase activity required for the first phosphorylation cycle is conferred by extracellular ligand binding and the subsequent destabilization of the inactive TKD conformation (*10*). This level of intracellular control via autoinhibition prevents the unintended initiation of RTK downstream signaling.

2.3.6 Downstream pathways in RTK signaling

RTK activity is tightly controlled regarding the spatial and temporal organization of phosphorylation events. The "first phase"-substrates are tyrosines of the receptor (see paragraph 2.3.5) causing the release of autoinhibition. These events occur in a precise order, gradually increasing kinase activity and creating a positive feedback loop essential for full RTK signaling (*46, 47*). The next steps or "second phase" involves the phosphorylation of tyrosine in the C-terminal tail of the receptor (or on adaptor proteins like insulin receptor substrate (IRS) for the insulin receptor) creating binding site for proteins involved in downstream signaling. Specialized domains like Src homology 2 (SH2) or phosphotyrosine binding (PTB) domains associate with the phosphorylated amino acids at the receptor (*48*) initiating either a direct response or serving as adaptor or docking proteins (Fig. 2.4). For instance, the adaptor protein growth factor receptor-bound protein 2 (Grb2) recruits the guanine nucleotide exchange factor Son of Sevenless (Sos), which in turn activates the small GTPase p21/Ras. This leads to the activation of several pathways including the mitogen activating pathway (MAP) that is characterized by a cascade of phosphorylation events on the MAP kinases Raf, Mek and Erk (*49*). This ultimately leads to the initiation of gene transcription and results in cellular proliferation.

In other cases effector proteins are directly recruited to the receptor. They are multidomain proteins that are recruited to the correct location by phosphotyrosine, membrane and protein binding domains. Phospholipase C γ (PLCγ) is a prominent example responsible for the signal transduction of different RTKs. It has SH2 domain for the interactions with the receptor and pleckstrin homology (PH) domains that facilitate binding to phospholipids in the plasma membrane. The multivalency of different binding sites increases the affinity of signaling molecules for the appropriate location and also provides specificity ("coincidence detection", (*50*)) since single binding modules are not sufficient for recruitment (*51*). PLCγ itself is phosphorylated by the RTK and cleaves the phospholipid phosphatidylinositol 4,5 bisphosphate (PIP_2) into inositol 1,4,5 trisphosphate (IP_3) and diacyl glycerol (DAG), thereby mediating signal transduction via Protein kinase C (PKC) and Ca^{2+} (*52*).

The variety of interacting modules, downstream distribution of the signal, and control elements that ensure specificity, allow complex signaling networks to work efficiently, thus providing another level of robust control for downstream RTK activity. Since most

of the RTK associated pathways have implications in cancer biology (*53*), a tight control of initiation and efficient ways to terminate signal transduction are crucial to prevent malignant transformation.

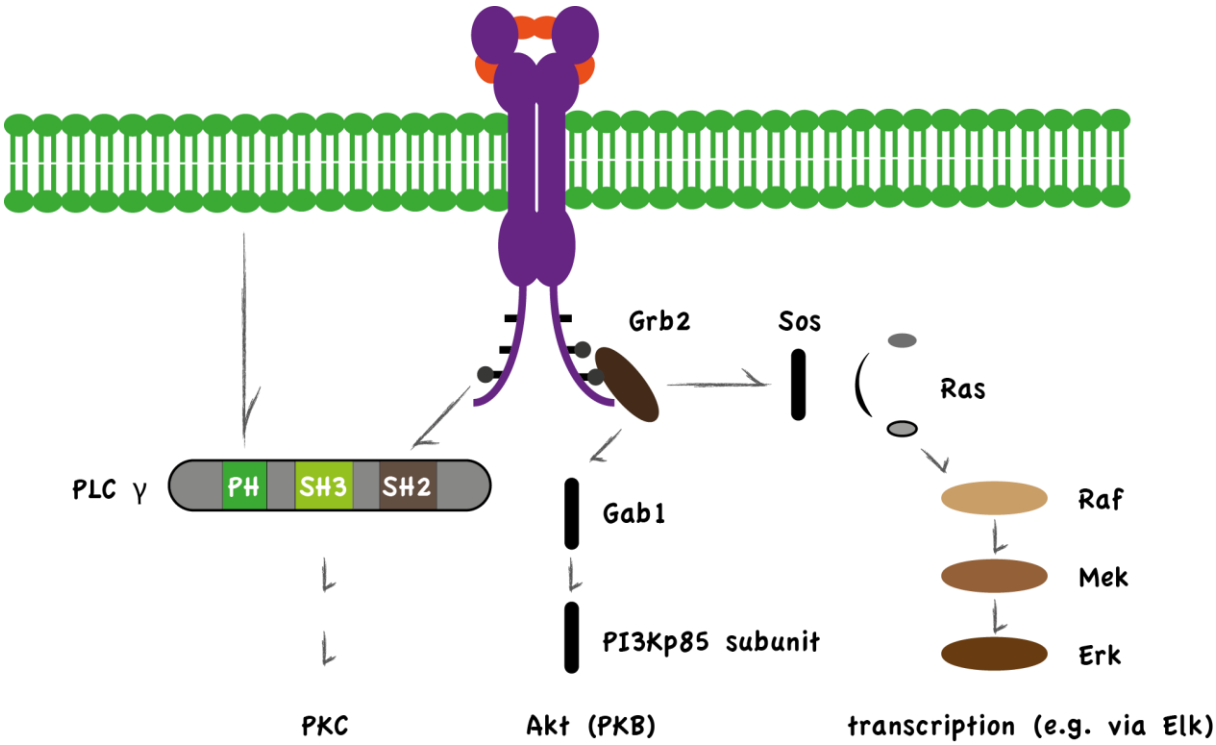

Fig. 2.4 Signaling pathways associated with receptor tyrosine kinase activation. Activation of RTKs results in a wide variety of different cellular responses such as activation of MAP kinase cascades or the activation of major serin/threonine kinases. Different sets of adaptor molecules are employed and specialized domains facilitate recruitment of involved proteins to the appropriate sites inside a cell.

2.3.7 Termination of RTK signaling

Receptor tyrosine kinases are never fully inactive but rather stabilized in an inactive conformation that can rapidly be resolved by conformational changes upon extracellular ligand binding. This, however, leads to spontaneous phosphorylation events even in the absence of ligand. One mechanism that is essential to avoid random receptor activation is governed by protein tyrosine phosphatases (PTPs). These proteins have a constant basal activity that reverses stochastic phosphorylation events and therefore prevents receptor activation. PTPs are important for maintaining the cellular signaling equilibrium. Their inhibition leads to general activation of RTKs even in the absence of ligands (*54*) and pathophysiological malfunction of PTPs are associated with cancer (*55*). However, PTPs are also important for normal termination of regularly activated

RTK signaling. They are recruited via SH2 domains to phosphotyrosines at the receptor and hence promote its inactivation in a very efficient negative feedback loop (*56*).
Another mechanism for the termination of RTK signaling is controlled by endocytosis, ubiquitination and receptor degradation in the lysosomal compartment. After stimulation, RTKs undergo endocytosis both in a clathrin dependent and independent manner. After endocytosis, RTKs are sorted in the endosomal compartments either to be degraded in the lysosome or to be recycled to the plasma membrane (*57*). The way of endocytosis and the fate of activated receptor molecules are influenced by the ligand type, abundance and phosphorylation events that occur after stimulation. Some RTKs (directly or via adaptor proteins) recruit RING type E3 ubiquitin ligases of the Cbl family that facilitate ubiquitination of receptor molecules (*58*). The resulting ubiquitination pattern determines, besides other factors, how endocytosed receptor molecules are sorted and whether they are rapidly degraded or maintain to transmit their signal. Although endocytosis and lysosomal degradation leads to termination of RTK signaling, it is important to mention that receptor signaling continues and is modified during the endosomal sorting process (*59*). It was even proposed that different cellular locations of active receptors are associated with pathophysiological relevant signaling outcomes. While the bulk transcriptional response seems to be derived from signaling RTKs located at the plasma membrane, some cancer relevant targets are expressed in response to continuous signaling from internalized receptors (*60, 61*).
All described mechanisms of RTK activation, downstream signaling and termination of the response illustrate the importance of tightly regulated biochemical pathways to maintain cellular homeostasis. A prominent family of RTKs will be discussed below to introduce a specific example in more detail and emphasize the characteristics of a "special case".

2.4 The ErbB family of receptor tyrosine kinases

The ErbB (named after the vErb oncogene from avian erythroblastosis virus, (*20*)) family of receptor tyrosine kinases consists of four members that associate in homo- or heterodimers to initiate signaling.They have important functions in control of proliferation and differentiation, are essential during mammalian development (*62*) and aberrant activity is frequently found in human cancers (*63*).

ErbB family members are activated by epidermal growth factor (EGF) related peptide growth factors like EGF or the neuregulins (NRG). These ligands share an EGF like domain and are further characterized by three disulphide-bonded intramolecular loops. The ligands have preferred binding partners, with EGF or TGFα primarily binding to ErbB1 and NRG isoforms associating with ErbB3 and ErbB4 (*64*).

ErbB1 (or EGFR) and ErbB4 (or Her4) are fully functional and can bind extracellular ligand, dimerize and phosphorylate substrates. In contrast, both ErbB2 (Her2/Neu) and ErbB3 (Her3) exhibit impaired functionality on different levels of receptor activity. ErbB3 shows sequence alterations in parts of the tyrosine kinase domain (e.g. the αC helix and the activation loop, (*32*)), which leads to severely reduced activity (*65*). On the other hand, no high affinity ligand could be identified for ErbB2 (*66*). However, heterodimerization with other family members enables both ErbB molecules to contribute to signaling that involves a variety of downstream effectors, e.g. MAP kinases, PLCγ or PI3 kinase (Fig. 2.4, (*67*)).

2.4.1 Ligand binding and heterodimerization contribute to the complexity of ErbB signaling

The ErbB family is distinct from other RTKs regarding several aspects of their activation. In crystal structures of extracellular domains (ECDs) the dimer interface is solely formed by parts of the receptor, without any structural contribution of the ligand (*68, 69*). Instead, ligand binding induces a conformational change in the extracellular part of the receptor that releases a “dimerization arm” in domain II (of IV) of the ECD. In the absence of ligand, an intramolecular “tether” between domain II and IV buries this element, thus inhibiting dimerization (*70, 71*). Once released, receptor association is strongly supported by the dimerization arm and conformational changes required for full activation take place (*72*). ErbB2 has no high affinity ligand but association with other ErbB isoforms results in high kinase activity due to an intrinsically active conformation in its extracellular domain (*73*).

The fact that one ligand only contacts one receptor molecule and that the dimerization requires no structural ligand contribution explains why different ligands can bind to receptor molecules and induce hetero- or homodimers between different ErbB isoforms, utilizing a common dimerization motif (the dimerization arm on the receptor). Both the bound ligand and interaction partner influence the phosphorylation pattern and thereby

the signaling outcome of a receptor pair. The combination of several ligands that can initiate the association of a variety of receptor dimers renders the ErbB signaling network one of the most complex pathways in cell biology (*10*).

In contrast to the canonical way of ligand-dependent dimerization, recent studies suggest that EGF receptor molecules form dimers or oligomers at the plasma membrane even in the absence of an extracellular stimulus (*27*). Interaction between the transmembrane domains (TMDs) and contributions of parts of the juxtamembrane domain (JMD) could explain this observation since both a TM-JM and a JM-TKD construct are able to form dimers independent of the ECD (*13, 17*). The ability to spontaneously dimerize raises the question how undesired EGFR activation is prevented in the absence of ligand. Again, a specialized mechanism is employed to regulate the tyrosine kinase activity of intracellular ErbB domains.

2.4.2 An asymmetric dimer represents the active conformation of EGFR kinase domains

In contrast to other RTKs, ErbB family members are not obviously autoinhibited in cis by structural elements of the receptor. Although there is a tyrosine residue (Y845) present in the activation loop that is readily phosphorylated upon kinase activation, this residue is not essential to maintain the inactive state as observed for many other RTKs (*74, 75*). Instead, the kinase appears to be intrinsically inactive (*76*) and activation via ligand binding involves the formation of an unusual asymmetric dimer (*77, 78*). In this head-to-tail configuration of two receptor molecules one serves as the “activator” making contact with parts of its C-lobe to the N-lobe of the second kinase, the “receiver”. This stabilizes the active conformation characterized by a swung in αC helix and an extended activation loop ready for substrate docking. In a monomer, this conformation would expose hydrophobic residues to the aqueous environment explaining its intrinsic instability (*32*). Interactions in the asymmetric dimer cover the hydrophobic area and stabilize the active conformation. First shown for EGFR, this mechanism is also employed by other members of the ErbB family and seems to represent a general concept (*79, 80*).

Most other tyrosine kinases are stable in their active conformation and have to employ autoinhibitory mechanisms to avoid unintended activity while the EGFR behaves more like the Ser/Thr kinase CDK (*40*). This protein requires the presence of cyclins to be

activated by forming a hydrophobic interaction that induces the appropriate kinase conformation. Therefore, ErbB receptors prove to be distinct from classical RTKs on different levels of their biochemistry.

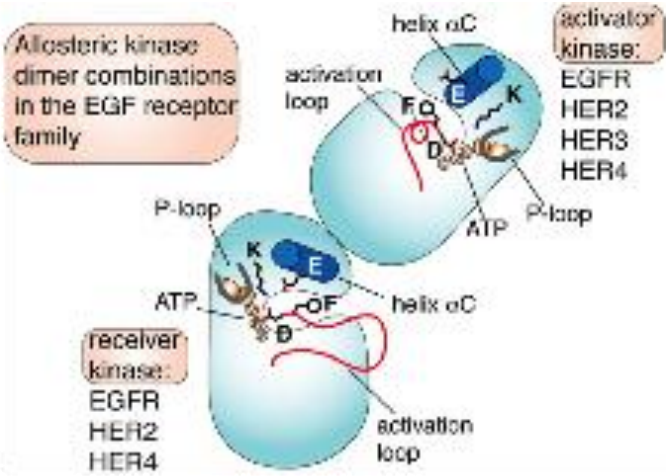

Fig. 2.5 The asymmetric dimer formed by two molecules of ErbB family members. All members of the family can act as activators. However, ErbB3 has a very low kinase activity and is therefore a bad receiver. The activator induces structural rearrangements in the receiver that facilitate enzymatic activity (for structural details of an active kinase see Fig. 2.3). Figure from Jura et al. (*32*).

2.4.3 Intramolecular modulation of EGFR activity

The tyrosine kinase domains (TKD) of the EGFR can form an asymmetric dimer that composes a signaling competent receptor. However, the affinity of this interaction alone is not sufficient to promote dimerization (*13*). Instead, an additional structural element is required for dimerization and activation: the juxtamembrane (JM) segment. This domain is usually involved in negative regulation of RTK activity (*44*) but is essential for EGFR activation upon ligand binding (*81*) and allows for *in vitro* dimer formation of EGFR intracellular domain constructs (*13*). Crystallographic studies show that the C-terminal part in the JM domain (JM-B or juxtamembrane latch) of the receiver kinase binds to the C-lobe of the activator kinase thereby stabilizing the dimer (*15*). The JM latch binding site at the activator kinase is crucial for the interaction and elements that block the interface reduce kinase activity. This could explain the regulatory role of the C-terminal tail of EGFR (*82, 83*). In an inactive conformation observed for EGFR intracellular domains (*13, 32*) the JM latch binding site is occluded by the C-terminal tail providing a mechanism for autoinhibition.

Apart from the JM latch increasing the affinity in the asymmetric dimer, the N-terminal part of the JM domain (JM-A) is also essential in EGFR activity (*84*). This element forms a small coiled-coil structure that promotes receptor association in solution (*13*). When coupled to the transmembrane domain (TMD), the coiled coil interaction needs to be

induced by dimerization of the TM helices at their C-termini. However, both the TM and the JM-A region support dimerization and thus the activation of EGFR (*17, 18*).
The full length receptor is inactive when not bound to an extracellular ligand. Negatively charged phospholipids sequester both the TKD and JM-A, leading to inhibition of the kinase (*18, 85*). This inhibition is only released after ligand binding to the extracellular domain, inducing the N-terminal association of the TM helices that forces the JM domains and in turn the TKDs to associate in an enzymatically competent dimer (*17, 18*). The described model suggests that many structural elements of the EGFR promote dimerization, but are intrinsically restrained from activation in the absence of a ligand. This autoinhibitory mechanism is unique among the members of the RTK family and further shows the distinct properties of the ErbB family RTKs.

2.4.4 Modulation of EGFR activity by other proteins

Positive and negative feedback loops are crucial aspects of all signaling cascades to provide both robustness of signal induction and allow for rapid termination of the signaling (*10*).
Negative control of EGFR activity is conferred by phosphorylation events in the JM domain. Downstream receptor activity via PLCγ results in protein kinase C (PKC) phosphorylation of Thr654 in the JM domain (*9*), which blocks high affinity ligand binding. Another threonine (Thr669) is phosphorylated by the MAP kinase Erk, leading to EGFR inactivation (*86*). Other negative feedback loops involve the described recruitment of PTPs to abolish signaling, and the endocytosis and degradation of receptor molecules after Cbl mediated ubiquitination (paragraph 2.3.7). Transcription products of the signaling pathway often mediateda delayed negative feedback. A well understood example is mitogen induced gene 6 (Mig6). Mig6 competes with the JM latch for binding to the C-lobe of the activator kinase, thereby blocking the formation of the asymmetric dimer (*87*).
These observations further emphasize the importance of the JM domain for EGFR activation and as a major site for regulation of activity and signaling.
Upon initial EGFR activation, positive feedback loops ensure a rapid and robust signaling response. Activation of ADAM proteases leads to the cleavage of membrane bound heparin-binding EGF like growth factors that enhance receptor activation via an autocrine loop (*88*). Another interesting example involves PI3K and Rac mediated activation of NADPH oxidase,

leading to the production of reactive oxygen species (ROS) that temporarily inactivate PTPs in the whole cell by lateral diffusion, thereby driving a more general cellular EGFR response (*89, 90*).

Factors that directly bind to the receptor molecule and positively influence their activity are rare. The few known examples belong to the family of guanine nucleotide exchange factors (GEFs) for small GTPases and will be discussed at the end of the next chapter.

2.5 Small GTPase and their role in cell biology

In contrast to the trimeric G proteins known from GPCR signaling, small GTP binding proteins (GTPases) are monomeric and function as "molecular switches" to control biological responses. They are involved in various processes, ranging from signaling and transport to cell motility and migration, therefore representing one of the most diverse regulatory molecules in a cell.

2.5.1 The Ras superfamily of small GTPases

The Ras (Rat sarcoma) GTPases represent the founding members of the large superfamily of small, monomeric GTPases, currently comprising over 150 members in humans (*91*). Based on sequence relationship and biological function they are classified into five subgroups: Ras, Rho (Ras homologous), Rab (Ras related in brain), Arf (ADP ribosylation factor), and Ran (Ras related nuclear protein). The Ras GTPases are key components in signal transduction and initiate signaling in response to growth or survival signals (*92*). Their importance is demonstrated by the abundance of mutations in Ras genes that can be observed in cancer (*93*). Rho GTPases participate in the regulation of cytoskeletal organization and signal transduction. (*94*). Rab and Arf GTPases are implied in the trafficking of membrane vesicles. Arfs are predominantly involved in traffic between the endoplasmic reticulum and the Golgi along the secretory pathway and control endocytosis and recycling to the plasma membrane(*95, 96*). Traffic between different endosomal compartments after endocytosis is regulated by the Rab family GTPases (*97*). Ran, the single member of the fifth class, regulates the transport of cargo from and to the nucleus; this protein is crucial for processes as diverse as transcriptional control and assembly of the nuclear envelope after mitosis (*98*).
Due to the key role these classes of proteins play in essential cellular processes, regulatory proteins tightly control their guanine nucleotide binding state and in turn their activity.

2.5.2 Small GTPases function as biological switches that are controlled by GEFs and GAPs

Small GTPases function as "molecular switches" that are active when bound to guanine nucleotide triphosphate (GTP) and inactive in complex with guanine nucleotide

diphosphate (GDP). The active conformation allows for interaction with effector proteins that mediate the associated cellular response (Fig. 2.6). Most GTPases bind to nucleotides with low nanomolar affinity causing a slow intrinsic nucleotide exchange. Regulatory proteins are required to enable rapid activation of GTPases by promoting the exchange of GDP for GTP (*99*). Guanine nucleotide exchange factors (GEFs) destabilize the interaction with nucleotides by inducing conformational changes in the switch 1 and switch 2 regions as well as the phosphate binding loop of the GTPase (*100-102*). The resulting GTPase-GEF complex is in turn dissolved by other nucleotides that displace the GEF and establish a fresh GTPase/nucleotide complex. GDP is usually exchanges for GTP due to the higher concentration of nucleotide triphosphates in the cell. Consequently, GEF activity leads to activation of the GTPase (Fig. 2.6; (*103*)).

GEFs itself are also regulated in a variety of ways to ensure proper initiation of GTPase downstream signaling. Localization in the cell, release of autoinhibition and allosteric control are possibilities to modify GEF activity. Most GEFs are multidomain proteins that contain elements that localize to membranes or interact with other proteins. Moreover, intramolecular inhibition by blocking the GTPase binding site is a common theme (*104*) and allosteric regulation, e.g. positive feedback via the active GTPase (*105*), is employed in robust GEF activation. Hence, GEFs integrate a plethora of signals to accurately adapt to a given cellular situation.

To fully function as a molecular switch, GTPases need to return to their original state after initial activation. Although the name implies that the proteins are able to hydrolyze bound GTP, the intrinsic catalytic activity is low. Efficient inactivation is facilitated by GTPase activating proteins (GAPs, Fig.2.6). They induce conformational changes in the GTPase that allow coordination of an attacking water molecule required for hydrolysis. Moreover, the transition state of the reaction is stabilized by proper orientation of suitable amino acids of the GTPase or the GAP (*106*). Although the detailed mechanism varies between different GAPs, the general concept of GTPase activation is very similar (*103*).

The complete GTPase cycle is required for correct function and problems with either activation or inactivation lead to aberrant cellular behavior. Therefore, GEFs and GAPs are crucial in the biology of small GTPases by providing accurate control of their activity.

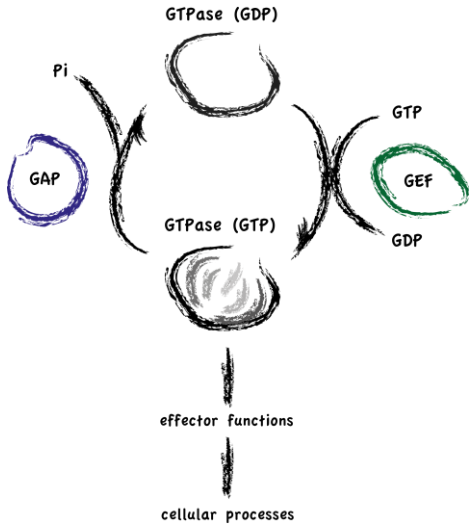

Fig. 2.6 Small GTPases are regulated by GEFs and GAPs. GTPases that are bound to GTP initiate downstream effector signaling. Regulation of the nucleotide binding state is facilitated by guanine nucleotide exchange factors (GEFs) and GTPase activating proteins (GAPs). Both protein classes are essential to establish small GTPases as molecular switches.

2.6 ADP ribosylation factor (Arf) GTPases

The ADP ribosylation factor (Arf) class of small GTPases was originally named for their ability to work as cofactors in the ADP ribosylation of Gα proteins by cholera toxin (*107*). However, their physiological role is that of a GTPase molecular switch.

The six mammalian members of Arf proteins can be categorized into 3 subclasses based on their sequence identity (*108*). The best-studied member of class I (next to Arf2 and 3) is Arf1. Playing an important role in membrane transport along the secretory pathway, Arf1 regulates the formation of COPI coated vesicles at the Golgi membrane and promotes budding of clathrin coated vesicles (CCVs) on endosomal membranes by recruiting adaptor proteins like AP-1 (*96*). Moreover, Arf1 regulates cytoskeletal elements that are required for maintaining the integrity of the Golgi network (*109*). The function of class II Arfs (Arf4 and Arf5) is still unclear, but they are thought to be involved in membrane trafficking by formation of heterodimers with class I Arf proteins (*110*). Arf-like (ARL) proteins resemble Arfs structurally, but their functions in cell biology are distinct from the classic Arfs (*111*).

Arf6 is the sole member of mammalian class III Arf proteins. It has widespread influence on cellular behavior with special importance in endocytosis and endosomal recycling (*96*).

2.6.1 Arf6 is implicated in endocytosis, endosomal recycling and cytoskeletal organization

Arf6 is the least conserved member of the mammalian Arf family. This is also reflected in its function and localization. While the other Arf proteins are found predominantly on Golgi membranes, Arf6 localizes to endosomes and the plasmamembrane to promote vesicle formation.

Arf6 in endocytosis

Arf6 regulates endocytosis at the plasma membrane, both in a clathrin dependent and independent manner. Clathrin mediated endocytosis is regulated by the presence of phosphatidylinositol 4,5 bisphosphate ($PI(4,5)P_2$) in the membrane, which is produced by Phosphatidylinositolphosphate 5 kinase (PIP5K). This enzyme is directly activated by Arf6 and needs phosphatidic acid, generated by Arf6 regulated Phospholipase D (PLD), as a cofactor (*112*). Clathrin independent endocytosis is regulated by shaping the lipid landscape in a similar way (*96, 113*). Full completion of endocytic trafficking requires the inactivation of Arf6 after vesicle budding. ArfGAPs are essential for this process and hydrolysis-deficient Arf6 mutants result in the accumulation of aberrant vesicle structures (*114*).
Endocytosis has implications in cell signaling since GPCRs and some RTKs (like c-Met and VEGFR) are internalized in an Arf6 dependent manner after activation (*115, 116*). Thereby, Arf6 activity has a regulatory effect on receptor function.

Arf6 in endosomal recycling and cytoskeletal organization

Membrane proteins such as the different receptor classes discussed before are internalized via endocytosis and sorted into the endosomal compartment. From there, they can either be degraded by lysosomal targeting or recycled to the plasma membrane. Thus, small GTPases can influence signaling processes governed by endocytosed proteins through regulating their fate regarding endosomal sorting (*117*).
Arf6 is involved in different endosomal recycling processes. Stimulation-dependent recycling of membrane proteins requires Arf6 activation and subsequent signaling involving PLD (*118*) and components of the “exocyst” complex (*119*). Furthermore, GTP hydrolysis stimulated by ArfGAPs is essential to complete the process (*120*). This is also

true for constitutive recycling of "bulk membranes" and proteins, a process that depends on the Arf6 GTPase cycle and ensures an equilibrium in membrane trafficking (*121*). Moreover, transport of membrane components to defined sites in a cell and reorganization of the membrane environment is crucial for phagocytosis and cell migration (*96*) suggesting a role for Arf6 in these vital processes.

Arf6 influences the remodeling of actin filaments, leading to the formation of "membrane ruffles", an initial step in cell migration (*122*). This involves the recruitment and regulation of Rac1 and is accompanied by changes in the lipid environment (*123*). Additionally, endocytosis of cell-cell-contact mediating proteins like E-cadherin allows cells to leave their microenvironment in an Arf6 dependent manner (*124*). All these processes are essential in normal cell migration; and deregulation in certain cancers leads to invadopodia formation and metastasis (*125*), making Arf6 a crucial target for cellular activity control.

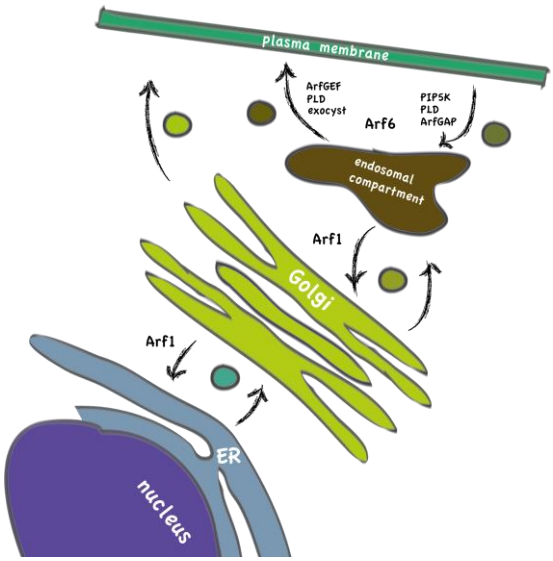

Fig. 2.7 The role of Arf GTPases in vesicle transport. Arf1 regulates vesicle transport along the secretory pathway. In contrast, Arf6 is involved in endocytosis and endosomal recycling. Hence,it influences important cellular processes associated with and at the plasma membrane.

2.6.2 Guanine nucleotide exchange factors (GEFs) for Arf GTPases

Activation of Arf GTPases is facilitated by specific GEFs. The common structural motif in Arf GEFs is the Sec7 domain. This domain is approximately 200 amino acids long and got its name from the yeast homolog Sec7p that is involved in Golgi-associated protein transport (*126*). High molecular weight Arf GEFs can be found in all eukaryotes, with orthologs from yeast to mammals. They are big multidomain proteins and predominantly act on class I and class II Arfs (*127*). Thus, they control membrane

trafficking along the secretory pathway and their inhibition via brefeldin A (BFA) leads to the disintegration of the Golgi (*128, 129*). In contrast, small molecular weight Arf GEFs are BFA resistant, function mainly at the plasma membrane and also catalyze exchange on Arf6. The four members of the cytohesin family and EFA6 represent this class of Arf GEFs.

The structure of Sec7 domains in complex with Arf proteins shows that the α helices F,G and H form a hydrophobic grove that is important for GTPase binding. Furthermore, a hydrophilic loop formed between helix F and G (the F-G loop) is highly conserved and crucial for GTPase binding and exchange activity (*101, 130*). Particularly important is a glutamate residue (position 156 in cytohesin 2), which catalyzes nucleotide exchange by displacing the magnesium ion important for nucleotide binding in the GTPase. This glutamic finger is essential for exchange activity (*131*).

Apart from a Sec7 domain-containing GEF, Arf GTPases require the presence of lipid membranes for their activation. An N-terminal myristoyl modification on the GTPase mediates membrane recruitment of the active form. When inactive, it blocksthe Sec7 binding site, inhibiting the exchange reaction (*132*). The presence of membranes promotes dislocation of the myristoyl moiety and the adjacent peptide helix, resulting in a modest nucleotide exchange rate (*133*) that is subsequently increased by efficient binding of Sec7 domain-containing GEFs.

The requirement for both, the correct membrane environment and a suitable GEF, provides a sophisticated way to limit the activation of Arf GTPases to the appropriate location and activating protein. Further control is provided on the level of GEF activity. A prominent example will be given with a more detailed introduction to cytohesins.

2.6.3 Cytohesins: a class of GEFs for Arf GTPases

There are four mammalian isoforms of cytohesins. They belong to the low molecular weight Arf GEFs and are characterized by a distinct domain structure. The central Sec7 domain responsible for the catalytic activity is flanked by an N-terminal coiled coil (CC) domain and a C-terminal pleckstrin homology (PH) domain. The CC domain mediates protein-protein interactions and can induce dimerization of cytohesins. On the other hand the PH domain is required for recruiting cytohesins to their target membranes through binding to phosphatidylinositolphosphates (*134*). Furthermore, the PH domain

has a binding site for active Arf6 that is employed to indirectly interact with the membrane via the GTPase, thereby creating a positive feedback loop (*135*).
Like other GEFs, cytohesins are intrinsically autoinhibited. A C-terminal polybasic region (PBR) is responsible for an intramolecular inhibition, which is resolved upon binding of the target membrane. By recruiting Arfs and GEFs to membranes, futile or deleterious GTPase activation is avoided, ensuring accurate control of Arf mediated cellular processes on the level of both proteins.
Although the exchange activity of cytohesin 2 or ARNO (Arf nucleotide binding site opener) *in vitro* is high for Arf1 and lower for Arf6 (*136*), the major physiological target for the GEF appears to be Arf6, due to its localization at the plasma membrane (*137*). Chemical inhibition of exchange activity results in reduced levels of Arf6GTP in cells. However, under the same conditions, Golgi integrity is not affected, indicating that Arf1 function is not impaired (*138*). This example illustrates how proper localization can regulate cellular processes independent of direct protein-protein interactions.
The different levels of Arf activity control provide further evidence for their importance in cell biology.

2.6.4 Known inhibitors for Arf signaling

The wide variety of Arf6 functions and control mechanisms indicate a complex network involved both upstream and downstream of the GTPase. A detailed dissection of the protein functions would be beneficial to gain a better understanding of the physiological and pathophysiological effects of Arf6.
One way to study the contribution of a protein in certain cellular pathways is to remove it from the cell and investigate the resulting phenotype. Genetic methods like knockout or RNA interference can be employed to reduce protein abundance. However, gene knockout is time consuming and even transient reduction of protein levels via RNA interference requires a cellular response over a longer period of time. Therefore, methods that directly inhibit the present protein pool are advantageous,providing a rapid way to generate effectsthrough loss of protein function. Small molecule inhibitors are an elegant tool to modulate protein function *in vitro*, in cells and even in animal models.

Brefeldin A (BFA) is a fungal toxin that inhibits Arf functions. Treating cells with this compound inhibits the secretory pathway and induces disintegration of the Golgi by inhibiting class I and class II Arfs (*139*). It was shown that the inhibition is mediated through stabilization of the complex between Arf and the Sec7 domain-containing exchange factor (*128*). This prevents the formation of a nucleotide-containing Arf complex and thereby terminates the GTPase cycle. However, BFA only binds to Arf in complex with specific GEFs (*140*). Low molecular weight Arf GEFs are not affected. A computational biology approach guided by structural data of an Arf1/ARNO Sec7-complex was employed to generate an inhibitor for low molecular weight GEFs. The identified compound, LM11, acted similar to BFA by stabilizing the Arf-Arf GEF interaction and preventing nucleotide binding (*141*) illustrating the broad applicability of this inhibitory mechanism.

Another small molecule inhibitor that is used in studies on Arf GTPases is SecinH3 (*138*). It inhibits the exchange activity of different cytohesins, thereby reducing the level of active Arf GTPases both *in vitro* and in cells and is frequently employed as an indirect Arf6 inhibitor (*142, 143*). Similar to the mode of action of BFA and LM11, SecinH3 modulates Arf activity upstream of the GTPase function by preventing its activation. This could cause unexpected side effects in cellular studies due to “off target” effects not mediated by the small molecule inhibitor itself but by the inhibited upstream protein. An interesting example is the effect of cytohesins on RTK signaling that was discovered with the help of SecinH3.

2.6.5 Cytohesins and RTK signaling

With the discovery of SecinH3 as a specific inhibitor for cytohesins, it was shown that Arf GEFs have functions in cellular pathways that are distinct from their canonical role in Arf activity control. Initially, an effect on insulin signaling was observed in mammalian cells and in Drosophila that was linked to reduced insulin receptor signaling caused by cytohesin inhibition(*138, 144*). Subsequently,the stimulatory effect of cytohesins on insulin signaling was found to be dependent on their direct interaction with the scaffold protein CNK1 (Connector enhancer of KSR 1, (*145*)).

The epidermal growth factor receptor (EGFR) is also regulated by cytohesins. However, in contrast to insulin signaling, cytohesins directly interact with the intracellular part of

the receptor and promote autophosphorylation and general kinase activity by inducing a conformational change (*146*). This represents the first example of a direct positive regulation of an RTK from the inside of the cell. The importance of this effect is illustrated by the overexpression of cytohesins in lung cancer cells and the inhibition of tumor growth observed in SecinH3 treated mice (*146*). Therefore, cytohesins emerge as a potential new target in tumor therapy. However, the detailed mechanism behind the activating effect of cytohesins on EGFR is elusive and more information is required to fully harness the potential of this novel discovery.

In several other cases, GEFs were found to be involved in RTK signaling. Cytohesins were also implicated in VEGFR signaling by promoting surface expression of the receptor (*147*) and a role in several cancer types is described (*148, 149*). Very recently, the GEF DOCK7 was found to regulate bouton formation in specialized interneurons. The effect was caused by modulating the activity of the EGFR family member ErbB4 and involved an interaction of between receptor and GEF (*150*). Interestingly, both the effect of DOCK7 on ErbB4 and of cytohesins on EGFR are independent of the catalytic activity of the GEF proteins, suggesting important physiological roles apart from their canonical functions. It is important to note that SecinH3 inhibits cytohesin's activity on Arfs as well as RTKs, demonstrating that a small molecule inhibitor can influence different aspects of protein biochemistry.

These examples demonstrate potential problems that can arise when using upstream inhibition to study protein functions and make an argument for different approaches that are currently rare in research focused on small GTPases.

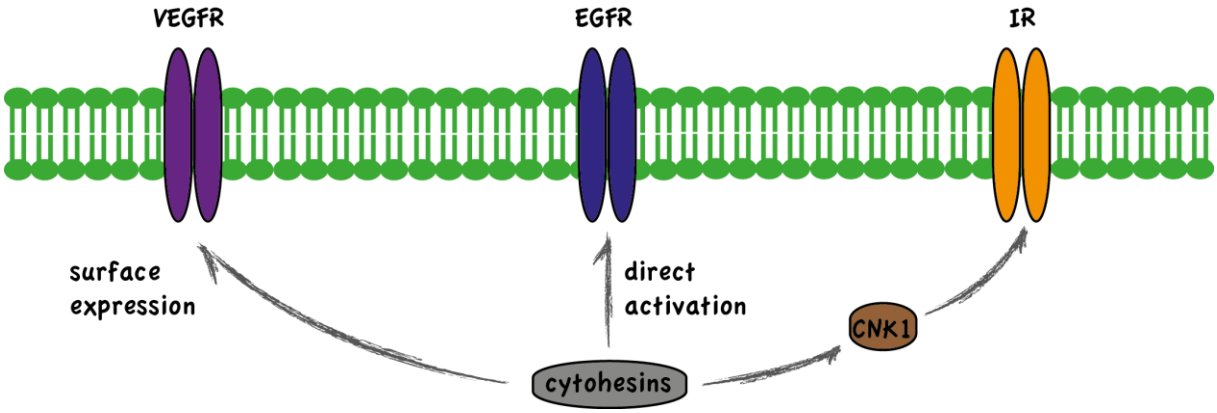

Fig. 2.8 The influence of cytohesins on different receptor tyrosine kinase pathways. Cytohesins regulate RTK associated signaling pathways on different levels. This complex contribution to receptor signaling was only recently discovered and raises important questions about RTK activity regulation.

2.6.6 The Arf6 effector protein JIP4

An alternative to upstream inhibition of GTPase function is downstream inhibition. Active GTPases bind to a variety of effector proteins to mediate different cellular functions. Effector proteins are expected to bind to the switch I, switch II and interswitch regions on Arf GTPases given that these structural elements undergo major conformational changes upon nucleotide exchange (*151*). Blocking effector interaction abolishes downstream effects and can be employed to control Arf signaling. Although different Arf proteins have distinct roles in cell biology, the GTP associated conformation in their switch region is very similar (*151, 152*). This is reflected by the fact that some Arf effectors bind to more than one isoforms, preventing discrimination on this level (*96*).

However, there are effector molecules that provide specificity towards single Arf isoforms. The protein c-Jun N-terminal kinase (JNK)-interacting protein 4 (JIP4) is a well-described example for a specific Arf6 effector. JIP4 serves as a scaffold protein in JNK and MAPK signaling and coordinates the recruitment of kinesins and dyneins to microtubules (*153, 154*). By competing with kinesin 1 for JIP4-binding, active Arf6 modulates microtubule transport and is required for successful abscission during cytokinesis (*155*).

Recently the binding site of Arf6 on JIP4 was narrowed down to the second leucine zipper domain (JIP4 LZII) and a fragment comprising only amino acids 392-462 was co-crystallized to obtain a detailed structural picture of the interaction (*156*). Therefore, JIP4 LZII represents the minimal Arf6-binding motif, making it suitable to screen for inhibitors that abolish the protein-protein interaction in order to modulate Arf6 downstream signaling.

3 Aims and Significance

Receptor tyrosine kinases (RTKs) are key players in the regulation of vital cellular processes like survival, growth and proliferation. The identification of cytohesins as intracellular activators of epidermal growth factor receptor (EGFR) signaling opens new possibilities for the therapeutic use of specific inhibitors to counteract aberrantly activated EGFR signaling, for example in cancer. To fully explore the therapeutic potential and understand the molecular events behind the observed effects, a more detailed understanding of the structural interplay between EGFR and cytohesins is required. This study aims to elucidate the mechanism involved in ARNO (cytohesin 2) mediated EGFR activation by employing biochemical methods to investigate the interaction and enzymatic regulation. Different constructs of ARNO and EGFR are analyzed to define the binding interface of the complex and to evaluate their enzymatic activity *in vitro.* Additionally, x-ray diffraction analysis of protein crystals should yield a high-resolution structure of the interacting proteins. A comprehensive model of the EGFR interaction with ARNO will help to understand and experimentally address this novel biochemical phenomenon.

Furthermore, identification of an Arf6-specific small molecule inhibitoris approached by a high throughput screening (HTS) effort. The small GTPase Arf6 is a molecular regulator of vesicle trafficking between the plasma membrane and the endosomal compartment. It is crucial for the regulation of receptor signaling, cell motility and the final steps of cell division. Hence, it has a multitude of different implications in both normal and aberrant cellular behavior (e.g. metastasis in cancer). The scientific interest in this protein is high, as illustrated by various studies using indirect Arf6 inhibitors. A prominent example is the cytohesin inhibitor SecinH3 that is frequently used to indirectly decrease Arf6 activity. However, the recently identified Arf6-independent functions of cytohesins in RTK signaling complicate the interpretation of results obtained with these inhibitors. Thus, this study aims to develop an assay for the discovery of Arf6 inhibitors that act downstream of its activation. The specific Arf6 effector JIP4 is employed in an assay that monitors complex formation, and can therefore be used in a high throughput screening to identify small molecules that block the interaction. Potential hits have to be verified in independent assays in order to obtain suitable molecules with the desired inhibitory activity.

4 Results

4.1 High throughput screening (HTS) for a small molecule inhibitor of the GTPase Arf6

There are six members in the family of mammalian Arf proteins that are characterized by high sequence homology and very similar 3D structures (*96, 152, 157*). Discrimination between different family members is a big challenge in the development of inhibitory molecules. Attempts to select an aptamer specifically binding and inhibiting Arf6 have not been successful in the past (unpublished data). This excludes the very promising option of establishing an aptamer displacement screen similar to the ones successfully used before to identify small molecules inhibiting different domains of the guanine nucleotide exchange factor (GEF) ARNO (*158, 159*). However, natural effector molecules of Arf GTPases are able to distinguish between the different Arf family members. A direct screen for inhibitors that can displace a selective effector from an active GTPase provides a promising alternative to the aptamer based method and exploits a new and promising area of drug development.

The effector molecule c-Jun N-terminal kinase interacting protein 4 (JIP4) was shown to bind to Arf6 but only weakly to Arf1 via its leucine zipper 2 (LZII) domain. Furthermore, a crystal structure of the complex is available that enables rational modifications in the process of assay development (*156*).Therefore, this protein is well suited for the envisioned task. To establish an *in vitro* binding assay it is required to:

1. Provide a sufficient amount of pure protein.
2. Establish and *in vitro* assay to monitor binding of the interaction partners.
3. Optimize the established assay for high throughput screening (HTS) applications.

The experimental steps leading to achieve the mentioned goals are described in the following paragraphs.

4.1.1 Expression and purification of stΔ13 Arf6 and JIP4 LZII (AA 392-462)

An n-terminally truncated form of Arf6 was expressed as a strep-tagged protein in E.coli and purified via a single step purification protocol using streptactin high capacity resin (data not shown). The obtained protein was at least 95% pure and could be purified in sufficient amounts (20mg protein from 1l bacterial culture) for the following experiments.

The JIP4 LZII domain was expressed as a fusion protein with glutathione S transferase (GST; expression plasmid pGST1 JIP4LZII was a kind gift of Julie Menetrey, Laboratoire d'enzymologie et biochimie structurales, Gif-sur-Yvette). After affinity purification of the fusion products with glutathione resin the GST tag was cleaved using recombinantly expressed Tobacco Etch Virus (TEV) protease (*160*). After removing TEV using a NiNTA resin, free JIP4 LZII was further purified via a Superdex 200 size exclusion chromatography column (Fig. 4.1). This final step removes higher molecular weight impurities and small aggregates that are not possible to be separated from the target protein via centrifugation but could disturb the intended binding assays by unspecific association.

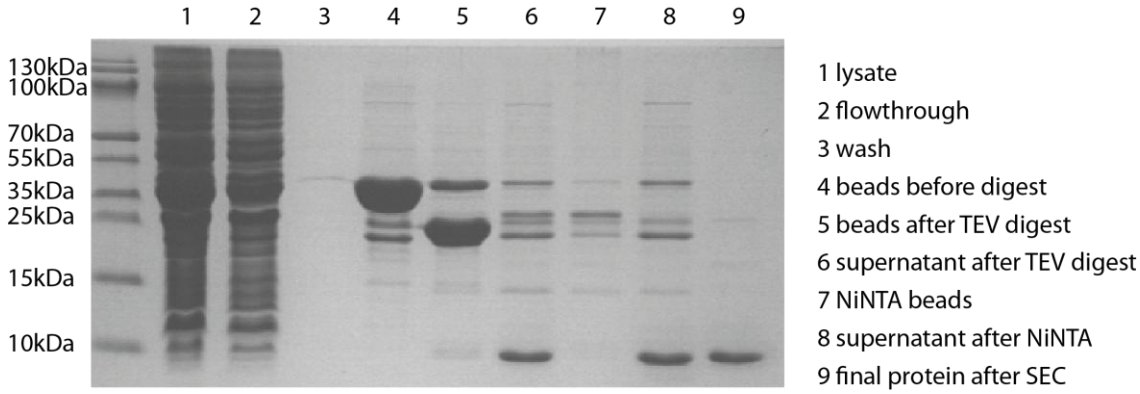

Fig. 4.1 Purification of JIP4 LZII (392-462). The indicated samples were taken during the purification process, separated on a 10% Tris-Tricine PAGE gel and stained with Coomassie Brilliant Blue. JIP4LZII runs slightly below the 10kDa marker band (expected MW: 9kDa). For purification details see text and Materials and Methods.

4.1.2 Exchange activity of the purifiedstΔ13Arf6 in an *invitro* assay

To proof that the recombinantly expressed GTPase is suitable to be used as a model for the physiological situation, the ability of the guanine nucleotide exchange factor (GEF) ARNO to exchange GTP for GDP was investigated. Arf6 preloaded with GDP is incubated

with the ARNO Sec7 domain in the presence of excess GTP. An increase in tryptophan fluorescence can be observed when nucleotide exchange takes place.

Despite the fact that ARNO was described to be a better GEF for Arf1 than for Arf6 (*136*) it is suitable for investigating Arf6 functionality *in vitro*(*161*). A clear exchange could be observed on Arf6 with concentrations of GEF down to 12.5nM (Fig. 4.2). As expected the exchange activity on Arf1 is higher (Fig. 4.2). However, it is clear that the recombinantly expressed truncated form of Arf6 used in this study is functional in a nucleotide exchange assay and therefore suitable for the intended screening approach.

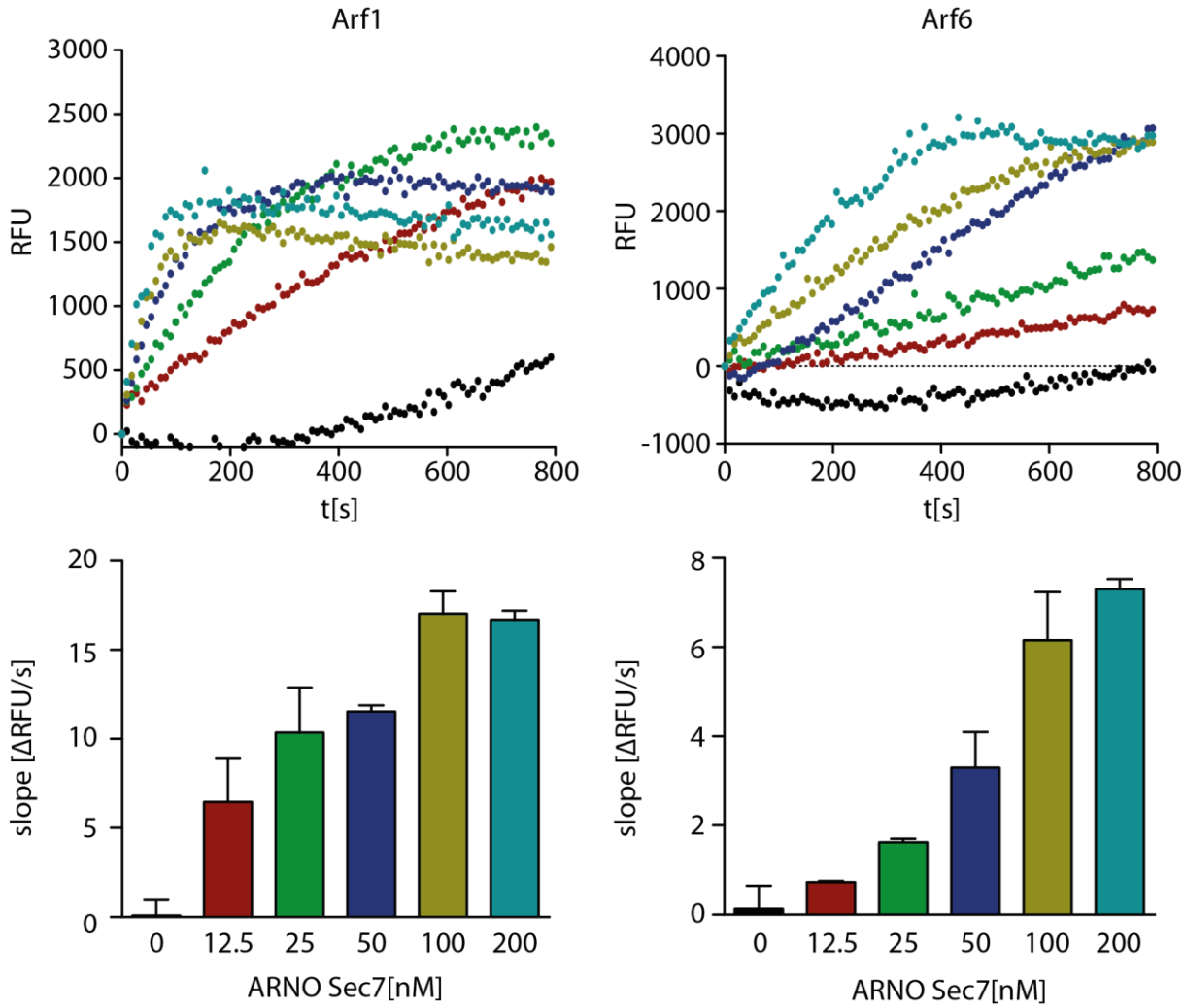

Fig. 4.2 Nucleotide exchange activity of ARNO Sec7 on Arf1 and Arf6. The indicated concentrations of ARNO Sec7 were incubated with GDP loaded Arf GTPases in the presence of excess GTP. Nucleotide exchange results in an increase in tryptophan fluorescence. The upper curves illustrate the change of fluorescence over the course of the experiment (one representative example). The early parts of the curves (150s for Arf1 and 300s for Arf6) were fitted to a linear regression model and the resulting slope is plotted in the column diagrams (n = 6).

4.1.3 Labeling of purified proteins for subsequent assay development

To find inhibitors that disturb the binding of JIP4LZII to active Arf6 an assay monitoring the interaction in an easy to evaluate readout needs to be established. Several biophysical methods are available (and described in paragraphs 4.1.4, 4.1.6 and 4.1.7) for this purpose and many of them require a non-reversible, e.g. covalent, modification of the interaction partners with chemical groups that provide them with certain characteristics (e.g. fluorescence) that are in turn employed to determine molecular interactions. Therefore, both of the purified proteins were covalently attached to either fluorescein or biotin for fluorescent detection or immobilization.

JIP4 LZII was labeled with fluorescein using iodoacetamido (IAA) functionalized reagent to selectively label thiol groups found in cysteine residues. The purified JIP4 LZII domain only contains one cysteine assuring a selective labeling at one position of the protein. Figure 4.3a and b show that the labeling is very efficient. Modification of JIP4 LZII can be observed in a band shift in a Coomassie stained SDS PAGE gel (Fig. 4.3a). Additionally UV irradiation shows that the altered migration behavior of the labeled protein can be explained by a fluorescent moiety covalently attached to the protein (Fig. 4.3b) since only the IAA fluorescein treated sample results in a visible band.

Arf6 was labeled with biotin using amine reactive NHS esters. These groups react with lysine residues as well as the N-terminus of a protein if those are surface exposed. NHS biotin treated Arf6 was immobilized on a nitrocellulose membrane and could be detected via an anti-biotin antibody conjugated to fluorescein while both unlabeled Arf6 and JIP4LZII were not detected (Fig. 4.3c). Although this assay is not quantitative it shows successful conjugation of biotin to Arf6.

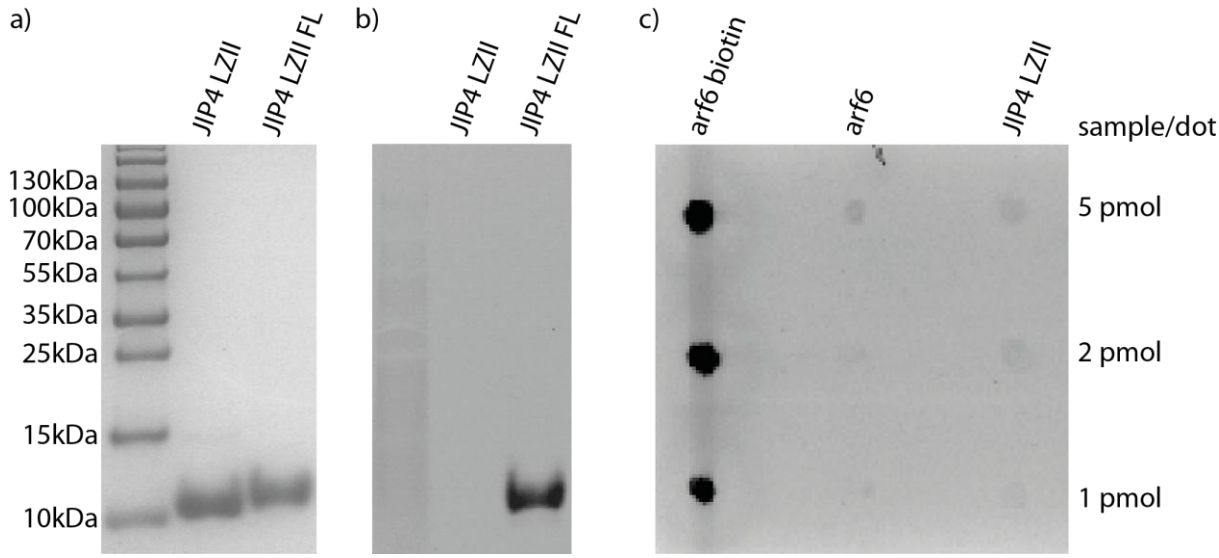

Fig. 4.3 Covalent modification of JIP4 LZII and Arf6. IAA fluorescein labeled JIP4 LZII (labeled "FL") was separated on a 10% Tris-Tricine SDS PAGE gel. Modification with fluorescein results in a change in running behavior of JIP4 LZII as observed in a Coomassie brilliant Blue stained gel (a). Furthermore, the

label is detected by UV irradiation (fluorescence, b). Biotin modified Arf6 is detected with anti-FITC antibodies after immobilization on a nitrocellulose membrane (DotBlot, c).

4.1.4 An luminescent oxygen channeling (LOC) assay detects the binding of different GTPases to their effector proteins

For luminescence oxygen channeling (LOC), or Amplified Luminescent Proximity Homogenous Assay (ALPHA) screen, experiment the interaction partners have to be immobilized specifically on either donor or acceptor beads. Interaction of the immobilized partners brings both beads in close proximity and allows the transfer of singlet oxygen generated by the donor beads upon irradiation with light of 680nm wavelength to the acceptor beads. This results in emission of light of 520nm-620nm by the acceptor beads. The singlet oxygen has a half-life of approximately 4µs and can diffuse up to 200nm from donor to acceptor beads. In contrast to techniques like Förster Resonance Energy Transfer (FRET) this allows for detection of a macromolecular interaction without detailed knowledge of the interaction site and the spatial orientation of the protein labels (*162*).

There are different options available for the immobilization of the proteins to ALPHA screen bead. Fluorescein modified JIP4 LZII and biotin conjugated Arf6 incubated with appropriate beads generate a signal that indicates the formation of JIP4 LZII complex with Arf6 and the attached donor and acceptor beads (Fig. 4.4a). Another option is the immobilization of one interaction partner using specific antibodies and protein A coupled beads. This circumvents the need to covalently modify one interaction partner and allows the detected of proteins in complex solutions, e.g. endogenous GTPases in cell lysates (see paragraph 4.1.5). The proof of principle was demonstrated using Arf1 and its effector protein GGA3 (Golgi-associated, γ adaptin homologous, Arf interacting protein 3; (*163*); Fig. 4.4b) and the Rho GTPase Rac1 with p21-activated kinase (Pak; (*164*); Fig. 4.4c). However, for Arf6 and both GGA3 and JIP4 LZII it was not possible to generate an ALPHA screen signal using the antibody based approach. Given that both proteins are described as Arf6 effector proteins (*156, 165, 166*) and are suitable to generate a signal in a LOC based assay with either biotin modified (Fig. 4.4a) or His tagged Arf6 (*167*) the problems observed could be attributed to antibody binding.

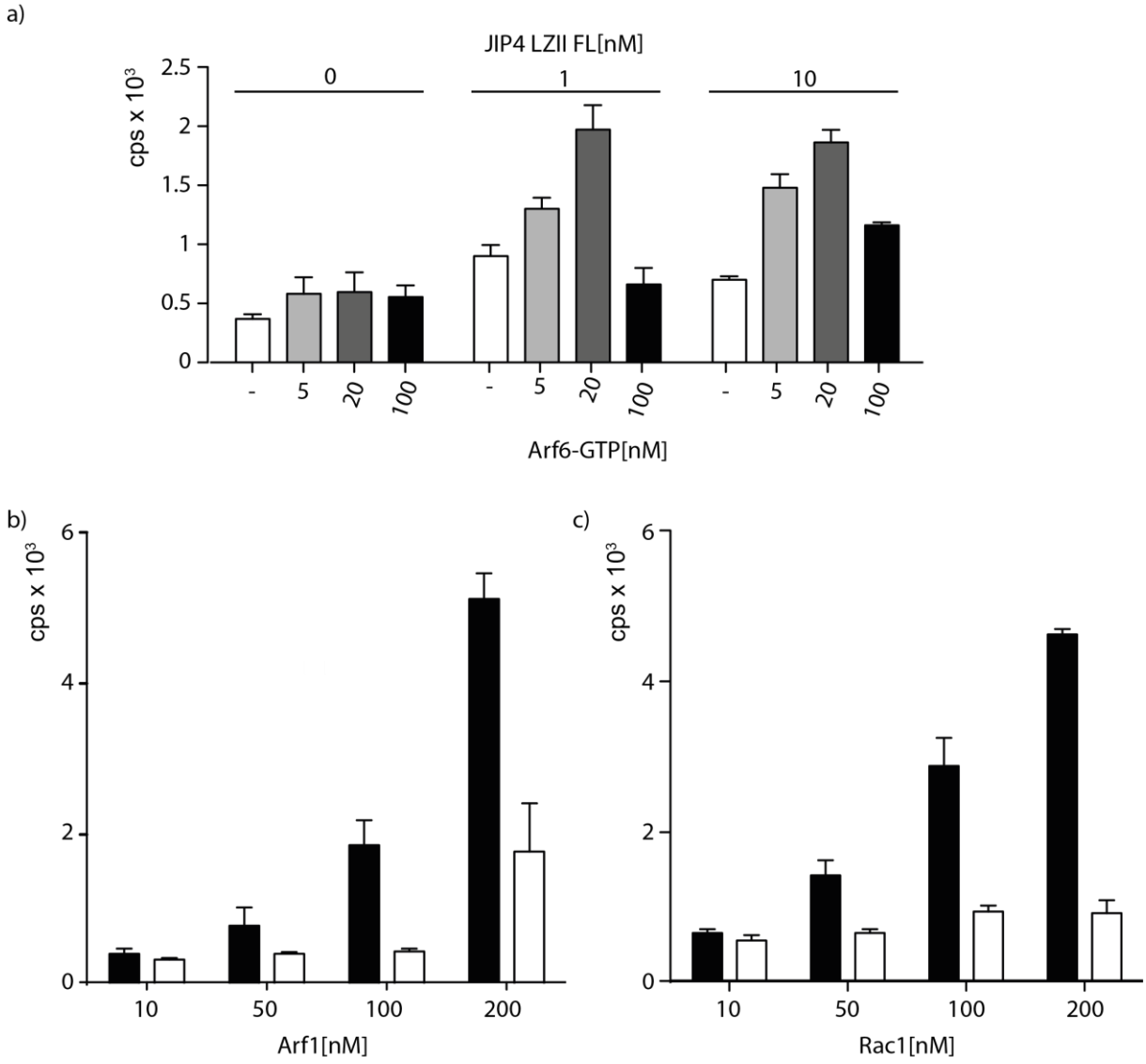

Fig. 4.4 A LOC assay to detect the interaction between small GTPases and specific effector molecules. a) JIP4 LZII fluorescein and Arf6 biotin were immobilized on appropriate donor and acceptor beads resulting in an increase in luminescence The decrease in signal observed for high concentrations of Arf6 is due to the "hook-effect". Free Arf6 biotin competes with binding of the immobilized proteins when the bead binding sites are saturated. b and c) Arf1 and Rac1 were immobilized via specific antibodieson protein A acceptor beads. The respective effector proteins GGA3 and PAK1 are biotin modified and coupled to streptavidin donor beads. The white bars indicate GDP bound GTPases while black bars represent GTP bound proteins.

4.1.5 An antibody based luminescent oxygen channeling assay measures GTPases activity in cell lysates

The described ALPHA screen assay with antibodies recognizing the GTPase allows the detection of unlabeled proteins in a complex mixture of components. Although it proved to be not suitable for the intended screening for Arf6 the assay provides an opportunity to establish a method to measure the activation state of GTPases in cell lysates.

It was possible to detect endogenous amounts of GTP loaded Rac1 in lysates of both NIH3T3 and HeLa cells (Fig. 4.5a and b). The amounts of lysate required to obtain a detectable signal are at least one order of magnitude lower than in conventional pulldown assays (Fig. 4.5c). This could prove to be a valuable alternative for those assays to quantify activation states of small GTPases given appropriate antibodies to detect the GTPase of interest.

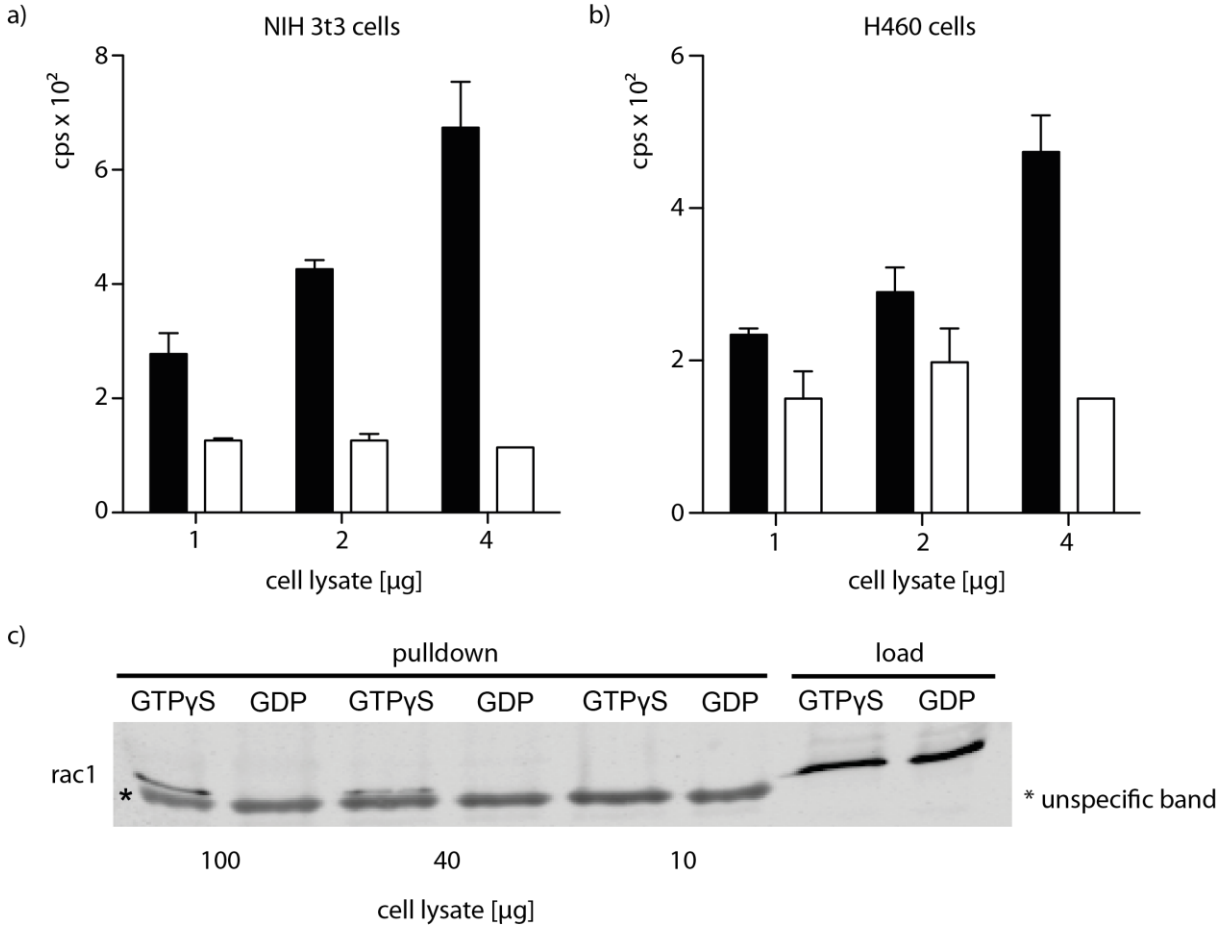

Fig. 4.5 LOC assay for the detection of active GTPases in cell lysates.A and b) The indicated amounts of cell lysate protein (preloaded with GTP or GDP) were incubated with the specific effector protein PAK1 immobilized on streptavidin donor beads. Specific antibodies are used to couple the endogenous GTPases to protein A acceptor beads. A specific signal was observed for both cell types with only 4µg of cellular protein. White bars indicate GDP loaded GTPases and black bars represent GTP loaded GTPases. C) Biotinylated PAK1 was immobilized on streptavidin agarose beads and incubated with the indicated amounts of cell lysate. Precipitated Rac1 was separated on SDS PAGE, blotted on a nitrocellulose membrane and detected with Rac1 specific antibodies. This experiment illustrates that 10 times more cell lysate (weak rac1 band detected with 40µg lysate) is required to detect GTP bound Rac1 when PAK1 is used to co-precipitate endogenous amounts of active GTPases from cell lysates.

4.1.6 A pulldown assay using GST tagged JIP4 LZII predominantly precipitates active Arf6

Pulldown assays are traditionally used to show complex formation between two proteins of interest. Precipitation of the complex is achieved by immobilization of one

interaction partner to an appropriate resin (e.g. agarose beads). If both proteins are precipitated with the resin it is expected that they form a stable interaction.

GST tagged JIP4 LZII can be immobilized on glutathione conjugated resin. Arf6 preloaded with GTP is efficiently co-precipitated with JIP4 LZII while GDP bound Arf6 and Arf1 do not bind as efficient to the effector protein. Furthermore, soluble JIP4 LZII without the GST tag can productively compete with the immobilized form indicating a specific interaction between active Arf6 and JIP4 LZII (Fig. 4.6a and b). In contrast, soluble JIP4 LZII does not compete with the precipitation of GTP loaded Arf1 by GGA3, a different effector protein for Arf GTPases (*163, 165, 166*). Both the specificity of JIP4 for binding Arf6 over Arf1 and the specificity in competing for effector binding argues for a very selective interaction that can be an excellent starting point to identify small molecules that selectively disturb Arf6 interaction with JIP4 or other effectors.

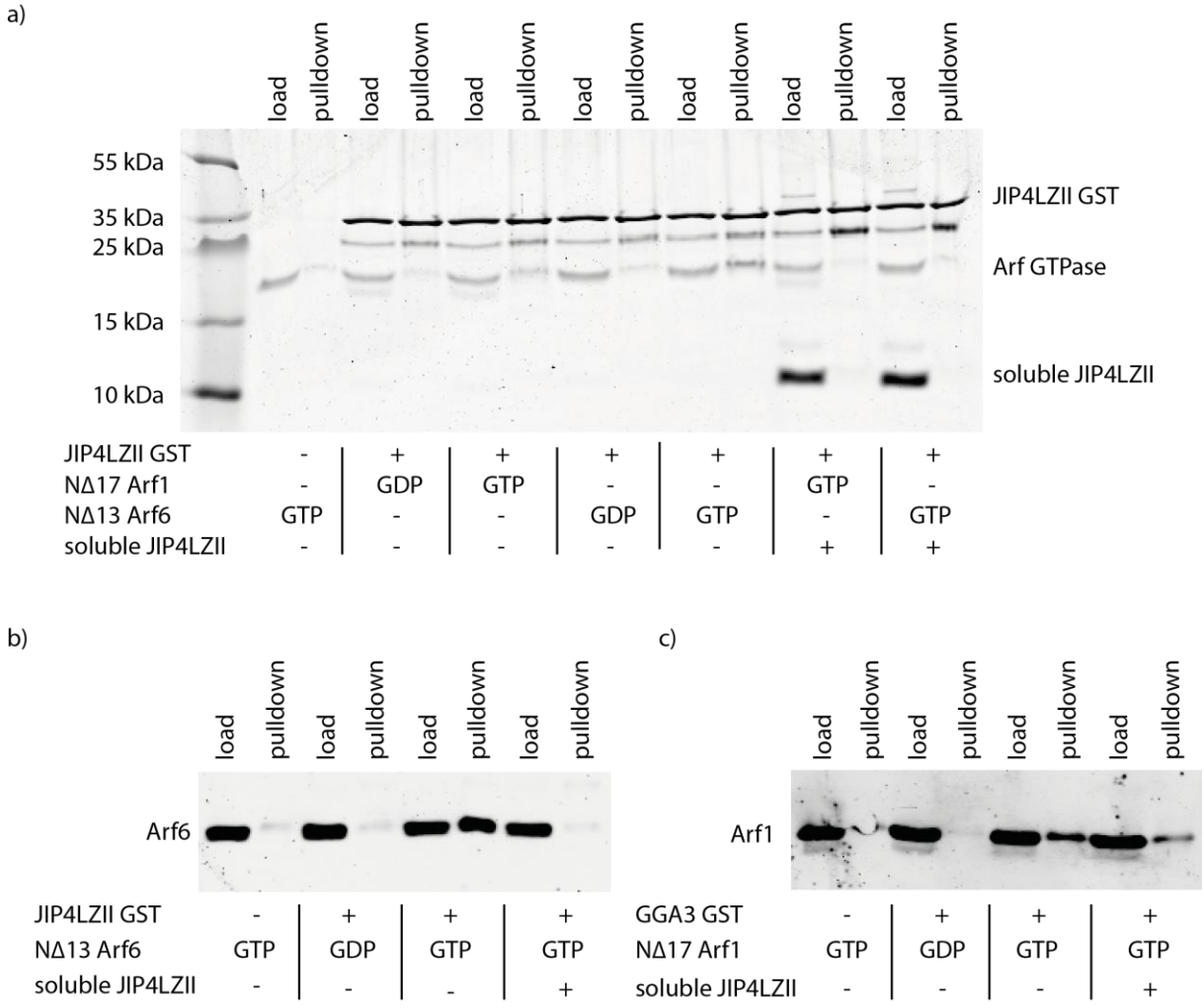

Fig. 4.6 Pulldown of Arf1 and Arf6 with specific effector proteins. JIP4 LZII GST was immobilized on glutathione agarose beads and incubated with Arf1 or Arf6, preloaded with either GDP or GTP, in the presence and absence of soluble JIP4 LZII as a competitor. GTP bound Arf6 is efficiently co-precipitated while Arf6 GDP and Arf1 GTP show only weak association with the effector bound beads (a, Coomassie stained SDS PAGE gel). Specific detection of both GTPases via Western Blot and antibody labeling shows that soluble JIP4 LZII competes for effector binding to Arf6 (b, JIP4) but not to Arf1 (c, GGA3).

4.1.7 A high throughput screening (HTS) compatible assay for protein-protein-interaction (PPI) inhibitors based on fluorescence polarization (FP)

High throughput screening for small molecule inhibitors requires the employed assay to be optimized for this special purpose. It has to be possible to perform the reaction in one tube (one well of a microtiter plate) in a homogenous mixture without the need for wash steps. Furthermore, the assay readout should be simple and stable over a definite time. If one or more of those criteria are not matched, screening will become complicated or even impossible with increasing quantity of small molecules. A co-precipitation assay as described in paragraph 4.1.6 is not suitable since it requires both extensive washing steps and evaluation of the results by separating the precipitated proteins via polyacrylamide gel electrophoresis (PAGE). Although the LOC assay described in paragraph 4.1.4 is suitable for HTS, it is a financially demanding method. To avoid problems associated with those two methods, a fluorescence polarization (FP) assay was established that provides an alternative that is easily applicable in a HTS setup.

Fluorescence polarization requires one molecule, ideally the smaller interaction partner, to be fluorescently labeled. When excited with polarized light tumbling and movement of the molecule during the time between excitation and emission (the fluorescence half-life) leads to a change in the polarization of the emitted light (*159, 168*). A small fluorescent molecule exhibits a low polarization of the emitted light. Binding of an interaction partner increases the size of the fluorescently labeled particle and in turn reduces the molecular motions that lead to a decrease in polarization. Hence, the FP value increases (Fig. 4.7a).

JIP4 LZII labeled with iodoacetamido (IAA) fluorescein was incubated with increasing concentrations of either GTP (active form) or GDP (inactive form) bound Arf6 and GTP bound Arf1. Active Arf6 binds with a K_d value of 0.6µM, which is in accordance to published data generated using surface Plasmon resonance (SPR) measurements (*156*). Inactive Arf6 (K_d=1.8µM) and active Arf1 (K_d=14µM) bind to JIP4 LZII with lower affinity. This demonstrates the specificity of the effector towards active Arf6. Additionally the FP values are stable over several hours (data not shown) further establishing this approach as suitable for HTS.

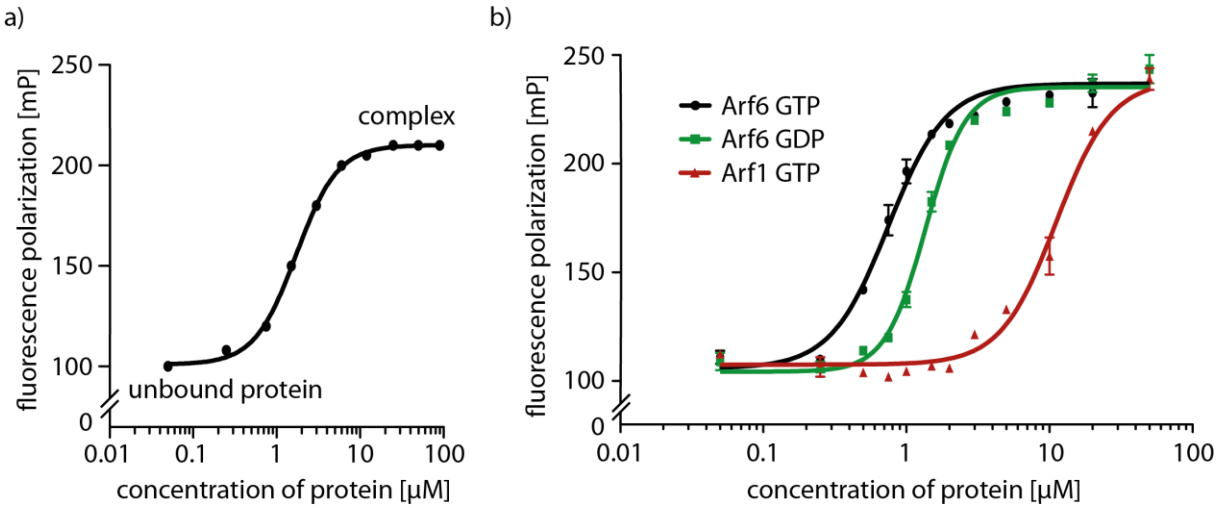

Fig. 4.7 Fluorescence polarization (FP) experiments with Arf GTPases and JIP4 LZII fluorescein. A small fluorescently labeled protein exhibits a low FP value due to a high molecular mobility. Binding of an interaction partner increases the size of the fluorescent complex, decreases the mobility and leads to an increase in FP (a). JIP4 LZII fluorescein was incubated with Arf6 loaded with GDP or GTP and Arf1 loaded with GTP. Arf6 GTP efficiently associates with JIP4 LZII while both GDP bound Arf6 and Arf1 exhibit a lower affinity for the effector protein (b).

4.1.8 The increase in fluorescence polarization is reversible and specific for JIP4 and Arf6

Further investigating whether the increased FP value observed when incubating JIP4 LZII fluorescein with Arf6GTP reflects specific association I used different control proteins. Only titration of Arf6 leads to an increase in FP but no change is observed with increased concentration of bovine serum albumine (BSA), Erk2 or the intracellular domain (ICD) of the EGF receptor (Fig. 4.8a). Furthermore, the FP values of JIP4 LZII FL in presence of Arf6 can be reduced by addition of increasing concentrations unlabeled JIP4 LZII (Fig. 4.8b) indicating both specificity and reversibility of the complex formation. In addition to the data from paragraph 4.1.7 the described results suggest that the assay is suitable for monitoring the specific interaction between Arf6 and its effector JIP4.

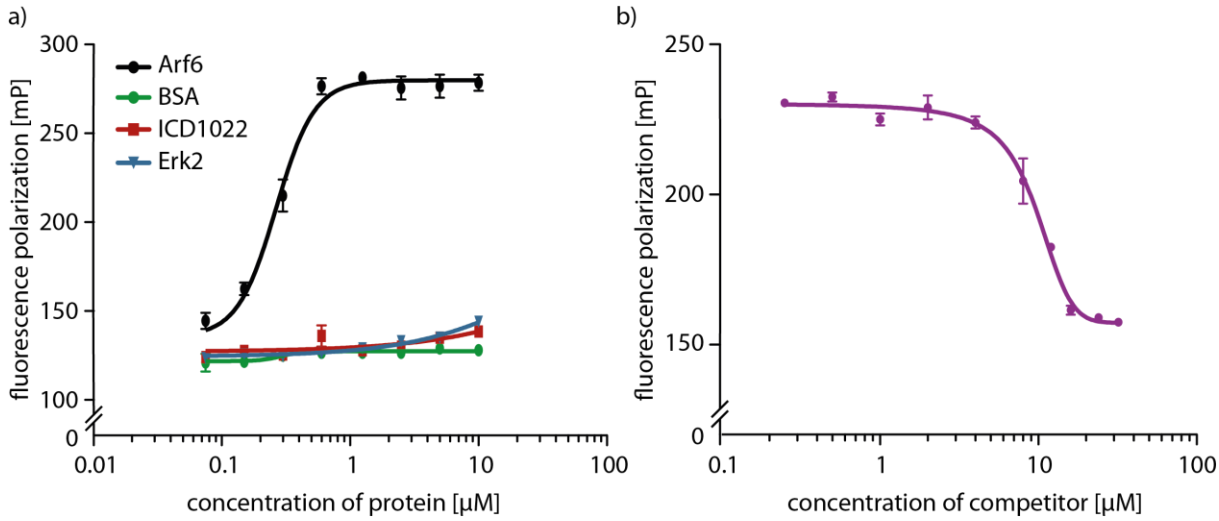

Fig. 4.8 JIP4 LZII and Arf6 generate a specific signal in a fluorescence polarization assay. The indicated proteins were incubated in increasing concentrations with fluorescein labeled JIP4 LZII. An increase in FP is observed for JIP4 LZII and Arf6 but not with the tested control proteins (a). A complex between Arf6 GTP and fluorescein labeled JIP4 LZII was incubated with increasing concentrations of unlabeled JIP4 LZII. This results in a decrease in FP indicating that complex formation is specific and reversible (b).

4.1.9 Neither addition of DMSO nor detergent impairs the fluorescence polarization assay

Another important aspect in the development of assays for drug development is their stability towards detergents or solvents used to store small molecules in libraries. The addition of detergents can reduce aggregation of small molecules, an effect that can lead to false positive results. Those "promiscuous" inhibitors (*169*) inhibit a wide variety of biological assays and are therefore not specific. Dimethylsulfoxide (DMSO) is a common solvent for the storage of stock solutions in compound libraries. The compounds screened in this study are stored in DMSO as well and therefore the biological assay needs to tolerate low concentrations of the solvent.

The addition of up to 0,1% Triton X 100 or 10% DMSO has no influence on the outcome of the FP assay (Fig. 4.9 a-c). Similar results are obtained with the detergent Tween 20 (data not shown). Furthermore, the assay readout was stable in reaction volumes as low as 10µl facilitating the use of 384 well plates.

An important parameter indicative of the quality of a HTS assay is the Z' value (*170*):

$$Z' = 1-(3*(\varsigma_{(positive)}+\varsigma_{(negative)})/(|\mu_{(positive)}-\mu_{(negative)}|))$$

The described assay had resulted in a Z' value close to 0.9 when performed under screening conditions (2µM Arf6, 250nM JIP4 LZII fluorescein, 384 well plate, 0,05% TritonX100, 5% DMSO) making the assay an excellent choice for the desired screening. HTS was performed with the help auf K. Rothscheid using an in-house compound library with 17000 small molecules and a final compound concentration of 30µM.

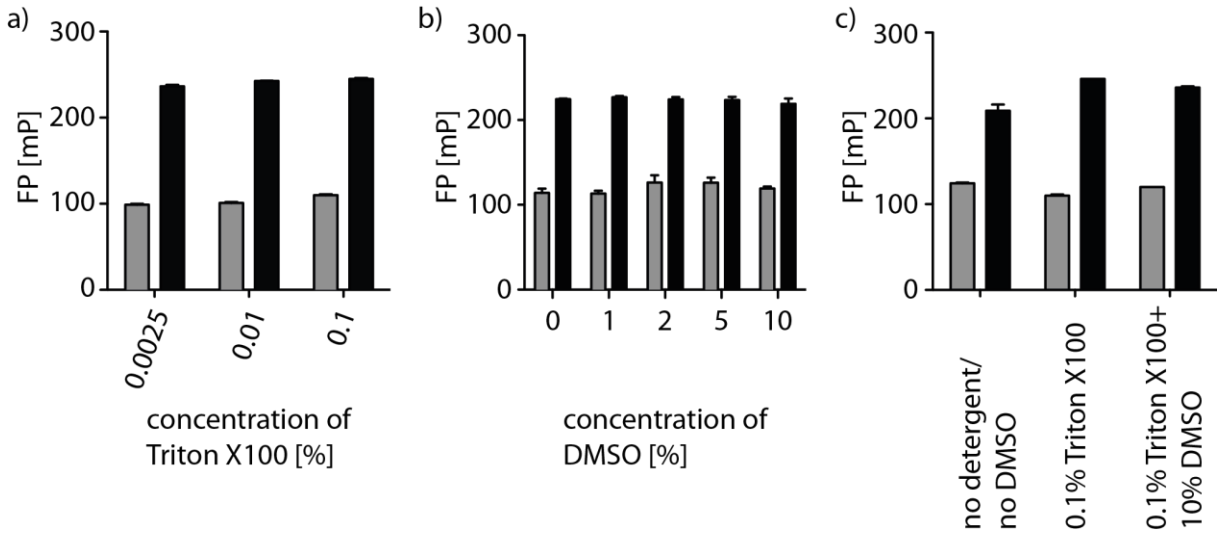

Fig. 4.9 Stability of the fluorescence polarization based screening assay towards Dimethylsulfoxide (DMSO) and detergent. Fluorescein labeled JIP4 LZII was incubated with the indicated reagents in the absence (grey bars) or presence (black bars) of saturating concentrations of Arf6 GTP. Neither DMSO nor Triton X 100 influence the change in FP observed (a and b). The combination of both reagents alsohas no effect (c).

4.1.10 Screening results and primary hit evaluation

The screening yielded nine compounds that reduced the FP value below the threshold of five standard deviations below the mean of the positive control (Fig. 4.10a). To confirm the results the assay was repeated manually using increasing concentrations of the initially identified compounds. Three of them had no effect in the rescreen while three more hits reduced the fluorescence polarization below the value of the negative control when used in high concentrations (30µM). Indeed those molecules exhibit a very high fluorescence in the range of fluorescein (Fig. 4.10b) and their presence in high concentrations leads to artificially reduced fluorescence polarization. The three remaining primary hits are depicted in Fig. 4.10c and were further analyzed.

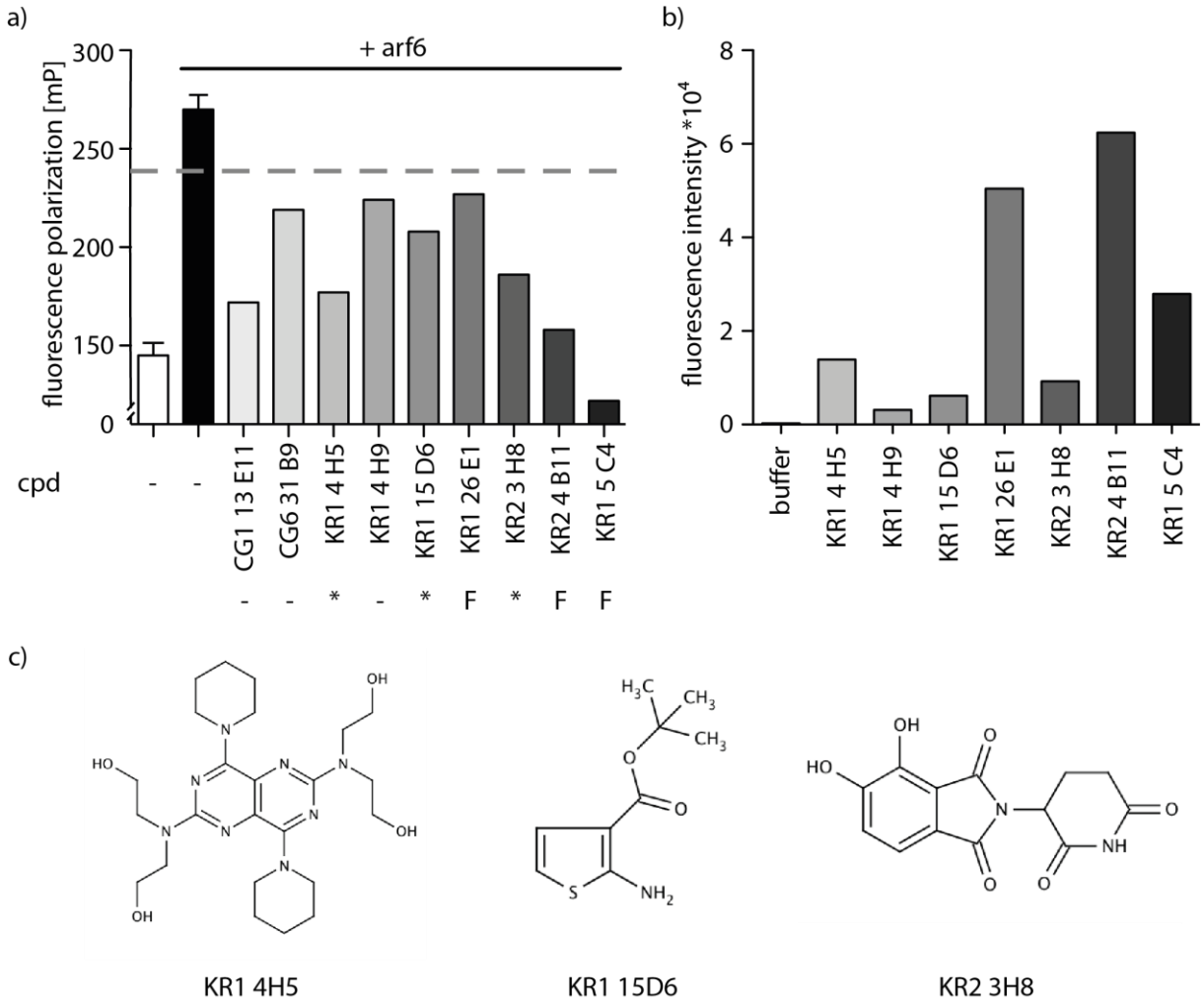

Fig. 4.10 Results of the screening for small molecule inhibitors of the Arf6 interaction with JIP4. Nine primary hits were identified in the screening (a). The dashed line indicates the threshold for primary hits (5 standard deviations below the positive control). No reproduction of the results was possible for three of the compounds ("-"). Furthermore, three different compounds exhibit a very high intrinsic fluorescence ("F") that interferes with the assay readout (b). The three remaining compounds shown in (c) were further tested.

4.1.11 Thalidomide has no effect in the FP assay employed in the screening

The hit compound KR2 3H8 (Fig. 4.10c) is structurally very similar to thalidomide (Fig. 4.11) a compound that became popular as a drug due to its tremendous effect on the development of unborn infants when consumed by the pregnant mother. Affected children exhibit defects in limb development resulting in shortened or missing arms (phocomelia or amelia). The malformations are caused by defects in angiogenesis during embryonic limb formation (*171, 172*). Migration of cells controlled by extracellular factors is extremely important for the angiogenic process (*173*) and a defect in the control of these events can lead to severe problems. Since Arf6 is involved in cell migration (*96*) inhibition of its function could provide another possible effect

explanation for the observed phenotype thalidomide and its derivatives were promising compounds for further analysis.

I tested both enantiomers of thalidomide, since they exhibit distinct biological activities. However, neither isomer changes the fluorescence polarization in the Arf6 JIP4 LZII interaction assay (Fig. 4.11). Furthermore, both forms of thalidomide have a lower autofluorescence than compound KR2 3H8. These results suggest the need for a fluorescent independent assay to confirm the initial hits.

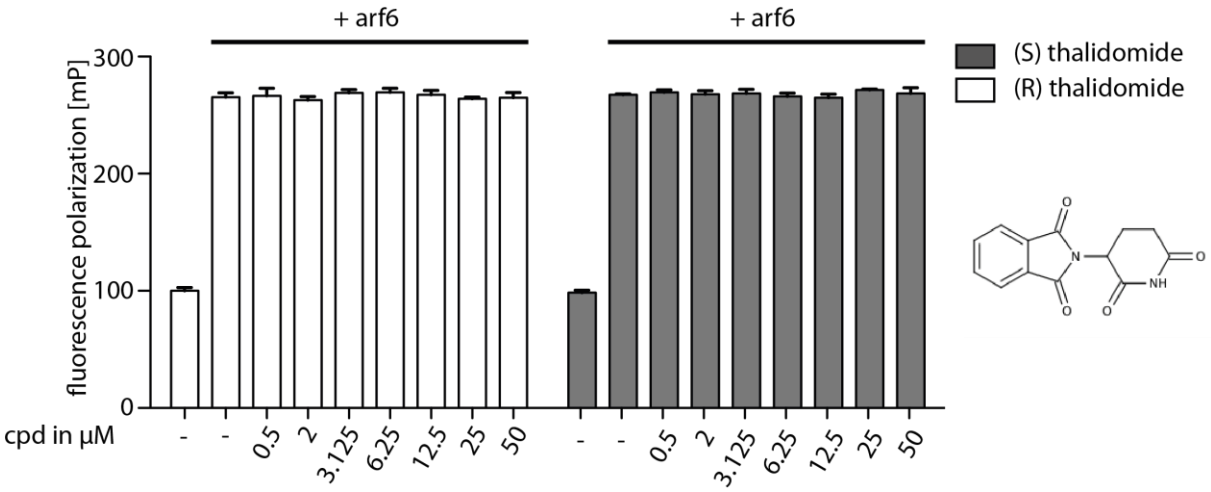

Fig. 4.11 Thalidomide has no effect on the association of Arf6 with JIP4 LZII in the fluorescence polarization assay. Up to 50µM of both enantiomers of thalidomide were incubated with fluorescein labeled JIP4 LZII in the presence of saturating concentrations of Arf6 GTP. No reduction of the FP values was observed even for the highest employed thalidomide concentration (n=3).

4.1.12 The hit compounds have no effect on binding of Arf6 to JIP4 LZII in a pulldown assay

Fluorescent assays are prone to yield false positive hits due to intrinsic fluorescent properties of the compounds used in the screening. A different assay was therefore employed to exclude false positive hits due to fluorescent artifacts. The pulldown assay described in paragraph 4.1.6 is well suited for this purpose. The initially identified small molecules had no effect on the amount of Arf6 co-precipitated with GST tagged JIP4 LZII (Fig. 4.12). The results indicate that the primary hits are false positive due to intrinsic fluorescence of the identified compounds.

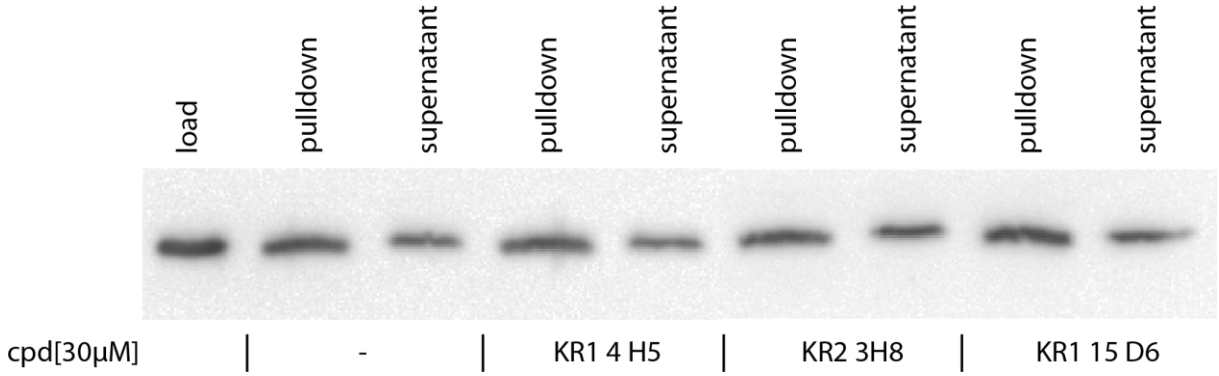

Fig. 4.12 Pulldown of Arf6 with immobilized JIP4 LZII in the presence of hit compounds. JIP4 LZII GST was immobilized to glutathione coupled agarose beads and incubated with GTP bound Arf6 in the presence of 30µM of each hit compound shown in Fig. 4.10 or DMSO ("-"). Samples were separated on a SDS PAGE gel and transferred onto a nitrocellulose membrane prior to decoration with specific antibodies against Arf6. The compounds have no influence on the amount of Arf6 co-precipitating with JIP4 LZII GST ("pulldown").

No small molecules that inhibit the interaction between Arf6 and JIP4 were identified. However, the screening assay developed is very stable, shows an excellent Z' value and is therefore easily applicable in HTS approaches. Furthermore, alternative methods are presented that can quickly exclude false positive hits or confirm the effect of identified compounds.

In addition to the established aptamer displacement screens (*158, 159*) and assays monitoring enzymatic activity (*174*) this assay provides another approach to identify inhibitory compounds for biological systems.

4.2 The influence of cytohesins on EGF receptor signaling

The recent identification of cytohesins as cytosolic factors that positively influence EGF receptor signaling revealed a novel aspect of this vital mitogenic pathway (*146*). A detailed knowledge of the mechanism behind the influence of cytohesins on the EGFR is required to understand implications of this finding in a specific physiological or pathophysiological situation, e.g. the control of normal cellular growth and malignant transformation in cancer.

The observed effect is dependent on a direct interaction between the Sec7 domain of cytohesins and the intracellular domain of the EGFR receptor and no additional factors are required to observe an effect *in vitro*(*146*). Further elucidation of the mechanism is approached by using purified components of the system. Therefore, both biochemical and structural (x-ray crystallography) methods were employed in order to dissect the interaction between the Sec7 domain of cytohesin2 (ARNO) and the intracellular domain of the EGFR.

4.2.1 Purification of proteins for crystallization and biochemical studies

Recombinant expression of the involved proteins was done in E.coli for the ARNO Sec7 constructs and in Sf9 insect cells for EGFR constructs respectively. All constructs were purified using NiNTA affinity chromatography followed by size exclusion chromatography (SEC) after cleavage of the His-tag using either TEV or Thrombin protease. Removal of the affinity tag yields recombinant proteins that closely resemble their endogenous form. This increases the chance to obtain proteins with natural conformations and therefore reduces artificial effects occurring in the *in vitro* setup.

Fig. 4.13 shows the three general steps during the purification process exemplified by the construct EGFR ICD1022 (EGFR 669-1022). The first purification step results in a crude product (Fig. 4.13a). The purity of the protein is thereafter increased after protease cleavage and gel filtration (Fig 4.13b and c). Other constructs used in this study are mentioned in their respective paragraphs and purified as described above. The employed EGFR constructs contain only the intracellular soluble part of the receptor. Both the extracellular domain and the transmembrane region are omitted to obtain a soluble protein. The resulting intracellular domain is kinase competent (*13*) and

sufficient to associate with ARNO (*146*). Additionally the receptor constructs lack the C-terminal tail (CTT), a flexible part of the protein that contains the major autophosphorylation sites. The presence of the CTT leads to difficulties observed during purification (data not shown, purification performed by Volkmar Fieberg) and is therefore avoided. However, Tyr1016 of the CTT remains in all employed constructs to investigate autophosphorylation activity.

A major difference between the EGFR constructs used in this study is the presence or absence of the juxtamembrane (JM) domain. While EGFR ICD1022 contains this n-terminal part of the protein, EGFR KC1022 (EGFR 672-1022) lacks it. These constructs can be used to investigate the binding site of ARNO at EGFR *in vitro*.

While most of the constructs were stable in solution, EGFR ICD1022 precipitates in concentration above 3 mg/ml. This poses problems for the use in crystallography when protein stability is required in highly concentrated solutions for a longer period of time (days to weeks).

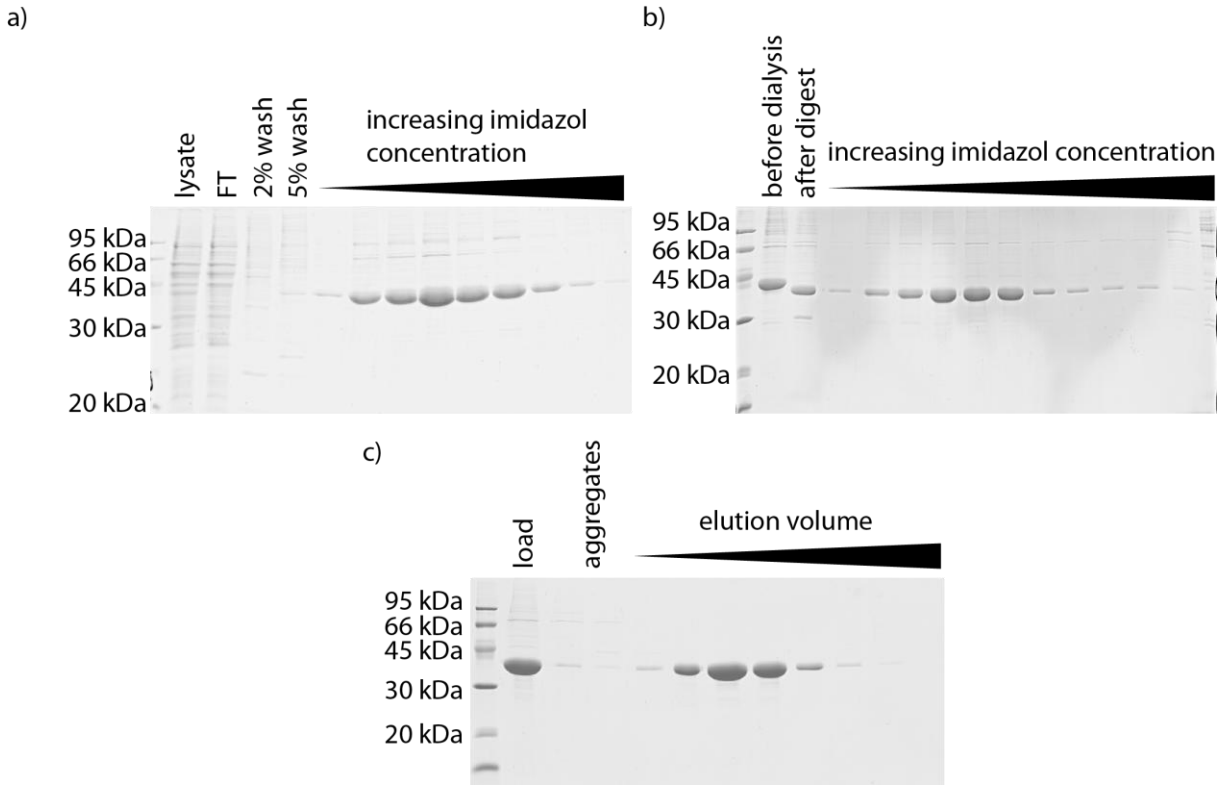

Fig. 4.13 Purification of Epidermal Growth Factor Receptor (EGFR) constructs (EGFR ICD1022). The indicated samples were taken during the purification process, separated on a 12% SDS PAGE gel and visualized with Coomassie Brilliant Blue staining. The gels show the enrichment of target protein via affinity purification using a NiNTA column (a), TEV cleavage of the affinity tag and inverse affinity purification to remove uncleaved protein and the protease (b), and a final size exclusion chromatography (SEC) step on a Superdex200 column (c). For details see Materials and Methods.

4.2.2 Dynamic light scattering (DLS) and circular dichroism (CD) spectroscopy of the purified proteins

Dynamic light scattering (DLS) can be used to evaluate the aggregation behavior of purified proteins and allows for estimation of the average particle size in a solution. Figure 4.14a shows that the ARNO Sec7 domain is not aggregating in solution and is represented by particles of approximately 30kDa (R=3nm) fitting the expected values very well ($MW_{ARNOSec7}$=24kDa). However, for EGFR ICD several more prominent populations of higher molecular weight peaks are observed (main peak at R=85nm; 30000kDa). It has to be considered that the intensity of the detected scattered light is not in a linear correlation to the absolute abundance of the corresponding particle size in a mixture. In fact particles of higher molecular weight scatter more and result in higher peaks. The first peak observed (Fig. 4.14b) corresponds to a dynamic radius of approximately 5nm (resulting in a molecular weight of 45kDa). Although it contributes only weakly to the total intensity of scattered light, the particles of the corresponding size still account for over 80% of the mixture. The EGFR ICD1022 monomer has a molecular weight of 44kDa and fits to the particle size observed in the first peak. In contrast to published data, no peak representing a dimeric EGFR is observed (*13*). Nevertheless other peaks indicate either aggregates or higher order oligomeric protein formations (Fig. 4.14b). A tendency to aggregate could explain the visible precipitation of EGFR ICD in solutions of higher concentration and would render the construct not suitable for crystallization.

Circular dichroism (CD) spectroscopy is employed to determine the secondary structure elements found in a macromolecule. For the ARNO Sec7 domain the peak at 222nm is typical for a predominant α helical structure that is expected in this protein (Fig. 4.14c). Although a second peak at around 208nm is characteristic for predominant helical elements in a protein too, the lack of this peak can be explained by the fact that the CD signal at lower wavelength is often disturbed by the buffer components and therefore not reliable. Other typical structural elements, however, exhibit a distinct spectrum with either a peak around 215nm (β sheet) or a peak below 200nm and a plateau in the higher wavelength region (random coil).

It was not possible to obtain suitable CD curves for EGFR ICD1022. Both the intensity and the shape of the curve are not of sufficient quality to deduce information about the

secondary structure of this construct (Fig. 4.14d). This finding is another indication for a heterogeneous population of macromolecules in the solution.

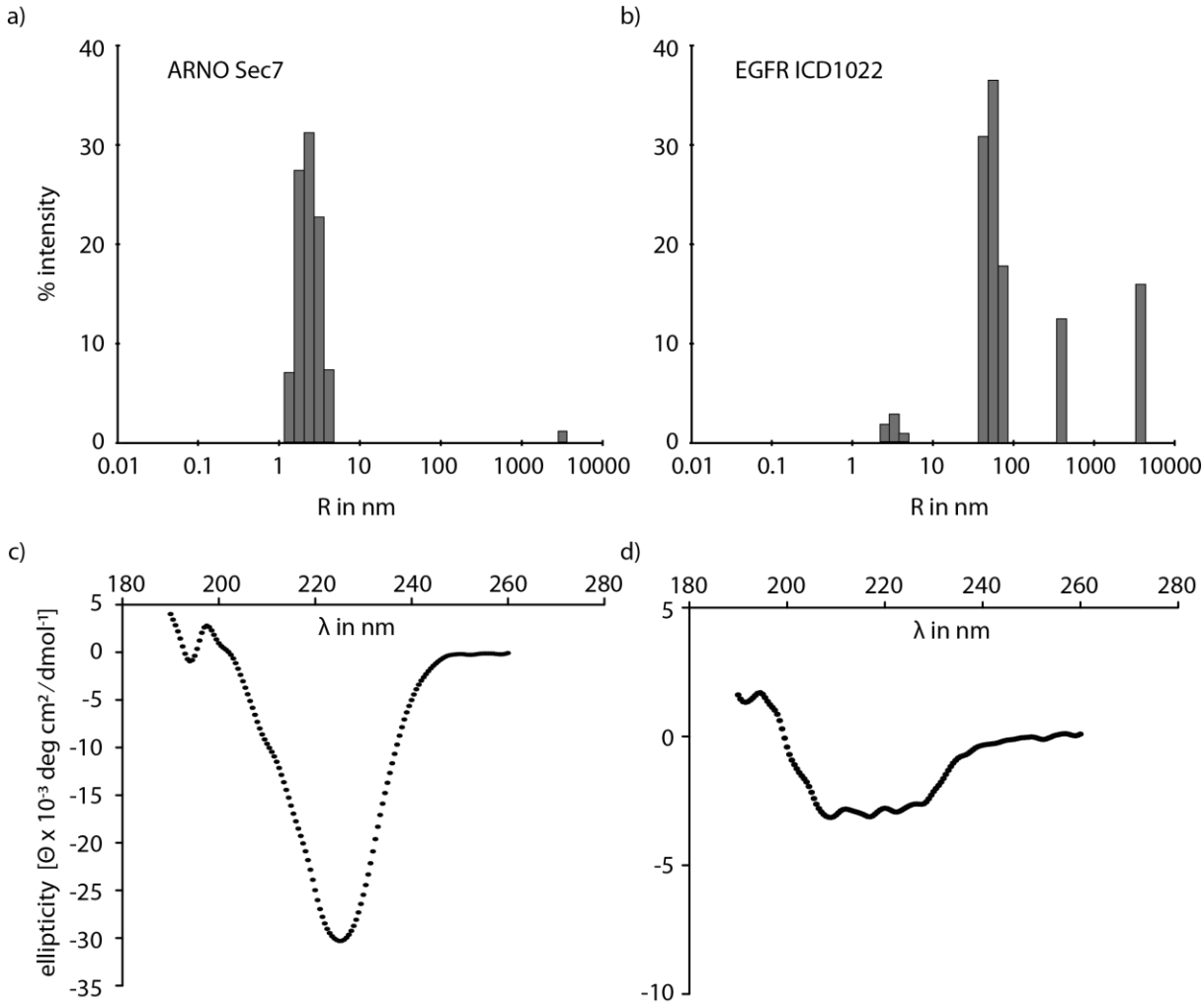

Fig. 4.14 Dynamic light scattering (DLS) and Circular dichroism (CD) measurements for ARNO Sec7 and EGFR ICD1022. DLS shows one homogenous population of particle size contributing to the detected scattered light for ARNO Sec7 (a) but several higher molecular weight particles result in light scattering in samples containing EGFR ICD1022 (b). Plotted are the relative intensities of scattered light that is calculated to be caused by particles of the corresponding size. The CD curve observed for EGFR ICD1022 shows low ellipticity values making interpretations regarding the secondary structure difficult (d). ARNO Sec7 results in a clear peak at 222nm (c). Although no complete α-helical spectrum is observed, the results argue for a secondary structure dominated by α-helices (see text).

4.2.3 Functional characterization of the purified constructs

Both ARNO and EGFR exhibit enzymatic activity that can be evaluated *in vitro* to examine functionality and therefore quality of the recombinant constructs. Using the assay described in paragraph 4.1.2 it was shown that the Sec7 domain of ARNO is able to exchange nucleotides on the GTPase Arf1 (Fig. 4.2a) proving its biological activity.

The kinase activity of EGFR constructs can be measured by evaluating the phosphorylation of tyrosine residues in the C-terminal tail (CTT) of the protein. However, the construct EGFR ICD1022 has a truncated CTT with only one phosphorylation site (Tyr1016). This results in a kinase to substrate ratio of 1:1 and is no good system to evaluate enzymatic activity. Therefore, a biological substrate of the kinase was used in molar excess to measure activity. The protein Phospholipase C γ (PLCγ) is phosphorylated at a tyrosine in its Src Homology 2 (SH2) domain. The SH2 domain was purified as a GST fusion protein and employed in a kinase assay that measured phosphorylation via Western Blot detection with phosphotyrosine specific antibodies. The EGFR construct lacking the juxtamembrane (JM) domain (EGFR KC1022) shows only weak activity with phosphorylation observed only after long incubation times (up to one hour). In contrast the presence of the JM domain in EGFR ICD1022 results in a dramatically increased activity leading to maximum phosphorylation after 5 minutes. This is in accordance with published data (*13, 15*) that highlights the importance of the JM domain for kinase activity.

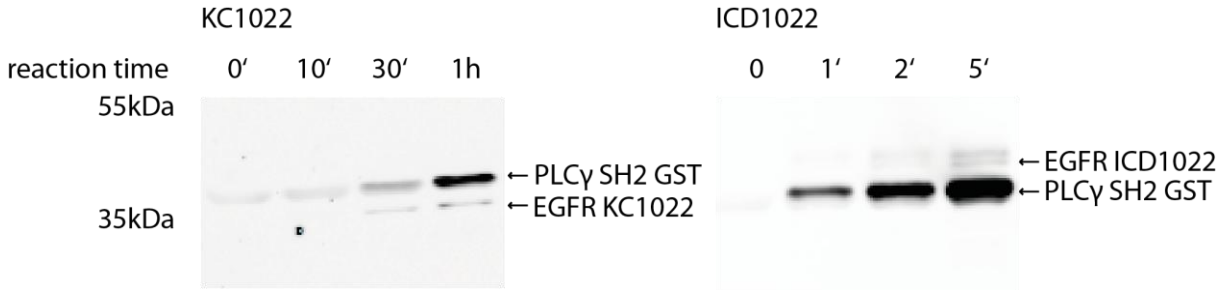

Fig. 4.15 Kinase activity assay for purified EGFR constructs. The described EGFR constructs were incubated with the SH2 domain of the natural substrate PLCγ in the presence of ATP. Samples were taken after the indicated times, separated by SDS PAGE and phosphorylation was detected using α-phospho-tyrosine antibodies (anti pY) after transfer of the proteins onto a nitrocellulose membrane. While EGFR KC1022 is only weakly able to phosphorylate the substrate, EGFR ICD1022 rapidly phosphorylates the SH2 domain of PLCγ .

4.2.4 Thermal stability of ARNO Sec7 and EGFR constructs

Purified EGFR ICD1022 is not stable when stored at high concentration and precipitates *in vitro.* To address this issue a quantitative stability assay was employed in order to optimize buffer conditions and increase stability of the protein. Using an environmentally sensitive fluorescent dye (SYPRO Orange) it is possible to follow the unfolding of proteins in solution and determine their thermal stability by monitoring the change in fluorescence in a temperature gradient (*175*). SYPRO Orange increases its fluorescent intensity upon binding to hydrophobic patches that are exposed in unfolded proteins. Plotting the fluorescence intensity against the temperature results in a curve as seen in Figure 4.16a and c. The inflection point of the curve marks the melting temperature and represents a quantitative value to measure the thermal stability of the protein. Determination of the melting temperature is facilitated by plotting the change in fluorescence at a certain temperature against the temperature (the derivative of the aforementioned curve). Here the local maximum represents the melting temperature and is easy to observe as a peak in the curve (Fig. 4.16b and d).

ARNO Sec7 and the EGFR construct lacking the JM domain (EGFR KC1022) have a similar melting temperature around 51°C. However, the presence of the JM domain in EGFR (EGFR ICD1022) results in a lower thermal stability and a melting temperature of 44°C (Fig. 4.16a and b).

In order to increase the thermal stability of EGFR ICD1022 I tested different buffer conditions and additives to evaluate their influence on the observed melting temperature. The non-hydrolysable ATP analogue Adenylyl-imidodiphosphate (AMPPNP) competes with ATP for binding to the active site of the kinase and therefore blocks catalytic activity. The addition of AMPPNP increases the thermal stability of EGFR ICD1022 resulting in melting temperature of 55°C (Fig. 4.16c and d). These findings suggest that a reduction in kinase activity leads to increased thermal stability since both EGFR KC1022 and AMPPNP blocked EGFR ICD1022 have a higher melting temperature than fully active EGFR ICD1022.

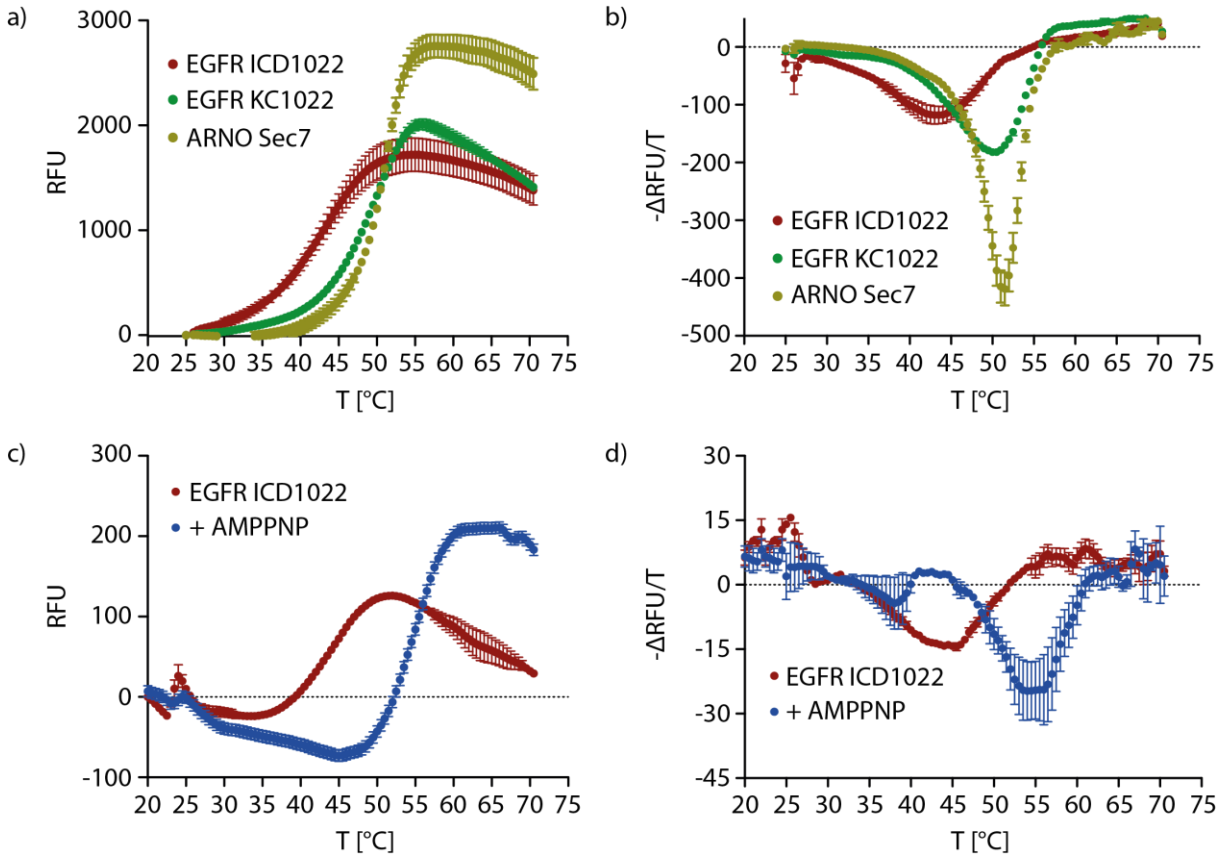

Fig. 4.16 Thermal stability of purified proteins determined by a Thermal Shift assay. The indicated proteins were slowly heated in the presence of the environmentally sensitive fluorescent dye SYPRO Orange. Unfolding of the protein results in an increase in fluorescence and unfolding at low temperature indicates instability of the tested proteins. While ARNO Sec7 and EGFR KC1022 exhibit a comparable melting temperature, EGFR ICD1022 unfolds earlier in the gradient (a and b). The addition of AMPPNP strongly enhances the thermal stability of EGFR ICD1022 indicated by the shift in melting temperature (c and d). Plotted are the fluorescent intensities against the temperature in a) and c) or the change in fluorescence intensity at a temperature against the respective temperature in b) and d) (n=3).

4.2.5 Investigation of the interaction between ARNO and the EGF receptor

Recently it was shown that the Sec7 domain of ARNO directly interacts with the intracellular part of the EGFR (*146*). To further investigate the interaction an assay based on chemical crosslinking was established. Crosslinking reagents such as Bis(sulfosuccinimidyl)suberate (BS3) are bivalent molecules that can form covalent bonds to specific reactive groups in biological macromolecules. BS3 has two succinimidyl groups that react with primary amines present at the N-terminus of a protein and at lysine side chains. If two amines on two different molecules react with the same BS3 molecule both are covalently connected and the complexes becomes visible on a denaturing polyacrylamide gel. Since the linker between the two reactive groups is short (11.4 Å for BS3) only molecules that are in close proximity to each other (e.g. due to direct interaction) can be crosslinked.

This approach allows detection of transient interactions since the binding partners are irreversibly coupled once they form a crosslinking susceptible conformation.

As a proof of principle, known interaction partners for ARNO and the EGFR intracellular domain were crosslinked. The GTPase Arf1 forms a complex with ARNO during the nucleotide exchange reaction (*176, 177*) and Mig6 (mitogen induced gene 6) is an intracellular negative regulator of EGFR activity (*87, 178*). Both proteins can be crosslinked to their respective interaction partners *in vitro* (Fig. 4.17 a and b) demonstrating the feasibility of the assay to detect molecular interactions involving the two proteins of interest.

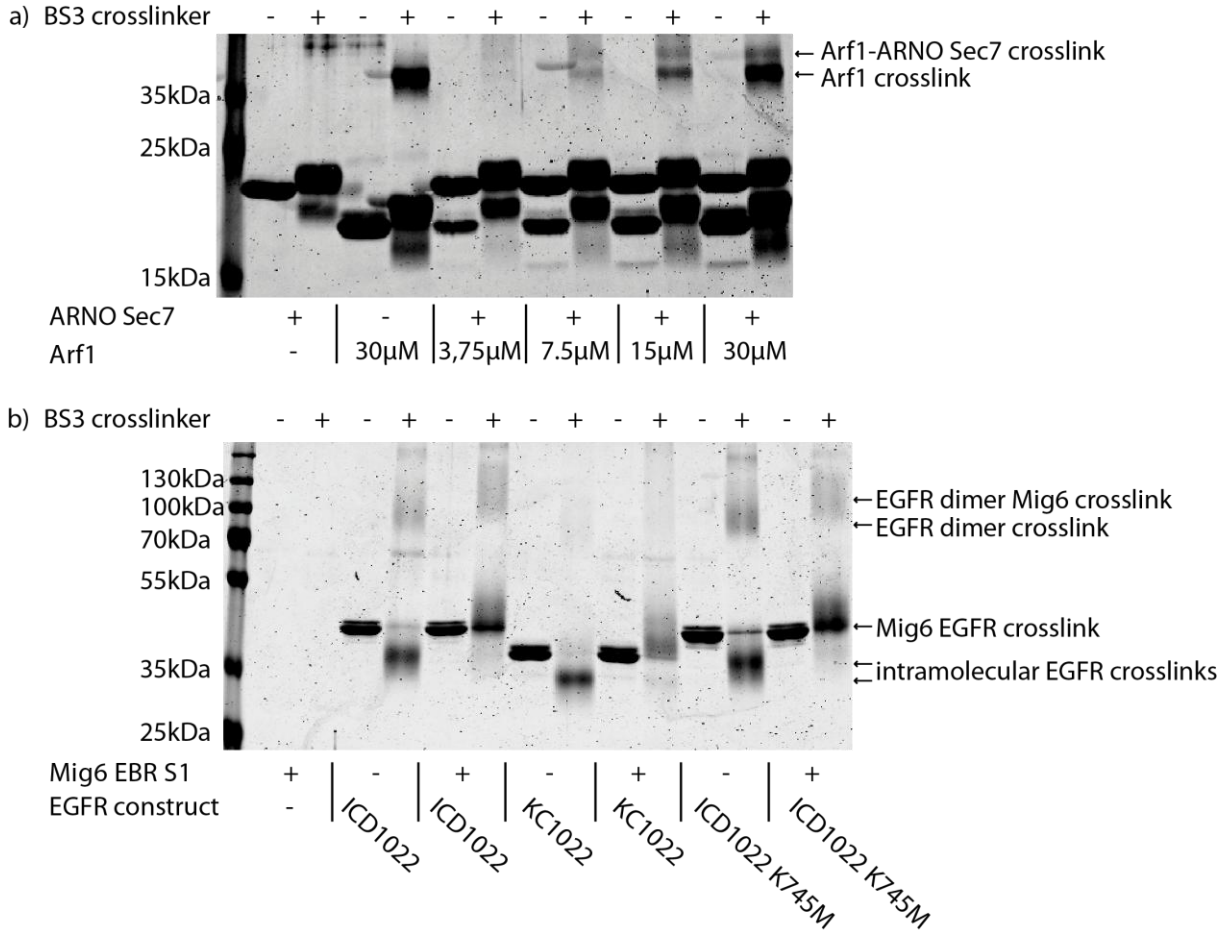

Fig. 4.17 Chemical crosslinking of ARNO Sec7 and EGFR construct with known interaction partners. The bivalent amine specific crosslinker Bis(sulfosuccinimidyl)suberate (BS3) was employed to covalently connect protein complexes. ARNO Sec7 and Arf1 (a) and different EGFR constructs with Mig6 EBR S1 (b) were incubated with BS3. Crosslinks were visualized via Coomassie Brilliant Blue stain after separation of the reaction on SDS PAGE gels. Mig6 associates with the kinase core of EGFR and therefore forms crosslinks with all EGFR constructs. EGFR K745M is a kinase inactive mutant that no longer binds the ATP essential for enzymatic activity.

4.2.6 EGFR constructs containing the juxtamembrane domain can be crosslinked to ARNO Sec7

The EGFR receptor intracellular domain is known to associate in homo-dimers and this conformation is required for activity of the kinase (*77*). The juxtamembrane (JM) domain is crucial for dimer formation (*13, 15*) and lack of this domain results in severely reduced kinase activity (Fig. 4.15). Crosslinking of EGFR ICD1022 results in an additional band at 90kDa (Fig. 4.18a, lane 4). The same band is observed for EGFR ICD1022 K745M (Fig. 4.18a, lane 6). Lysine at position 745 (position 721 in the mature EGFR) is crucial for ATP binding and therefore kinase activity (*179*). Replacing this amino acid with methionine renders the receptor catalytically inactive. However, both constructs contain the JM domain and the molecular weight of the observed band fits to an EGFR dimer. In contrast no crosslink is observed for EGFR KC1022 (Fig. 4.18a, lane 8) supporting the importance of the JM domain for dimer formation.

In addition to the 90kDa crosslink another band appears when ARNO Sec7 is added to the EGFR constructs containing the JM domain (Fig. 4.18a lane 10 and 12). With a molecular weight of 65kDa this crosslinking product fits the size of an EGFR-ARNO complex. The presence of the JM domain is required for the formation of this complex since EGFR KC1022 is not crosslinked to ARNO Sec7 (Fig. 4.18a, lane 14). These results highlight the importance of the juxtamembrane domain for the interaction of EGFR and ARNO and are supported by results from microscale thermophoresis (data not shown, experiments performed by Anton Schmitz) and fluorescence polarization experiments (Supplementary Figure 7).

Furthermore, no crosslinking is observed between EGFR ICD1022 and the GTPase Ran (Fig. 4.18b, lane 14) indicating specificity of the assay. Although the nucleotide exchange active domain of the bacterial protein DrrA forms a crosslink with EGFR ICD1022 (Fig. 4.18b, lane 12) this interaction is not dependent on the presence of the JM domain since EGFR KC1022 can also be crosslinked (Supplementary Figure 9).

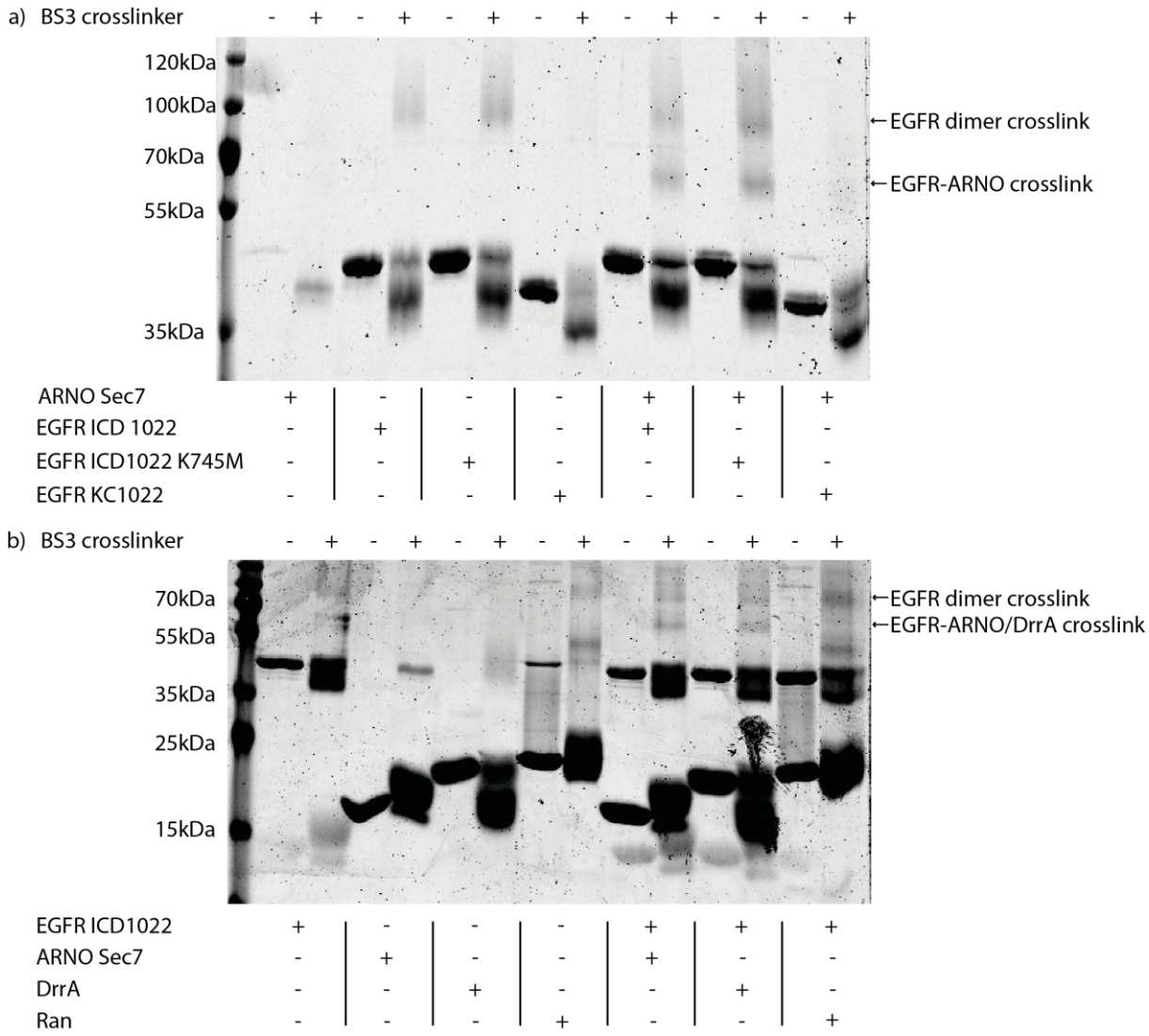

Fig. 4.18 Chemical crosslinking of EGFR with ARNO Sec7 and control proteins. The indicated proteins were incubated with BS3 and the resulting crosslinking products were separated on SDS PAGE gels and stained with Coomassie Brilliant Blue. EGFR forms a crosslink with ARNO Sec7 when the juxtamembrane (JM) domain is present in the employed construct (a). Other proteins do not crosslink to EGFR in a JM dependent manner (b and Supplementary Figure 9).

4.2.7 The EGFR juxtamembrane domain is a binding site for ARNO Sec7

The presence of the JM domain is important for crosslinking to ARNO Sec7. However, it is unclear whether the JM domain binds to ARNO or dimerization of EGFR molecules induced by the presence of the JM domain is required for binding and the formation of crosslinks. The EGFR JM domain was solid phase synthesized and contained both the JM-A and JM-B region of the domain (*13*). Two N-terminal tryptophans were added to the peptide to allow concentration determination in solution using absorbance at 280nm.

Crosslinking of the EGFR JM domain in the presence of ARNO Sec7 results in an additional band at approximately 27kDa (Fig. 4.19a, lane 10). This indicates the

formation of an ARNO Sec7 complex with EGFR JM. Both a scrambled version of the JM domain peptide and the unrelated JM domain of the insulin receptor (IR) show no crosslinks when incubated with ARNO Sec7 (Fig. 4.19a, lane 12 and 14).

The two control proteins Ran and DrrA form no crosslink with ARNO Sec7 (Fig. 4.19b) supporting the hypothesis that the JM domain of EGFR is a specific binding site for ARNO.

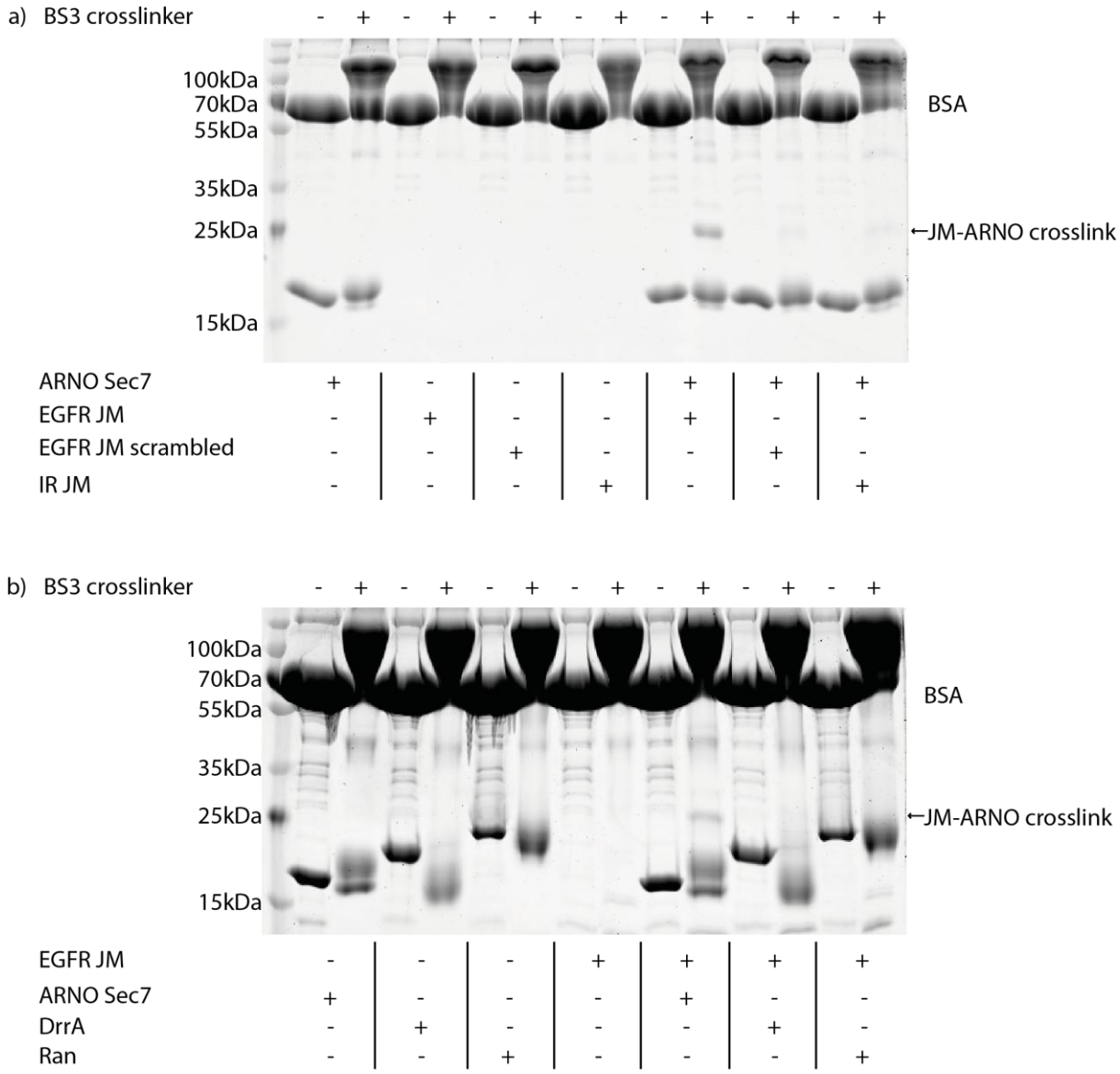

Fig. 4.19 Chemical crosslinking of the juxtamembrane domain of EGFR with ARNO Sec7. The indicated constructs were crosslinked using BS3, separated on a SDS PAGE gel and stained with Coomassie Brilliant Blue. ARNO Sec7 crosslinks only to the JM domain of EGFR but not to a scrambled EGFR JM construct or the JM domain of the insulin receptor (IR) (a). Furthermore, EGFR JM forms no crosslinks with DrrA or Ran (b).

4.2.8 Crosslinking with lysine mutants of ARNO Sec7

Chemical crosslinking with amine reactive groups depends on the presence of lysine residues in the interacting proteins. Therefore, mutation of lysines close to the interaction site would reduce crosslinking efficiency and vice versa reduced crosslinking efficiency indicates that a lysine residue is close to the interaction site.

The EGFR JM domain has only two potential crosslinking sites, the N-terminus and one lysine very close to the N-terminus (8th amino acids in the peptide). The close proximity suggests that both amines are redundantly involved in crosslinking. Indeed although the N-terminus is not required for crosslinking, its covalent modification results in a reduction of crosslinking efficiency between ARNO Sec7 and EGFR JM (Suppl. Figure 5).

In contrast the ARNO Sec7 domain contains 11 lysine residues making the identification of crosslinking relevant residues more complex. Constructs containing mutations of single lysines or groups of lysines located in certain parts of the protein were employed in order to investigate crosslinking behavior. The amino acids were replaced by arginines to minimize effects caused by a change in surface charge in the mutants.

Figure 4.20 shows the division of ARNO Sec7 in three parts in which lysines are mutated to obtain the constructs “N” (K->R 57,64,70,71,77,78), “M” (K->R 102,108,159) and “C” (K->R 207,244). In the following paragraph these mutants are employed to narrow down the potential binding site of ARNO Sec7 for EGFR JM.

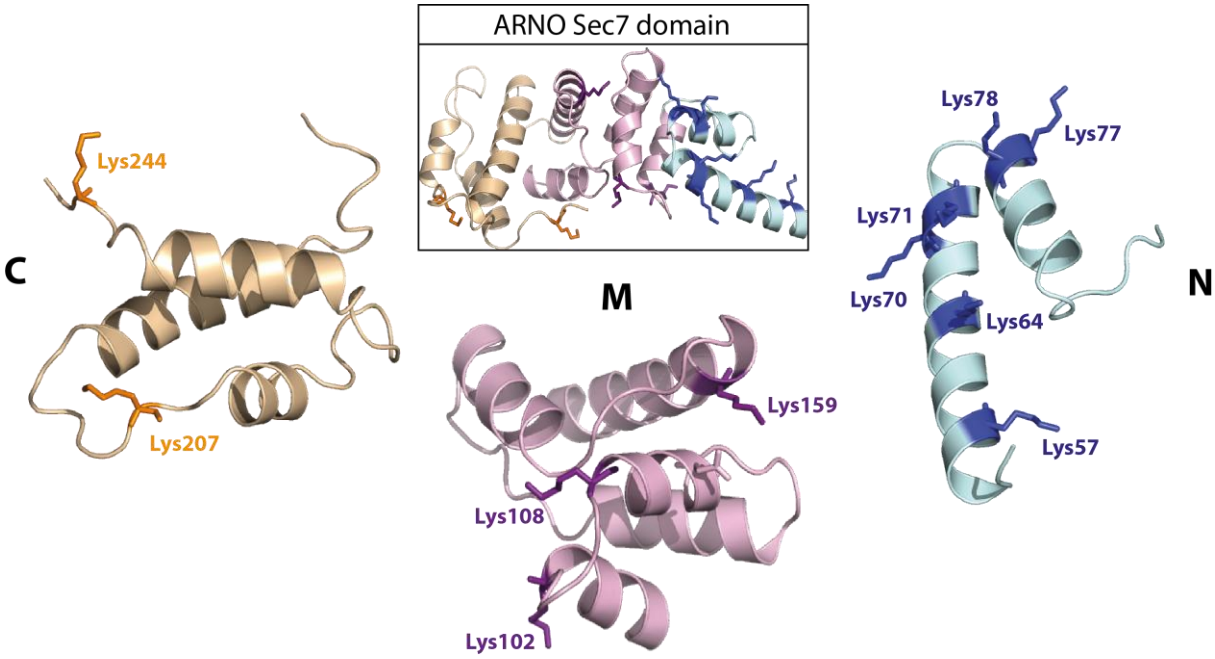

Fig. 4.20 Structural representation of the ARNO Sec7 lysine residues mutated for crosslinking analysis.

4.2.9 The C-terminal part of ARNO Sec7 is important for crosslinking

Mutation of the lysine residues at position 207 and 244 in ARNO Sec7 (construct "C") results in a decrease in crosslinking both with the EGFR intracellular domain (EGFR ICD1022) and with the JM domain peptide (Fig. 4.21a and b, compare lanes 4 and 6). In contrast mutation of all lysines in the N-terminal and the middle part of ARNO Sec7 (construct "NM") has no influence on crosslinking efficiency with EGFR ICD1022 (Fig. 4.21a, lane 8) indicating that lysines in the C-terminal part are required for efficient crosslinking. However, crosslinking of ARNO Sec7 "NM" to EGFR JM provides contradictory results since reduced crosslinks are observed (Fig. 4.21b, lane 8; see discussion). To substantiate the importance of the C-terminus for crosslinking the ARNO Sec7 constructs "M" and "MC" were employed (Fig. 4.22a and b). While mutation of lysine residues in the middle part ("M") of the protein has no influence on crosslinking with EGFR ICD1022 and EGFR JM, additional mutation of lysines 207 and 244 in the C-terminal part ("MC") results in significantly decreased efficiency (Fig. 4.22a and b, lane 12 and 14). This establishes one or both of the C-terminal lysines of ARNO Sec7 as important for crosslinking to EGFR.

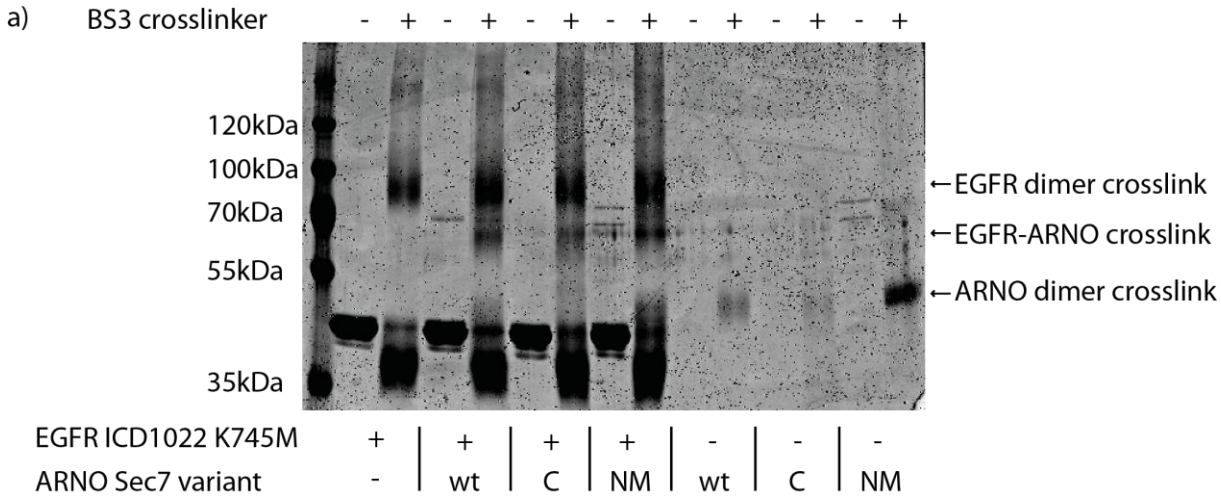

Fig. 4.21 (a) Lysines in the C-terminal region of ARNO Sec7 are important for chemical crosslinking with EGFR ICD1022. The indicated ARNO Sec7 mutants were crosslinked to EGFR ICD1022 using BS3, separated on a SDS PAGE gel and stained with Coomassie Brilliant Blue. The mutation K745M in EGFR ICD1022 has no influence on crosslinking but results in a stabilized protein. A reduction in crosslinking efficiency is observed when Lys207 and Lys244 are replaced by arginines ("C") but not when all other lysines are mutated in ARNO Sec7 ("NM", see Figure 4.20).

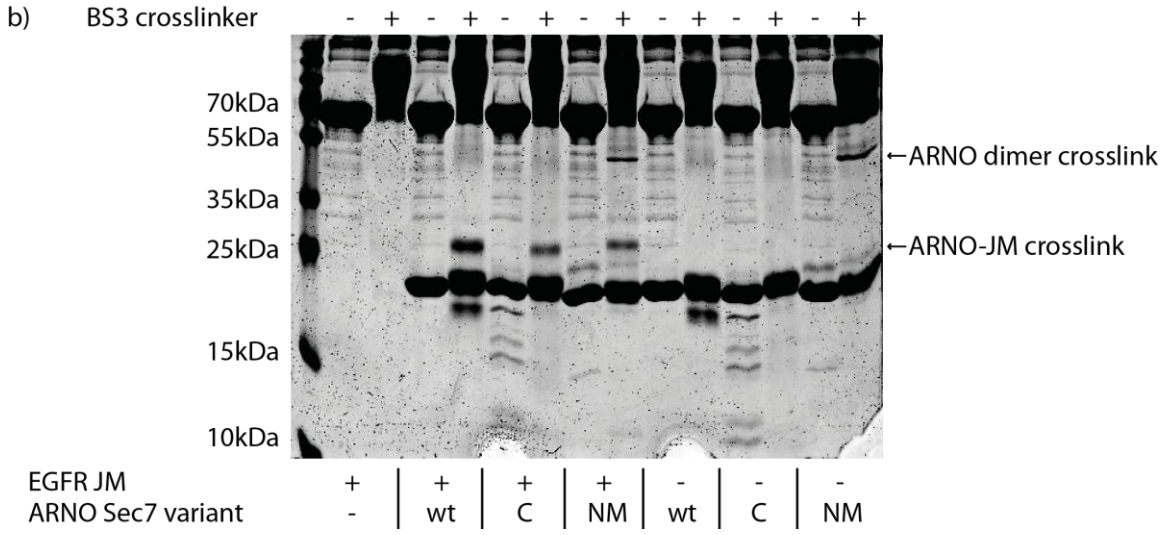

Fig. 4.21 (b) Lysines in the C-terminal region of ARNO Sec7 are important for chemical crosslinking with EGFR JM. The indicated ARNO Sec7 mutants were crosslinked to EGFR JM using BS3, separated on a SDS PAGE gel and stained with Coomassie Brilliant Blue. A reduction in crosslinking efficiency is observed when Lys207 and Lys244 are replaced by arginines ("C") and when all other lysines are mutated ("NM"). However, this also results in increased ARNO dimer crosslink formation.

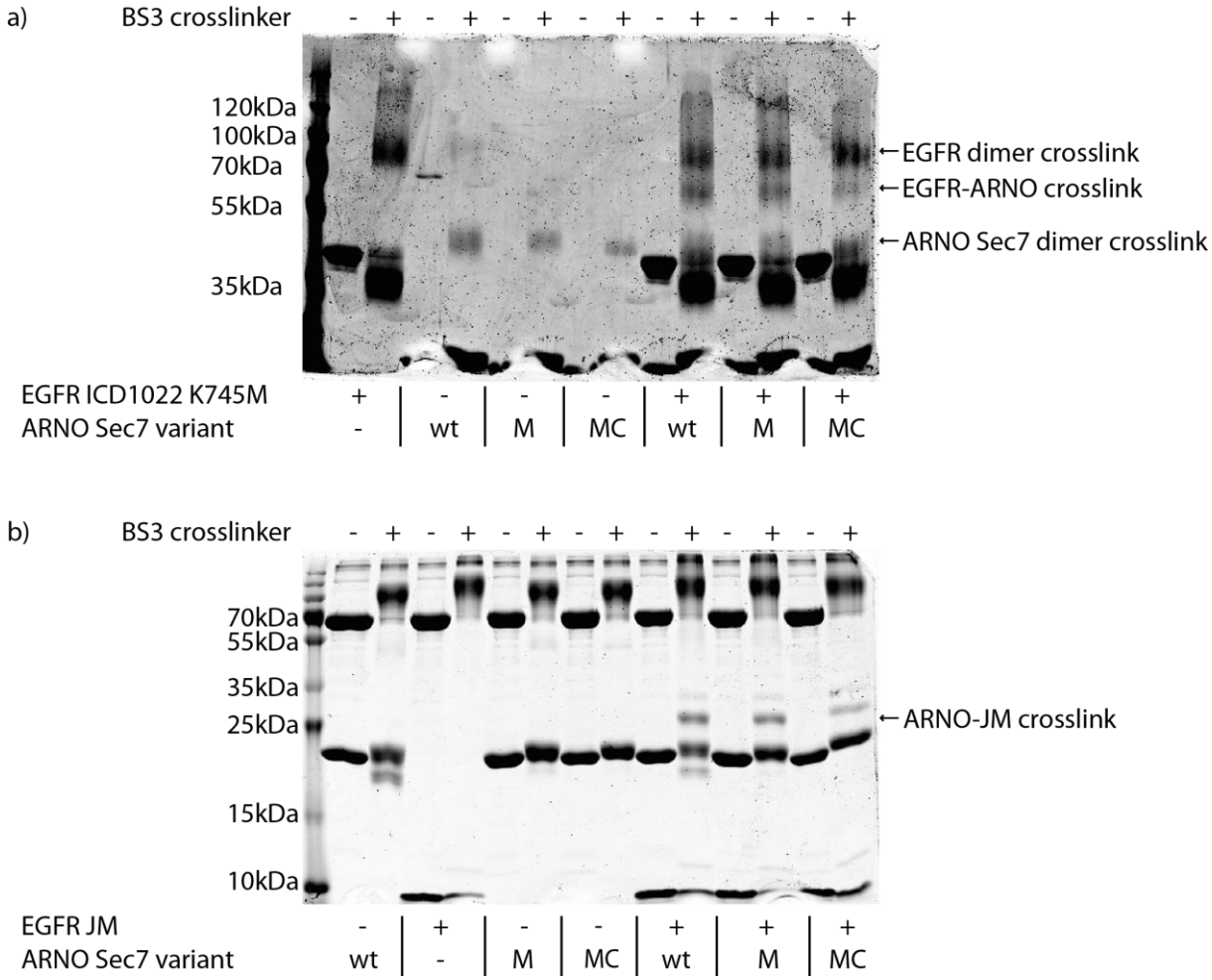

Fig. 4.22Lysines in the C-terminal region of ARNO Sec7 are important for chemical crosslinking with EGFR constructs. ARNO Sec7 mutants were crosslinked to EGFR ICD1022 (a) or EGFR JM (b) with BS3. The reactions were separated on SDS PAGE gels and stained with Coomassie Brilliant Blue. Mutation of lysines in the C-terminal part of ARNO Sec7 severely reduces crosslinking efficiency both to EGFR ICD1022 (a) and EGFR JM (b).

4.2.10 Lysine 244 is a major crosslinking site for EGFR at ARNO Sec7

Knowing that the C-terminal part of the ARNO Sec7 domain is critical for efficient crosslinking the question arises if both or actually just one lysine is responsible for the observed effect. ARNO Sec7 K244R shows reduced crosslinks both with EGFR ICD1022 and EGFR JM (Fig. 4.23a and b, lane 8). The reduction is comparable to the effect observed for double mutant at position 207 and 244 ("C", Fig. 4.23a and b, lane 6). Furthermore, replacing only lysine 207 by arginine has no effect on crosslinking (Fig. 4.24a and b, compare lane 4 and 10). These results establish lysine at position 244 in ARNO as an important determinant for crosslinking to EGFR constructs and allow for speculations about the binding site (see discussion).

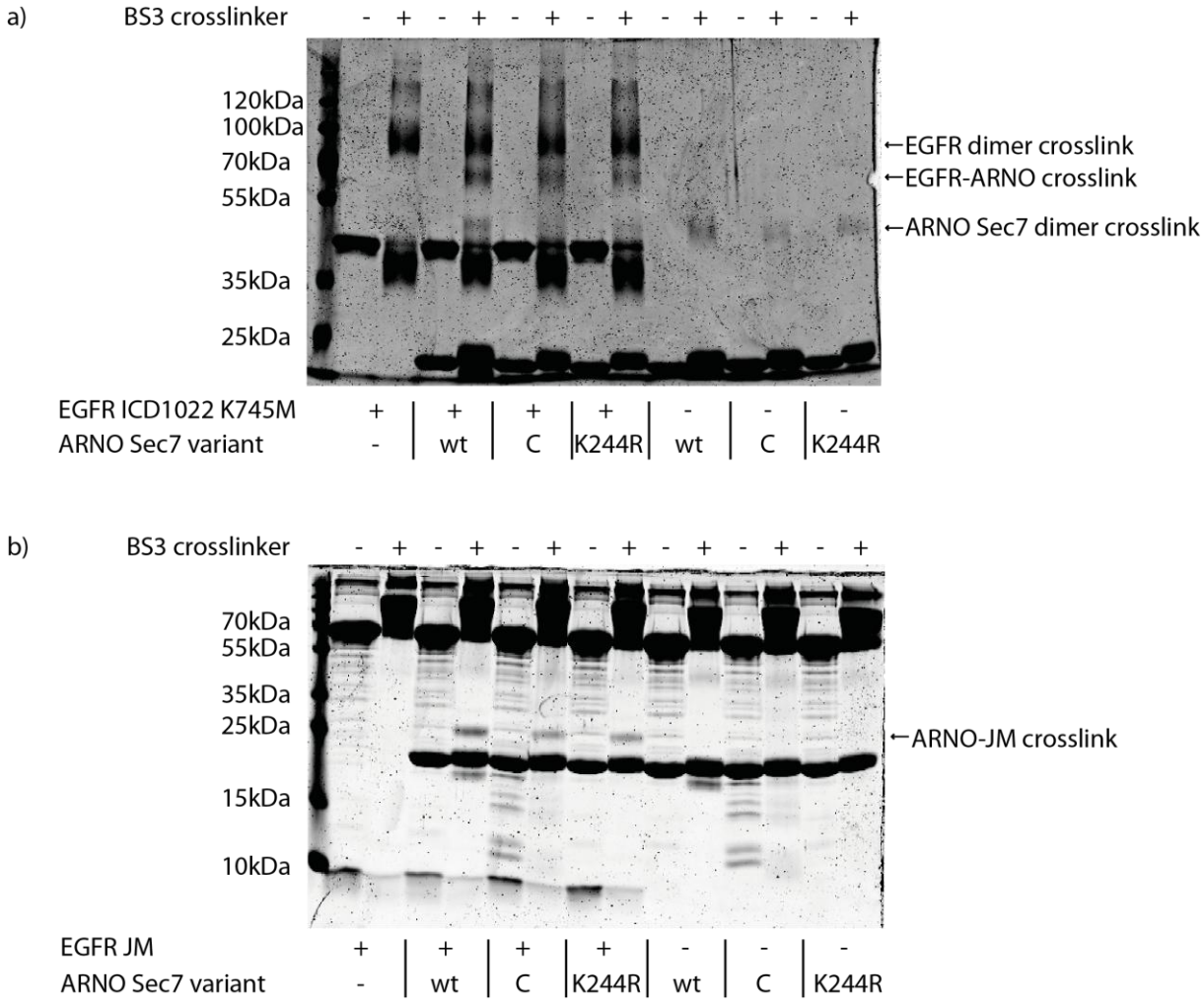

Fig. 4.23 Chemical crosslinking of EGFR constructs to ARNO Sec7 is reduced in the absence of Lys244. The indicated ARNO Sec7 constructs were crosslinked to EGFR constructs with BS3, separated on SDS PAGE gels and stained with Coomassie Brilliant Blue. Replacing Lys244 in ARNO Sec7 with arginine has the most pronounced effect on crosslinking to EGFR ICD1022 (a) and EGFR JM (b). No other lysine mutation shows comparable effects on crosslinking.

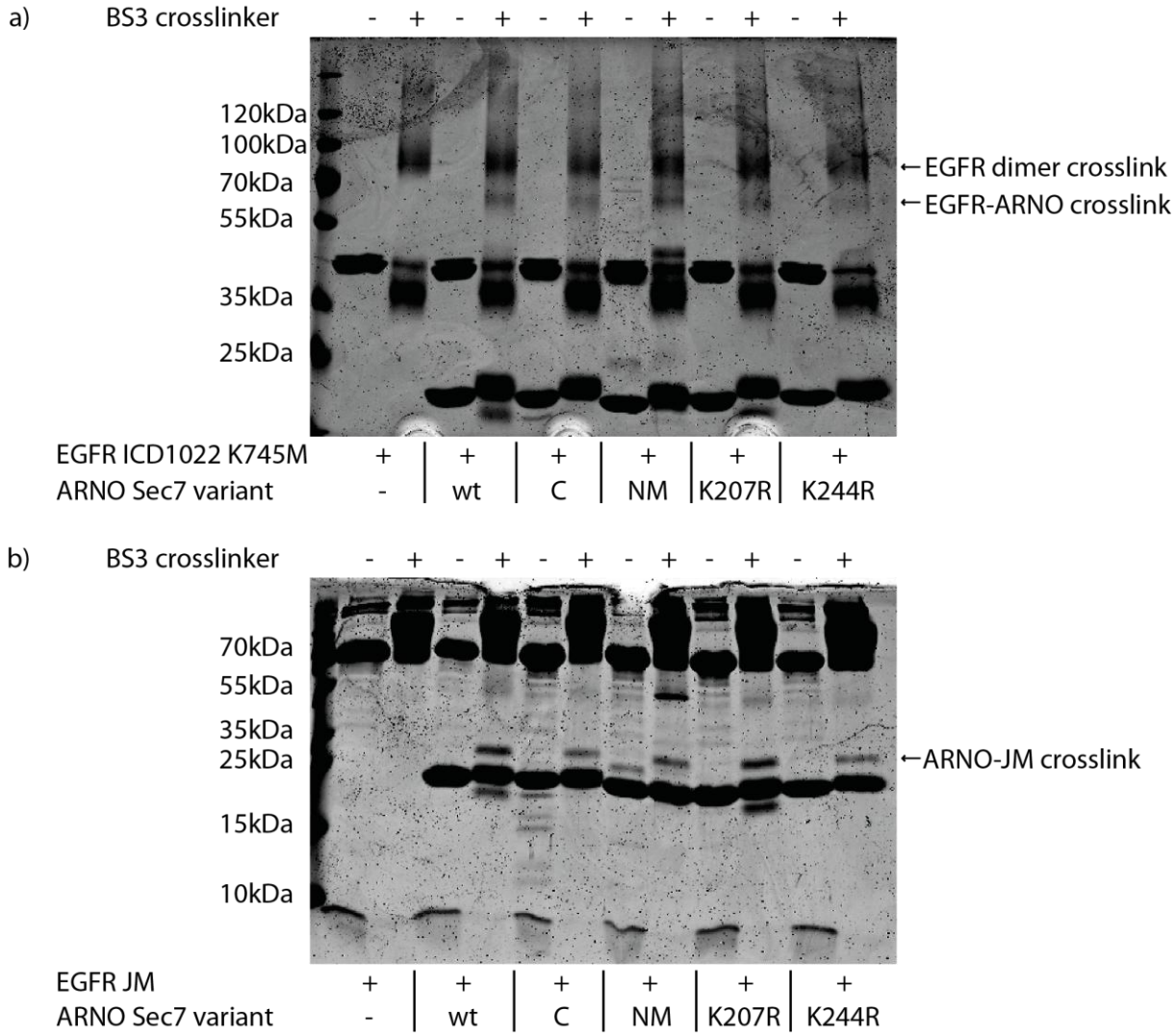

Fig. 4.24 Summary of crosslinking results obtained with ARNO Sec7 lysine mutants. The indicated ARNO Sec7 constructs were crosslinked to EGFR constructs with BS3, separated on SDS PAGE gels and stained with Coomassie Brilliant Blue. Only mutating Lys244 in ARNO Sec7 shows a consistent effect on crosslinking both to EGFR ICD1022 (a) and EGFR JM (b).

4.2.11 *In vitro* nucleotide exchange on Arf1 catalyzed by ARNO is inhibited in the presence of EGFR JM

The interaction between EGFR and ARNO raises the question whether it has an influence on other functions of ARNO. Therefore, the EGFR JM peptide was added to the nucleotide exchange reaction monitoring ARNO activity on Arf1. Indeed the exchange rate is reduced in the presence of EGFR JM in a dose dependent manner (Fig. 4.25) suggesting a functional effect of EGFR binding to ARNO.

The presented data strongly argue for a direct and specific interaction between ARNO and EGFR with functional consequences for both proteins (*146*). However, a detailed picture of this interaction is not possible to deduce from the results. Therefore, a different method is required to obtain more information on a molecular level.

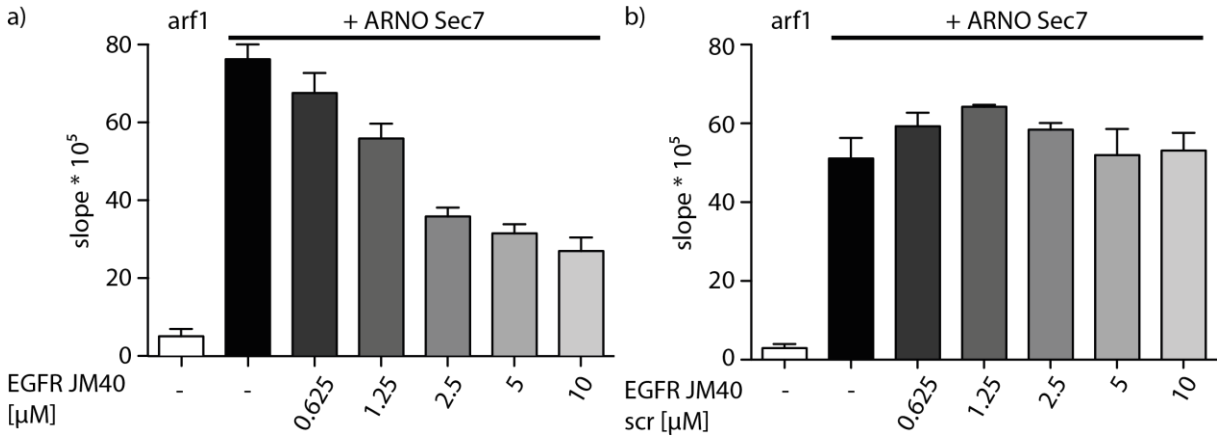

Fig. 4.25 ARNO catalyzed nucleotide exchange on Arf1 in the presence of the JM domain of EGFR. Arf1 preloaded with GDP was incubated with ARNO Sec7 and excess GTP in the presence of increasing concentrations of EGFR JM (a) or a scrambled version of the domain (b, EGFR JM scr). Error bars represent SEM (n=4 for EGFR JM; n=2 for EGFR JM scr).

4.3 Investigation of the ARNO EGFR interaction using x-ray crystallography

Obtaining detailed information about the structure of the complex between ARNO and EGFR can provide insights into the mechanism of ARNO dependant receptor activation. Protein crystallization and structure determination using x-ray diffraction provide an elegant method to generate structural data with very high atomic resolution.

4.3.1 Analytical gel filtration analysis of the ARNO EGFR complex

The formation of crystals suitable for x-ray diffraction analysis requires a pure and homogenous solution of the molecule of interest. For a co-crystal this involves the purification of a stable complex and the exclusion of single proteins from the crystal solution. Due to the higher molecular weight of the resulting complex, separation from monomers can be achieved via size exclusion chromatography (SEC).

In order to evaluate the suitability of SEC for this purpose ARNO Sec7 and Arf1 were mixed and applied to a SEC column. The resulting elution profile shows a peak at 31 min while the single proteins elute after 34 min (ARNO Sec7) or 36 min (Arf1) respectively (Fig. 4.26b). The earlier elution indicates a larger complex with a molecular weight of approximately 44kDa (Fig. 4.26a). The size of the complex fits to a 1:1 complex between ARNO Sec7 and Arf1. Additionally both proteins elute after the same time as seen by SDS PAGE analysis (Fig. 4.26b).

In contrast both EGFR ICD1022 and a mixture of the receptor with ARNO Sec7 result in the same elution profile with a peak after 33 min tailing towards later elution times (Fig 4.26c). The close proximity of the monomer peaks make it difficult to evaluate complex formation by SDS PAGE since both proteins elute at approximately the same time and co-elution is no indication for complex formation. The juxtamembrane (JM) domain of EGFR is sufficient to interact with ARNO Sec7 (paragraph 4..2.7) and its small size makes it separable from the exchange factor via SEC. Hence, co-elution of ARNO Sec7 and EGFR JM in an analytical gel filtration experiment would indicate complex formation. However, the JM domain interacts with the matrix of the SEC columns making interpretation of these results difficult (Supplementary Figure 8). These results suggest that complex purification via SEC is not possible prior to crystallization.

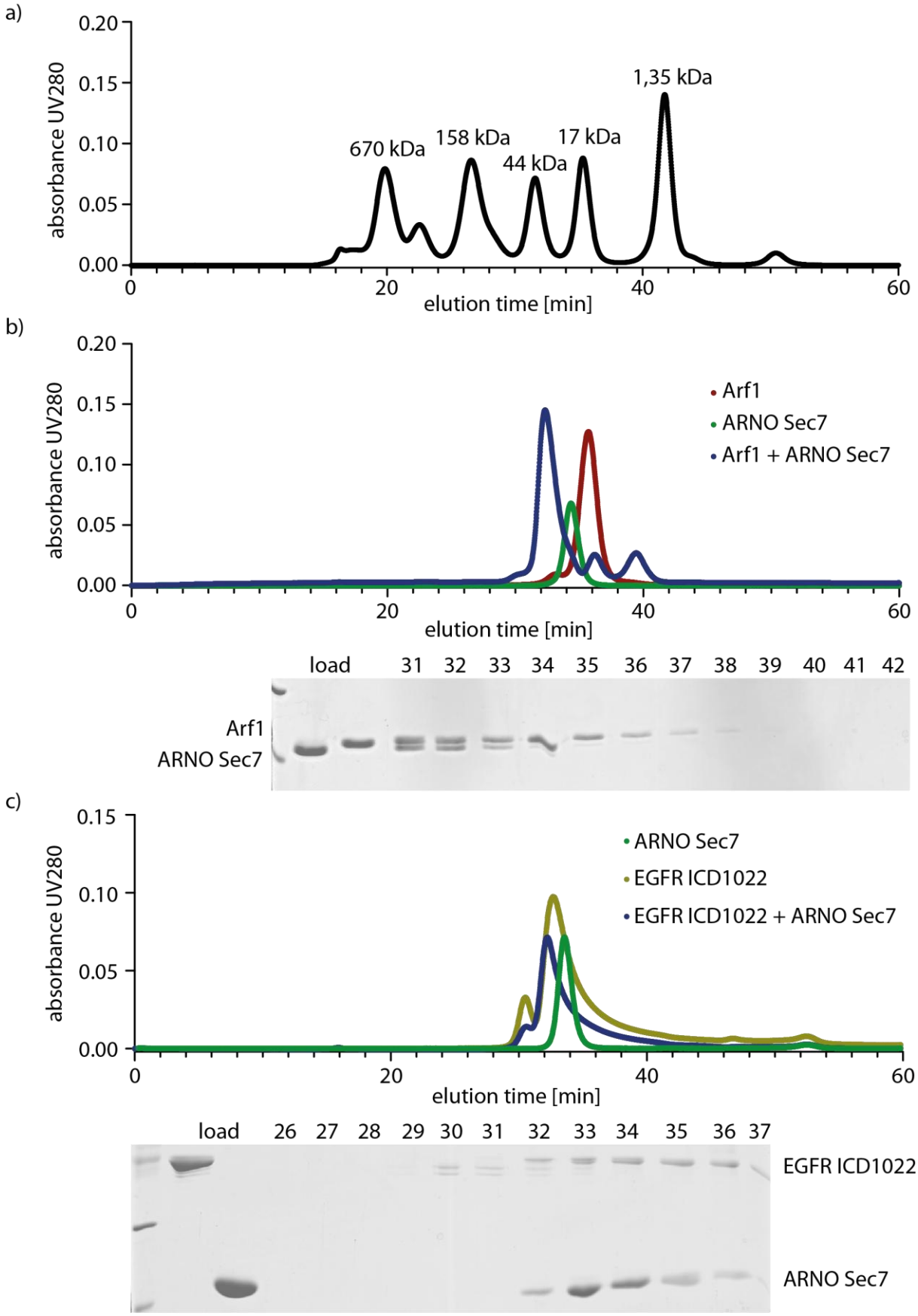

Fig. 4.26 Analytical size exclusion chromatography (SEC) of ARNO Sec7 complexes.ARNO Sec7 was incubated with Arf1 (b) or EGFR ICD1022 (c) and separated on a Superdex 200 column. Peak fractions were collected and analyzed on SDS PAGE gels using Coomassie Brilliant Blue staining. A molecular weight standard was employed to evaluate the size of the eluting proteins/complexes (a).

4.3.2 Crystallization trials for ARNO Sec7 in complex with the juxtamembrane domain of EGFR

Biochemical data suggests that the interaction between EGFR and ARNO involves and is dependant on the juxtamembrane (JM) domain of EGFR (paragraph 4.2.6 and 4..2.7). Furthermore, an intracellular EGFR construct containing the JM domain was not stable after purification (EGFR ICD1022, paragraph 4.2.4). Therefore, the initial crystallization screens were performed using a mixture of ARNO Sec7 with the JM domain of EGFR.

Two ARNO Sec7 constructs were used that differ at their N-terminus. While ARNO Sec7 52-256 is also used in other crystallization studies (*130, 180*), the shorter construct ARNO Sec7 61-246 represents the minimal functional domain as described in the studies. Both constructs are active in the exchange of nucleotides on Arf1 (data not shown) and crosslink to EGFR JM (Supplementary Figure 10). The JM peptide was used in molar excess to ensure saturation of ARNO Sec7 with the binding partner (from 2x to 20x molar excess).

For the shorter construct only one condition yielded crystals (Fig 4.27a) that could be reproduced and were suitable for further analysis. However, no x-ray diffraction was obtained from the crystals rendering them useless for the purpose of structure determination.

The longer ARNO Sec7 constructs could be crystallized in the presence of EGFR JM under many different conditions (e.g. Fig 4.27b and c). Unexpectedly all crystals analyzed from that screening did not show an additional electron density apart from the ARNO Sec7 structure indicating that either EGFR JM is not present in the crystal or it is too flexible to result in a clear diffraction pattern.

These results show two potential problems that need to be addressed to optimize crystallization efforts: the complex between ARNO Sec7 and EGFR JM is either not stable enough to allow co-crystallization or the tendency of ARNO Sec7 to crystallize alone renders this effort difficult.

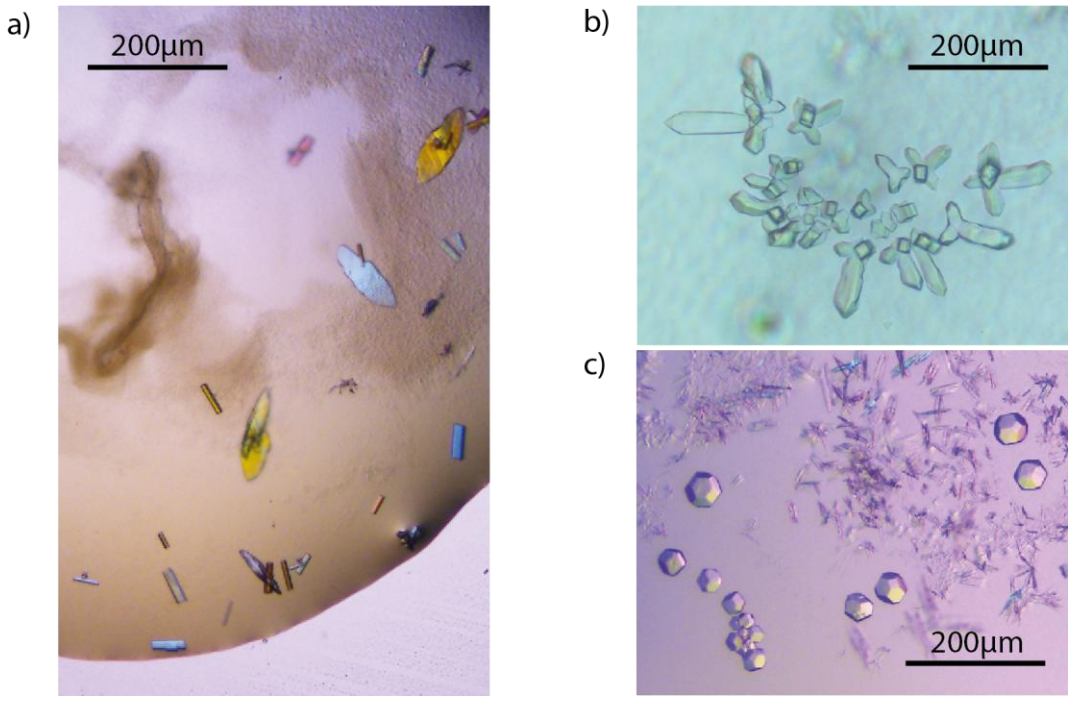

Fig. 4.27 Crystals obtained with ARNO Sec7 in the presence of EGFR JM. ARNO Sec7 61-246 was crystallized in the presence of 20x molar excess EGFR JM. Crystals appeared after 3 days (100mM NaOAc pH 4.6, 20mM CaCl2, 30% 2-methyl pentanediol) but show no diffraction (a). ARNO Sec7 52-256 crystallized in the presence of 2x excess EGFR JM under several conditions (b: 100mM MES pH 6, 20% PEG6000; c: 200mM di-ammonium-tartrate, 20% PEG3350).

4.3.3 N-terminal truncated ARNO Sec7 constructs show less efficient crystallization

ARNO Sec7 61-246 could not form crystals under many different buffer conditions while the longer construct ARNO Sec7 52-256 crystallizes readily (paragraph 4.3.2). Reducing the chances of ARNO Sec7 to crystallize alone could increase the chances to obtain a crystal of the desired complex. Therefore, several intermediate N-terminal truncations of the longer construct were designed to test their crystallization behavior. 127 buffer conditions were employed to evaluate six different ARNO Sec7 constructs.

Indeed a gradual decrease in the number of different conditions allowing for crystal growth is observed with reduction in N-terminal length (Fig. 4.28a). However, the crystals that do grow become visible after similar incubation times indicating that the kinetic of crystal growth is not impaired by N-terminal truncations.

Using the shortest construct that still crystallized (ARNO Sec7 59-256) another screen in the presence of 2x molar excess EGFR JM was performed. ARNO Sec7 in the absence of EGFR JM was crystallized in parallel under all tested conditions. From 1152 tested buffer conditions, 166 supported ARNO Sec7 crystal growth and 51 conditions allowed for crystal growth in the presence of EGFR JM (Fig. 4.28b). However, 50 of those conditions

did not distinguish between the absence and presence of EGFR JM (Fig. 4.28b). Nevertheless the found crystals were reproduced if possible and analyzed using x-ray diffraction (two out of 6 suitable crystals are shown in Fig. 4.28c).

None of the analyzed crystals yielded a structure with an additional electron density that represents the EGFR JM domain. These results indicate that a simple mixture of the two proteins might not be suitable to obtain the desired co-crystals.

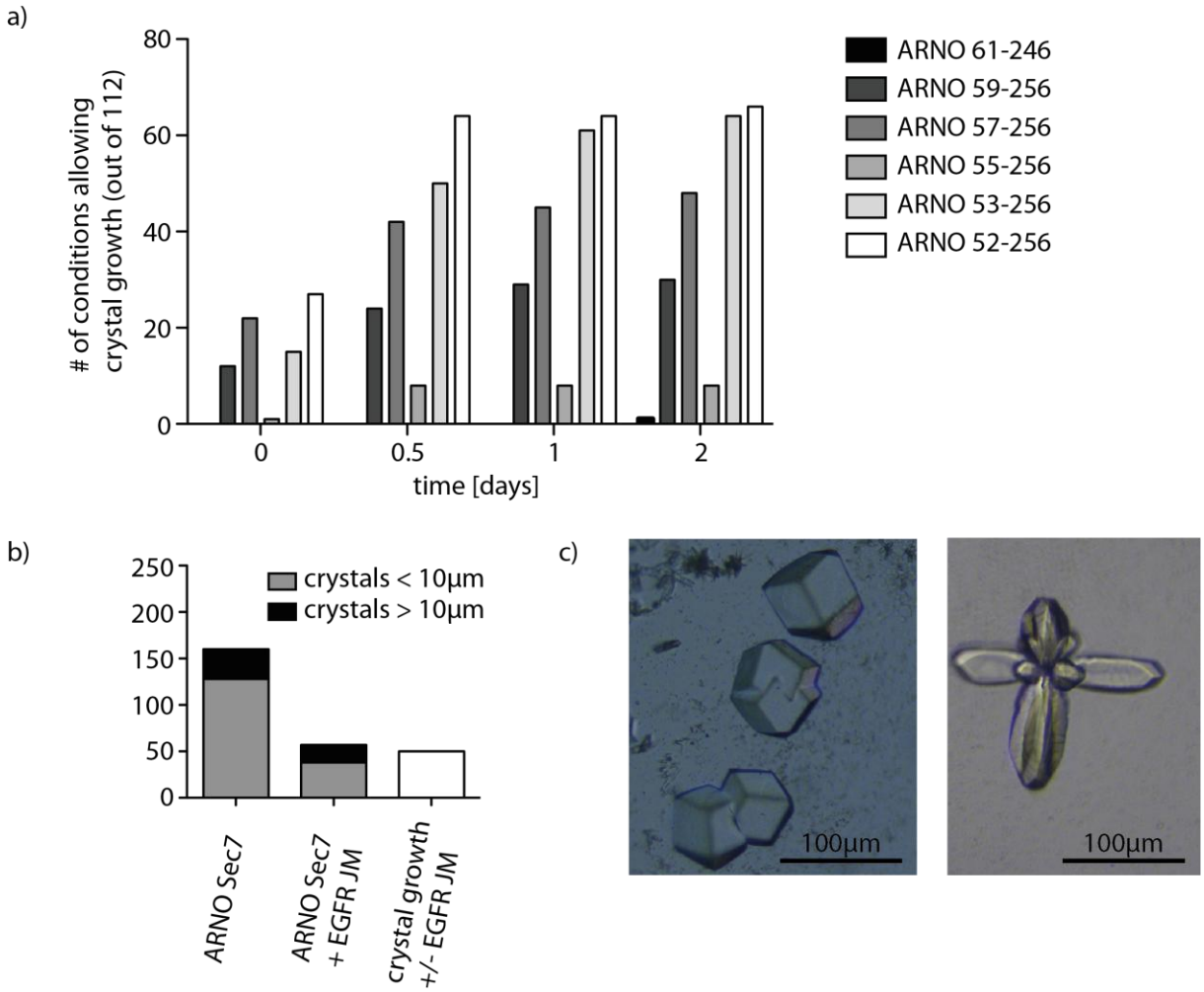

Fig. 4.28 N-terminal truncation of ARNO Sec7 results in less efficient crystallization. ARNO Sec7 52-256 was successively shortened at the N-terminus in two amino acid steps. 112 different buffer conditions that allowed for crystal growth of the longest construct in many cases were used to study the crystallization behavior. Truncation of the N-terminus results in decreased number of conditions that support crystal growth (a). The constructARNO 55-256 precipitated readily and therefore did not yield many crystals. The construct ARNO 59-256 was employed in a screen with 2x excess EGFR JM and yielded several crystals that were dependent on the presence of EGFR JM (in the initial screen) and sufficiently large to analyze (b). Two different crystals are shown as an example that could be reproduced after the initial crystallization screen (c: 180mM tri-ammonium citrate, 20% PEG3350 [left] and 100mM MES pH 6, 200mM CaAcetate, 20% PEG8000 [right]).

4.3.4 Genetic fusion of ARNO Sec7 to the EGFR JM domain

Proteins that are not able to form a complex in solution that is stable enough to promote crystal growth can be expressed as a single fusion protein. The constructs both interaction partners separated by a flexible linker of amino acids that allows for conformational changes required for physiological arrangements. An example for a suitable linker can be found in the transcription factor Oct1 connecting the DNA binding domain and the transcriptional activator domain of this protein (*181*). Different variants of this amino acid sequence have successfully been used to stabilize and crystallize low affinity complexes (*182*).

The JM domain of EGFR was fused to the N-terminus and the C-terminus of ARNO Sec7 using three different linker lengths to create a total of 6 different constructs (Fig. 4.29a).

Purity and quality of the constructs is important since long flexible parts like the employed linkers could lead to protein instability. However, purification of the different fusion constructs was possible and resulted in homogenous proteins (Fig. 4.29b). Moreover electrospray ionization mass spectrometry (ESI MS) analysis confirmed that the purified products have the expected molecular weight (Fig. 4.29c) making them suitable for crystallization.

4.3.5 ARNO Sec7 genetically fused to EGFR JM as constructs for crystallization

ARNO Sec7 modified with a flexibly attached EGFR JM domain at the C-terminus crystallizes under several different conditions (e.g. Fig. 4.30a). However, when modifying the N-terminus of ARNO Sec7 with the linker and EGFR JM sequence, crystallization is impaired. This is in accordance to the finding that the N-terminus of ARNO Sec7 is crucial for the formation of protein crystals (paragraph 4.3.2 and 4.3.3).

To obtain suitable results, a micro seeding approach was employed to improve both size and quality of the crystals (Fig. 4.30b, for details see Materials and Methods).

Suitable diffraction data for structure determination could be collected for all six different fusion proteins. However, again no electron density for the EGFR JM domain could be located in the structural models calculated with the obtained data.

a)

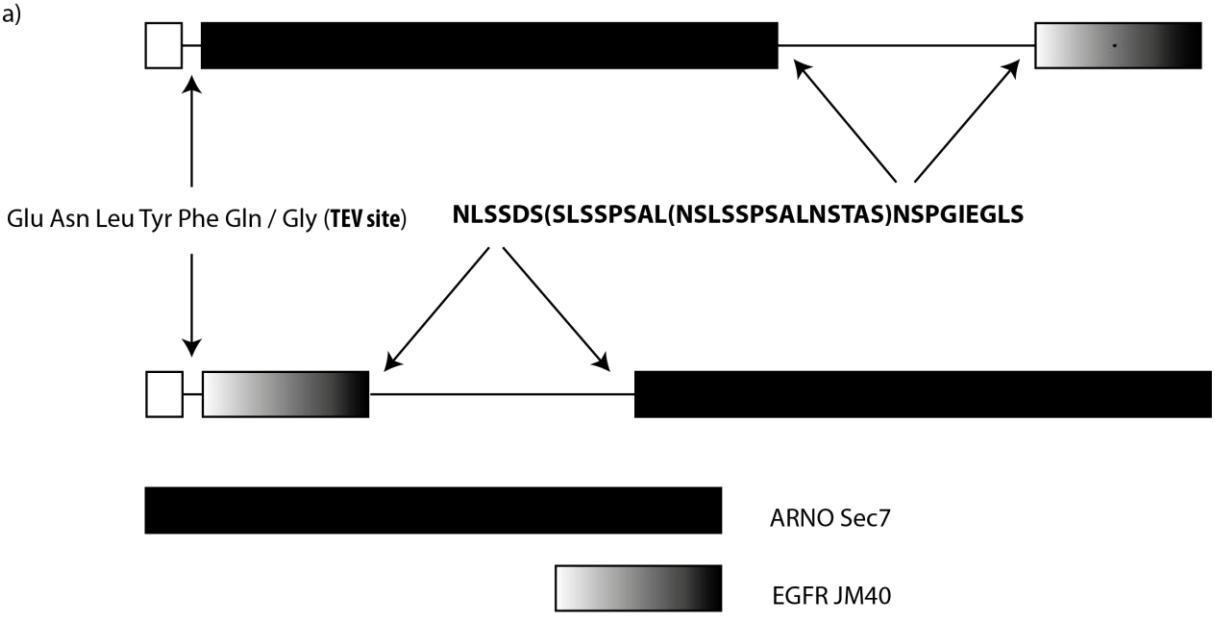

b)

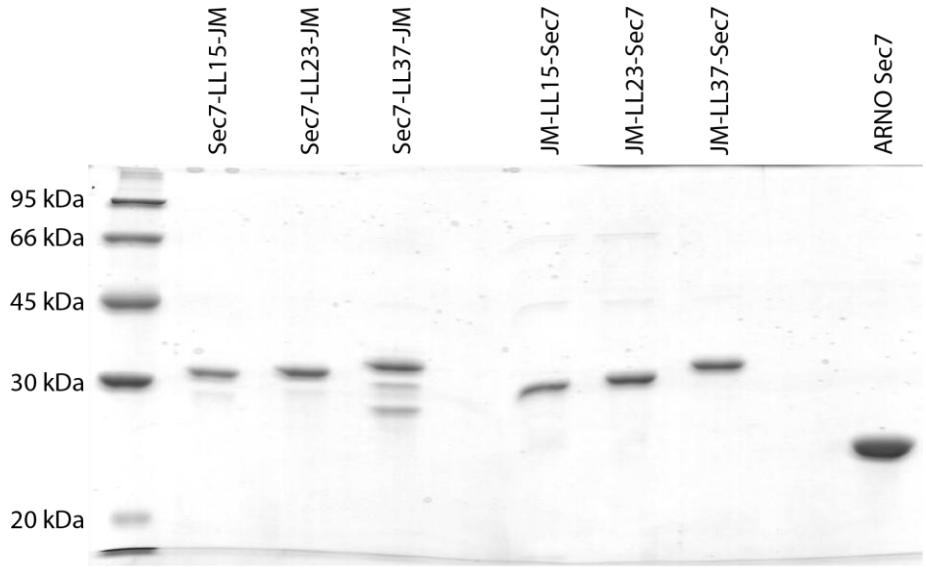

c)

	Sec7-LL15-JM	Sec7-LL23-JM	Sec7-LL37-JM	JM-LL15-Sec7	JM-LL23-Sec7	JM-LL37-Sec7
measured MW	30211	30955	32269	30207	30947	32261
calculated MW	30205	30948	32265	30205	30948	32265

Fig. 4.29 Fusion construct of the juxtamembrane domain of EGFR to ARNO Sec7. Using three different linker lengths (15, 23 and 37 amino acids, sequence depicted in (a), amino acids in brackets are only present in the long linker constructs), six constructs with EGFR JM connected to the N-terminus or the C-terminus of ARNO Sec7 were obtained. SDS PAGE analysis and Coomassie Brilliant Blue staining (b), and mass spectrometry (ESI MS, data summarized in c) confirmed the integrity of the fusion proteins.

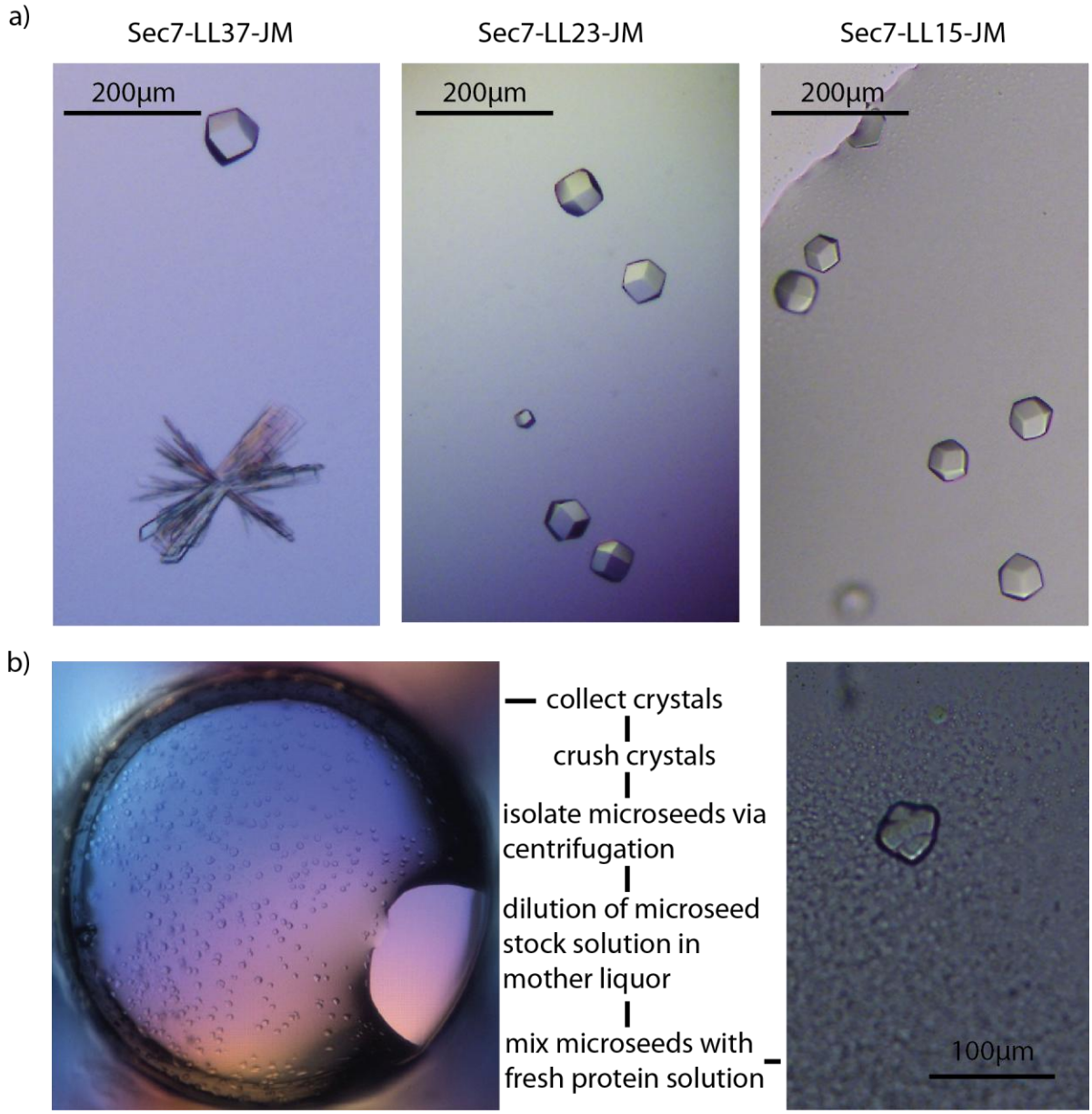

Fig. 4.30 Crystals grown from ARNO Sec7-EGFR JM fusion proteins. C-terminal fusion of EGFR JM to ARNO Sec7 resulted in readily crystallizing constructs (a, Sec7-LL15-JM: [100mM BisTris pH 6.5, 200mM NaI, 20% PEG3350], Sec7-LL23-JM: [200mM Tri-Lithium-Citrate, 20% PEG3350], Sec7-LL37-JM: [100mM Tris pH 8.5, 200mM $MgCl_2$, 20% PEG8000]). In contrast fusion of EGFR JM to the N-terminus of ARNO Sec7 reduced the ability to crystallize. Optimization of the initially found conditions via microseeding yielded crystals that were suitable for analysis (b, [100mM BisTris pH 6.5; 25% PEG3350]; for details see Materials and Methods).

4.3.6 Fusion of two copies of EGFR JM to ARNO Sec7

It is yet unknown whether the EGFR interacts with ARNO in a 1:1 ratio. Several studies suggest that the juxtamembrane domain indeed forms dimers via its N-terminal JM-A part (*13, 17*). If dimer formation is required for interaction with ARNO, a fusion construct with a 1:1 ratio between ARNO and EGFR is not feasible to support complex formation.

To exploit this possibility, two copies of the EGFR JM domain were genetically fused to ARNO Sec7. The two JM domains in these constructs are separated by a 23 amino acid linker sequence that is identical to one linker used to connect ARNO Sec7 with the first JM sequence (Fig. 4.31a). This linker length is sufficient to cross the distance required for JM-dimer formation as observed in NMR structures (*17*).

It was not possible to express and purify a construct of two JM domains N-terminally fused to ARNO Sec7 (Fig. 4.31b). In contrast C-terminal fusion of two JM domains to ARNO Sec7 results in a protein that can be purified (Fig. 4.31c). Although the resulting product is not very pure it was successfully employed in crystallization. The obtained crystals yielded good diffraction patterns. However, no part of the EGFR JM domain or the linker sequence could be identified in the resulting structural models of the fusion proteins.

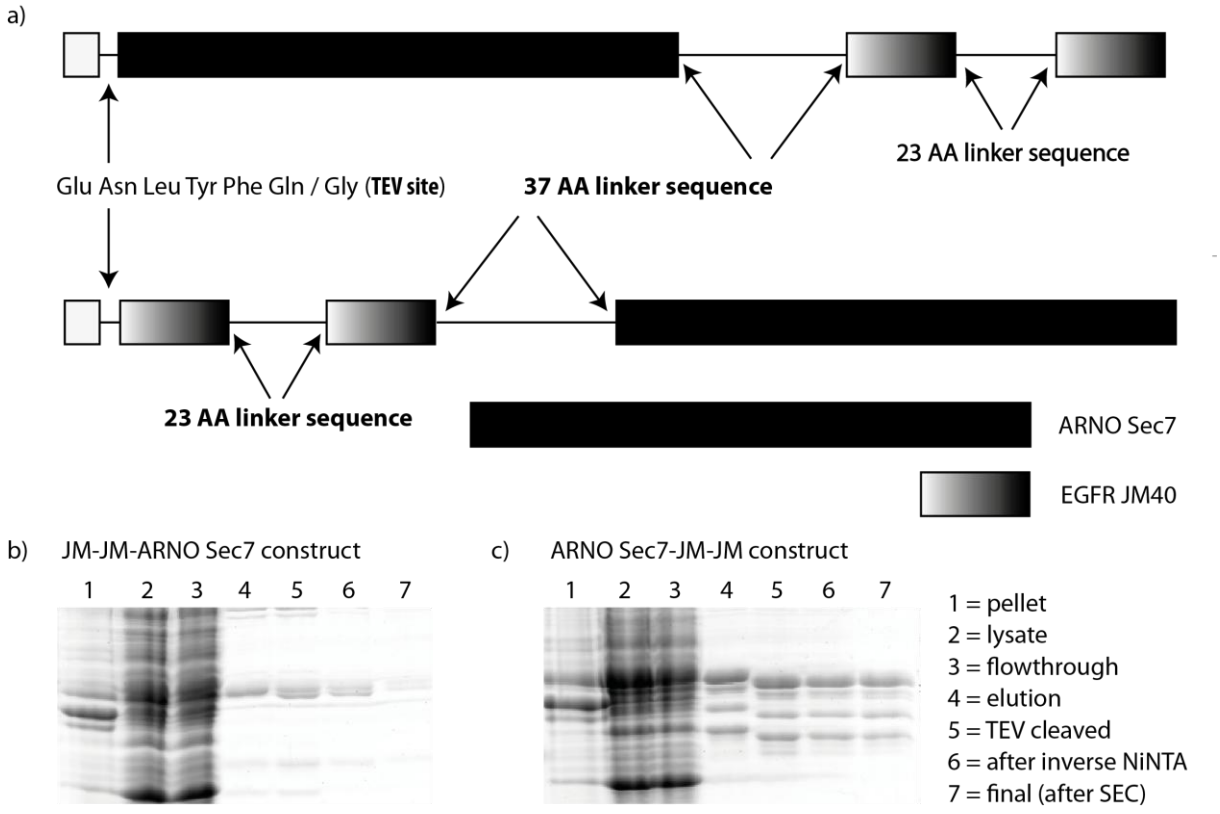

Fig. 4.31 Fusion of two copies EGFR JM to ARNO Sec7. The employed constructs are illustrated in (a). Protein purification was followed by analyzing samples on SDS PAGE gels stained with Coomassie Brilliant Blue (b and c). Fusion of two EGFR JM copies to the N-terminus of ARNO Sec7 resulted in an unstable protein that could not be purified efficiently (b). Fusion at the C-terminus of ARNO Sec7 was possible. The molecular weight of the main species was found to fit to the expected fusion protein as verified by mass spectrometry.

In summary x-ray crystallography was not successful to generate structures of a complex between ARNO and EGFR using the juxtamembrane domain as the interaction

partner for ARNO. Future studies should focus on different constructs or structural methods (e.g. NMR analysis) in order to circumvent the described problems.

5 Discussion

5.1 Screening for Arf6 specific small molecule inhibitors

5.1.1 Purification of the constructs NΔ13 Arf6 and JIP4 LZII 392-462

While purification of N-terminally truncated Arf6 was straight forward, some optimization of the purification process was required for the JIP4 LZII domain. In contrast to the published protocol (*156*) I employed size exclusion chromatography (SEC) as the final step of the purification.

While both the TEV protease (pI: 8,7) and other contaminating proteins could be removed by anion exchange chromatography as described by Isabet et al. (*156*), a high amount of free GST was still present after this purification step (data not shown, $pI_{JIP4LZII}$: 4,7 pI_{GST}: 5.7 GST). Not all of the free GST stayed attached to the glutathione matrix after over night digest. Therefore, it was a major issue to remove the remaining molecules. GST has a molecular weight of approximately 26 kDa and forms homodimers in solution (*183, 184*). The resulting difference in molecular weight between JIP4 LZII (18kDa/dimer, (*156*)) and the GST dimers (52kDa) made it possible to use size exclusion chromatography to separate both proteins and obtain pure JIP4 LZII. Two molecules that are supposed to be separated via SEC should have a molecular weight ratio of at least 2:1. In the described case the ratio is 2,9:1 and therefore suitable for successful separation. Indeed the purification data shows that both GST and other high molecular weight contaminations could be reduced using SEC (Fig. 4.1). One problem that remained with the modified method of purification was the TEV protease that was added for the cleavage of the GST-JIP4 LZII fusion protein. The molecular weight of the protease is approximately 27 kDa and therefore very close to the MW of a JIP4 LZII dimer. Hence, this protein was removed from the solution after cleavage but before SEC by incubation of the sample with NiNTA agarose matrix. The protease has a His tag for purification and can therefore be removed by incubation with such a matrix. The optimized protocol resulted in very pure JIP4 LZII in sufficient amounts for the high throughput screen and the following validation assays.

5.1.2 *In vitro*functionality of the purified Arf6 construct

The Sec7 domain represents the common structural element in guanine nucleotide exchange factors (GEFs) for Arf GTPases. To test the activity of purified Arf6 I employed and in vitro exchange assay with the Sec7 domain of cytohesin 2 (ARNO). It is described that ARNO Sec7 has a higher in vitro exchange activity towards Arf1 than towards Arf6 (*136*). However, Sec7 domains from two Arf GEFs that prefer Arf6 over Arf1 (EFA6 and GEP100) showed no activity on Arf6 in my hands (data not shown). Therefore, the assay was conducted using ARNO Sec7. In accordance with the literature the observed exchange activity was higher for Arf1 than for Arf6. However, the observed activity shows that the purified Arf6 construct is capable of binding to physiological interaction partners (*161*) and that nucleotide exchange occurs under appropriate conditions. Further evidence for a functional Arf6 construct is provided by the interaction assay with JIP4. The effector protein is able to discriminate between the active (GTP bound) and inactive (GDP bound) conformation of the GTPase. Moreover the K_d values observed are in accordance with published data using Surface Plasmon Resonance (SPR) technology. Moreover the affinity for active Arf1 was more than one order of magnitude lower than for Arf6, an observation that is also supported by the literature (Fig. 4.7, (*156*)). The obtained results suggest that the employed system of interacting proteins is suitable to resemble a physiological situation essential for Arf6 downstream signal transduction.

5.1.3 Differences between GDP and GTP bound Arf6 in binding to JIP4LZII

A clear discrimination between GDP and GTP bound Arf6 was possible in the JIP4 LZII based fluorescence polarization (FP) assay. However, the difference in affinity is lower that expected for GTPase-effector pairs.

The binding site of Arf6 on JIP4 was determined to the region between amino acids347-480(*155*) and later further reduced to amino acid 392-462 (*156*). However, it is not clear whether other parts of the protein play a role in discriminating between the active and inactive form of Arf6. In fact no binding studies were performed addressing this issue in the major publication describing the crystal structure of the GTPase-effector complex (*156*). The relatively small difference in binding affinity measured by fluorescence polarization could therefore bethe result of missing parts in JIP4that contribute to active/inactive discrimination under physiological conditions.

Another potential *in vitro* bias can be attributed to the GTPase side of the interaction. The Arf6 construct used in this study lacks the N-terminal 13 amino acids. In cells this part forms a small α helix that is lipid modified with a myristoyl moiety at glycine in position two of the protein. The lipid modified helix is involved in membrane binding and localization of Arf GTPases and plays an important role in the activation inside the cell (*132, 185*). The lack of the N-terminal helix allows for *in vitro* activity in the absence of membranes that are required for sufficient activation of full length Arf6.

The effector binding site of small GTPases is located to switch I, switch II and the bridging interswitch region (Fig. 5.1 shows a crystal structure of Arf6 highlighting the important regions in both conformations). Furthermore, the N-terminal helix is part of the switch machinery that undergoes drastic conformational changes upon nucleotide exchange (*101, 133, 152, 157*). In the Arf6 GDP structure, the helix associates with the core molecule (*152*) thereby stabilizing a conformation that buries the interswitch region in the protein. GTP binding results in a translocation of the interswitch region and a reorientation of the N-terminal helix that forms lipid contacts in the presence of membranes (*151*). This explains the requirement of lipids for proper nucleotide exchange since the hydrophobic moieties exposed upon GTP association destabilize the protein conformation in the absence of lipid bilayers.

The rather small differences in binding affinity of JIP4 LZII to active/inactive Arf6 can be explained in context of the lack of the N-terminal helix. The GDP bound conformation lacks the intramolecular contacts of the N-terminal helix. Hence, it is tempting to speculate that the resulting conformation is not stable and switches between the inactive form and an “active like” conformation that can still be recognized by effector proteins. Indeed it was shown that NΔ13 Arf6 GDP is partially unstructured in solution (*186*) supporting the idea of a heterogeneous mixture of different conformations. This could explain the small difference in the observed affinities for active and inactive Arf6 that is not expected considering other known GTPase-effector pairs like Ras and the Ras binding domain of Raf (*187*).

Further experiments are required to support these hypotheses. Full length myristoylated Arf constructs in the presence of membrane models, e.g. liposomes or NanoDiscs, and longer constructs of JIP4 provide a system that is closer to the physiological situation. This could elucidate the binding of both proteins and the differences between active and inactive Arf6 in effector recognition.

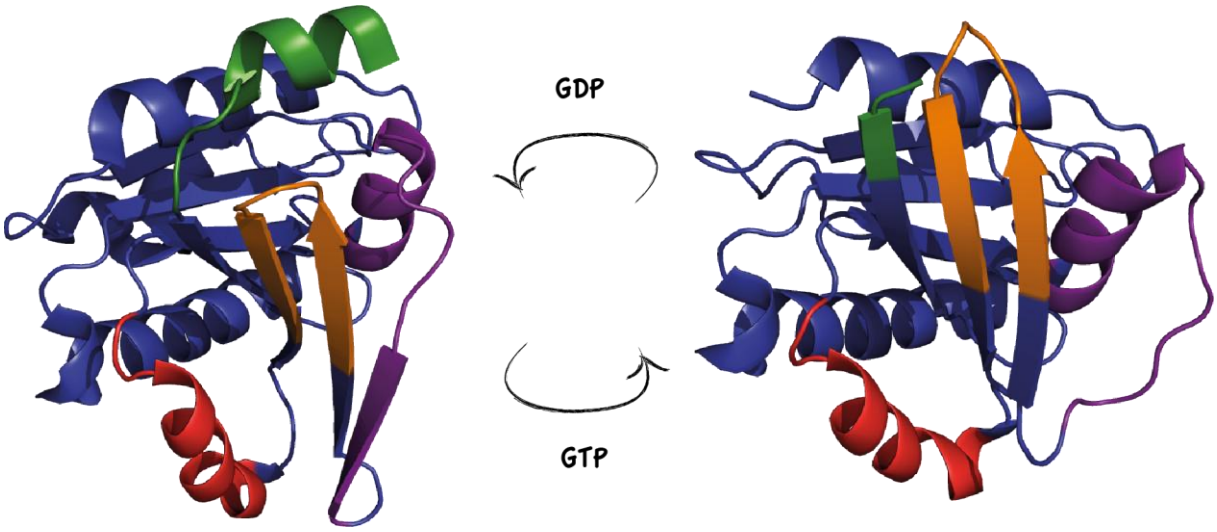

Fig 5.1 Crystal structures of Arf6 in the "active" and "inactive" conformation. The cartoon representation illustrates conformational changes observed upon nucleotide exchange in the GTPase Arf6. The most prominent features undergoing conformational rearrangement are: the N-terminal helix (green), switch I (purple), switch II (red) and the interswitch region (orange). Structural models: PDB 1EOS (*152*), PDB 2J5X (*151*).

5.1.4 Differences between the FP assay and the pulldown assay

While in the FP assay only a small difference in binding of active and inactive Arf6 to JIP4 LZII is observed, the pulldown assay employed in paragraph 4.1.6 shows that only a negligible amount of GDP bound Arf6 can be precipitated with immobilized JIP4 LZII. Insufficient loading with the respective nucleotide in the FP assay can be excluded by employing constitutively active or inactive mutants of Arf6 (Q67L and T44N respectively). Both constructs show binding as the wild type preloaded with the respective nucleotide (Supplementary Fig. 1). Hence, other factors seem to contribute to the differences observed in the pulldown and FP assay. A major difference between the two assays is that the pulldown works with immobilized, GST tagged JIP4 LZII while the FP assay is performed in a homogenous solution with only slightly altered JIP4 LZII. It is possible that immobilization of the effector or the GST tag itself has an influence on the binding of GDP bound Arf6.

Another possibility could be that kinetic aspects of the binding play an important role in the discrimination between active and inactive Arf6. If GDP bound Arf6 has a very fast off rate (k_{off}) when binding the effector JIP4, it is possible that the bound GTPase dissociates from the immobilized effector in the pulldown assay during the required wash steps of the assay. In contrast the same off-kinetic would result in a reasonably high dissociation constant in a homogenous steady state assay like the FP assay given an equally fast on kinetic (k_{on}). Since $K_d = k_{off}/k_{on}$, a protein-protein complex with a low Kd

value can still dissociate with high frequency and therefore appear not stable in a pulldown assay. A fast intramolecular dynamic induced by an unstable conformation could be one explanation for a fast dissociation for Arf6 GDP (see paragraph 5.1.3). The observed binding event might actually represent a mixture of several interactions with the inactive conformation of Arf6 as one extreme and an "active like" conformation due to the missing N-terminal helix as the other. In a steady state assay (like FP) this results in an average of the combined affinities. In contrast in a pulldown assay low affinity intermediates can get lost during wash steps and do not contribute to the observed association with the effector. The obtained results would argue for an unstable complex between Δ13 Arf6 GDP and immobilized JIP4 LZII that might be caused by structural artifacts due to the missing N-terminal α helix.

5.1.5 The concept of the screening assay

Arf GTPases have crucial functions in cells. They regulate membrane traffic along the secretory and endosomal pathway ensuring a tight balance of transport processes. From all mammalian Arf proteins Arf6 is the most distantly related one. Although it shares 67% sequence identity with Arf1 (*188*) it represents a special case. Knock down of single class I or class II Arf isoforms shows no severe membrane traffic phenotype indicating that their functions are partially redundant (*110*). In contrast, Arf6 is the sole member of class III Arf proteins and is involved and essential in diverse processes from membrane traffic and endocytosis to cytoskeletal organization and transport (*96*). Therefore, Arf6 is an interesting protein for cell biological research and small molecule inhibitors suitable for *in vivo* studies are of great interest in the scientific field (*142, 143*). However, all known inhibitors for Arf GTPases target the GTPase before or during their activation (*128, 138, 141*). Thereby they prevent the initiation of downstream effector signaling by indirect inhibition of the GTPase. Most GEFs have some intrinsic specificity towards certain Arfs, however, they rarely act on only one (*96, 136*). By inhibiting the upstream activator it is very likely to obtain "off target" effects that lead to difficulties in the interpretation of experimental data from complex systems like cells or animals. Although inhibitors like SecinH3 are excellent tools to study GEF biology, a direct correlation with the activity of a specific GTPase is hardly possible (*138, 146*).

For a more specific inhibition it would be beneficial to directly target the GTPase of interest and inhibit downstream signaling from this step on. Signal transduction via small GTPases always involves downstream effector proteins that associate with the active conformation of the GTPase. The structural features responsible for effector binding of Arf proteins are the switch I, switch II and interswitch regions (Fig. 5.1). Although the detailed interactions are distinct for different effector proteins the general binding site is limited to the mentioned elements. This leads to overlapping binding sites of different effectors (*156, 189*) and suggests that binding of one protein prevents the association of another (Fig. 5.2). Hence, by blocking the general binding site for effector proteins it can be possible to prevent downstream signaling in general. In contrast to many other Arf effectors, JIP4 shows a high degree of specificity towards binding of Arf6 (*156*), hence it occupies and blocks the Arf6 effector binding site but not that of other Arf isoforms. Indeed pulldown analysis shows that soluble JIP4 LZII can displace an effector from Arf6 but leaves the interaction between Arf1 and GGA3 intact (paragraph 4.1.6). This supports the hypothesis of a specific binding site block for Arf6. Small organic compounds that displace JIP4 LZII from Arf6 and obtain the mentioned characteristic have the potential to act as Arf6 downstream signaling inhibitors. However, it is also possible to identify compounds that specifically disturb the JIP4 interaction with Arf6 but no other effector binding. In this case a less general Arf6 inhibitor would result.

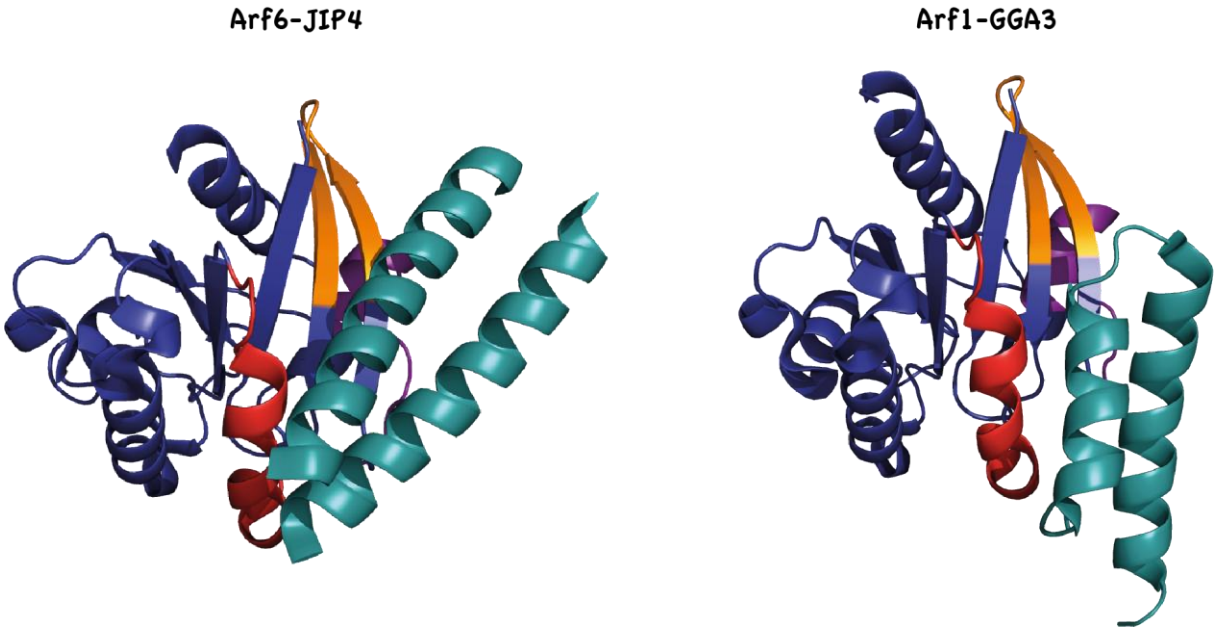

Fig. 5.2 Occupancy of the switch and interswitch regions of Arf GTPases by different effector proteins. The proteins JIP4 (PDB 2W83 (*156*)) and GGA3 (PDB 1J2J (*189*)) cover similar binding sites at the respective Arf GTPase. Indicated features: switch I (purple), switch II (red), interswitch region (orange), effector protein (cyan).

5.1.6 Results of the screen and challenges in finding PPI inhibitors

The search for small molecule inhibitors involves using big libraries of "drug like" compounds that can be systematically tested for their activity in a suitable assay. In this study a fluorescence polarization based assay was employed to monitor the binding between Arf6 and its effector JIP4. Throughout the screening of 17000 compounds the assay proved to be stable and the overall Z' value obtained was 0.85, which is very close to the initial test results of 0.9 indicating an excellent performance of the assay under real HTS conditions. The obtained values were stable even over night at room temperature. To summarize the FP assay performed robustly in a HTS setup and screening of approximately 1000 compounds per day was possible although this value could easily be increased when using a full automated pipetting setup.

Nine small molecules were identified as primary hits leading to a hit rate of 0.06%. This value is in the normal range for published HTS approaches (*190*). The primary hits were identified as false positives using a fluorescence free pulldown assay. The effect of the compounds on JIP4 LZII binding to Arf6 monitored in the FP assay was not confirmed when both proteins are co-precipitated. Indeed, the identified hit molecules exhibit an intrinsic fluorescence in the spectral range of fluorescein. This can be a major reason for false positive results when using fluorescence polarization. Therefore, an independent assay is required to verify compounds with suspiciously high fluorescence. The well-known molecule thalidomide shows striking similarity to one of the identified hit compounds (KR2 3H8). However, in contrast to the screening hits it has no intrinsic fluorescence and shows no effect in the fluorescence polarization assay further supporting that the screening hits are false positives.

No inhibitors for the JIP4 interaction with Arf6 could be identified in this study. Protein-protein interactions (PPIs) pose a general problem for drug discovery. Today's compound libraries are dominated by the drug discovery efforts of the past that were focused on GPCRs and enzymes (*191*). Some features of such drug-like small molecules are summarized by the "Lipinski rule of 5" and include the molecules to be not bigger than 500Da (*192*), a characteristic that decreases the chance to disturb a large PPI interface. Therefore, compounds employed in traditional screening approaches are not well suited for the discovery of PPI inhibitors and large libraries are required to find suitable hits (*193*). Although several studies exemplify that successful identification of PPI inhibitors is possible, the screening efforts behind the resulting compounds involved

large libraries and the logistic and financial support of big companies (*194, 195*). Moreover in contrast to other "druggable" protein-protein interactions (*196*) the JIP4-Arf6 interface is devoid of clear hotspots (*156*) indicating a more general contribution of the whole binding surface. This requires even more specialized and optimized libraries (e.g. by using larger molecules or natural products) to find hits that specifically disturb such interaction.

The studied interaction shows features that make it difficult to be targeted by small molecules when using traditional compound libraries for screening. However, distinct approaches were developed to tackle protein-protein interfaces in a specific manner.

5.1.7 Alternative approaches for the identification of protein-protein-interaction (PPI) modulators

Finding small molecule inhibitors for protein-protein-interactions (PPIs) is challenging and successful identification usually requires specialized compound libraries of sufficient size. A different class of molecules suitable for disturbing PPIs are stabilized α helical peptides designed with knowledge of the complex interaction surface. The interface involved in PPIs often contains α helical elements (*197*) and "hot spot" residues that are especially important for the interaction. Disturbing the binding site with small peptides that resemble crucial elements of the interface is therefore a promising approach in PPI inhibitor development. With this methods it was possible to inhibit the formation of a competent NOTCH transcription factor complex using hydrocarbon stapled α helical peptides (*198*) or prevent the activation of Ras by its GEF Sos with the help of hydrogen bond surrogate helices (*199*).

One method involves intramolecular covalent connections between non-adjacent backbone carbon atoms that replace a hydrogen bond formed between position i and i+4 in an α-helical structure (*200, 201*). Another approach confers helical properties by the introduction of artificial amino acids at appropriate positions in the primary sequence (*198, 202*). Modification of the resulting peptides is possible to optimize cell permeability or reduce side effects or toxicity (*203*). An active endocytic pathway facilitates the cellular uptake of peptides and enables intracellular effects without resulting in endosomal degradation due to high proteolytic resistance of the peptides (*198*, *199*).

The JIP4 LZII binding site forms a helical coiled coil domain (*156*) and hence represents a potential example for employing a short stabilized peptide to disrupt the Arf6-JIP4 complex. However, the formation of a JIP4 dimer is required for efficient binding to Arf6 since amino acids from both monomers make contact to one GTPase. To obtain a molecule that inhibits general effector association by blocking the binding site at Arf6, a peptide helix mimic needs to contain crucial elements for dimer formation as well as for Arf6 binding. The amino acids from position 412 to 424 of JIP4 form the major hydrophobic interface involved in the interaction with Arf6. Additional residues make hydrophilic contacts to Arf6 via hydrogen bonds. Hence, the minimal JIP4 motif containing all amino acids involved in binding spans position 412 to 432 (*156*). However, a peptide of 20 amino acids could pose problems regarding membrane permeability and limit the potential modifications due to the final size of the molecule. It is crucial to balance size and affinity in designing small α helical peptide mimics that can be suitable for blocking the Arf6 interface responsible for effector binding. In contrast to other Arf binding partners (*189*), there is no obvious "hot spot" residue essential for the interaction with JIP4. Therefore, selective removal of single residues is not expected to abolish binding but rather only slightly reduce the affinity.

Helical peptide mimics represent a promising alternative to small organic compounds when targeting PPIs. The JIP4 LZII binding to Arf6 shows some features that are also found in interactions that have been successfully disturbed by this method. Thus using peptide mimics is a promising approach to obtain inhibitors for Arf6 downstream signal transduction.

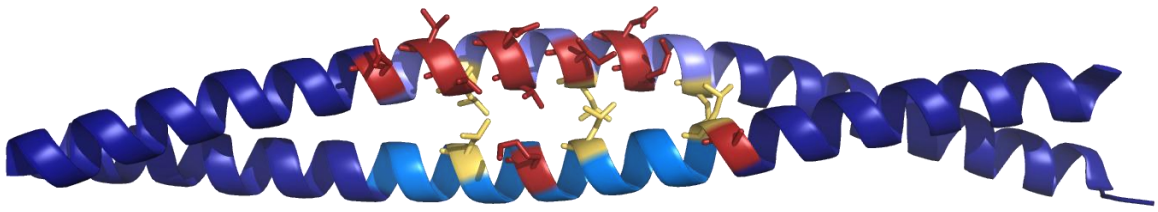

Fig. 5.3 JIP4 LZII dimer with highlighted structural features involved in Arf6 binding. Two molecules JIP4 LZII form a coiled coil structure that is stabilized by leucine residues (yellow stick representation). The amino acids colored in red (sticks) are involved in the binding to Arf6. The highlighted regions (pale purple and light blue) represent fragments of the protein that could be employed to design a small peptide inhibitor (for detail see text). PDB 2W83 (*156*).

5.1.8 Summary I

It was possible to purify functional Arf6 and JIP4 LZII of high quality that could be employed to establish a HTS assay. During a screen of 17000 compounds the assay was stable and proved to be robust in the presence of most of the small molecules. Although no inhibitor for the interaction of Arf6 with JIP4 was identified, the system is readily applicable for screening of bigger or more specialized compound libraries that are optimized for finding protein-protein interaction inhibitors. Moreover it is a convenient and reliable tool to test modulators of the interaction in vitro (e.g. peptide inhibitors).
Furthermore, an interesting observation is that JIP4 LZII only weakly discriminates between active and inactive Arf6. This either represents a physiological peculiarity of the interaction or points to an important structural role of the N-terminal helix in Arf6 to confer specificity in active and inactive conformations.

5.2 Structural and biochemical analysis of the interaction between EGFR and ARNO

5.2.1 Inactivation of the EGFR kinase construct increases its stability in solution

The purification of constructs for crystallography was straightforward for ARNO Sec7. In contrast the EGFR intracellular domain (including the juxtamembrane (JM) region, ICD1022) was unstable after purification and visibly precipitated when stored at concentrations suitable for crystallography. Investigation of the thermal stability in a fluorescence based thermal shift assay revealed that the presence of the JM domain results in a decreased melting temperature when compared to the JM free intracellular EGFR (KC1022). Since the JM domain is crucial for kinase activity of the soluble receptor, one can speculate that an "active" conformation causes protein instability. Different conformations are required to enable phosphotransfer catalyzed by protein kinases (*32*). While the ones represented in crystal structures are likely stable, some others could result in destabilized proteins in the absence of factors that are present in the cell during the physiological process.

This idea is supported by the fact that addition of a non-hydrolysable ATP analogue (AMPPNP) stabilizes EGFR ICD1022 leading to an increase in the melting temperature observed in the assay mentioned above. AMPPNP blocks the catalytic cycle of the kinase in a pre-phosphotransfer step thereby prohibiting conformations that occur afterwards. Furthermore, it is important to mention that crystal structures of the EGFR intracellular domain are generated with inactive forms of the kinase by either omitting the JM domain from the protein (*13, 77*), adding small molecule inhibitors (*76*) or by introduction of inactivating mutations (*15*). In accordance with the published information regarding the EGFR constructs employed for crystallization the EGFR mutant K745M was stable after purification in the presence of the JM domain.

The mutant EGFR construct is promising for the generation of co-crystals with ARNO Sec7 since it still binds to the exchange factor as shown by crosslinking and exhibits increased stability.

5.2.2 Activity of the purified EGFR constructs*in vitro*

The purified EGFR construct intracellular domain 1022 (ICD1022) contains the juxtamembrane (JM) domain and is therefore expected to be competent to phosphorylate substrate proteins. Indeed it was shown that the purified protein phosphorylates the SH2 domain of phospholipase Cγ, a natural substrate of the kinase. Furthermore, autophosphorylation of Tyr1016 is observed indicating full functionality of EGFR ICD1022 both as a kinase and a substrate. In accordance with published data it was shown that the juxtamembrane (JM) domain is essential for efficient phosphorylation of substrates by EGFR since the construct kinase core 1022 (KC1022) shows only weak catalytic activity. These results demonstrate that the recombinantly expressed EGFR variants employed in this study behave similar to full length constructs in cellular assays (*13*). Therefore EGFR ICD1022 and EGFR KC1022 are suitable to study receptor biochemistry using purified components.

5.2.3 The juxtamembrane domain is the binding site for ARNO at EGFR

The juxtamembrane (JM) domain of EGFR is a crucial structural element in the activation of the kinase (*13, 15*). Interestingly binding of the positive EGFR regulator ARNO is also dependent on the presence of the JM domain indicating that it either directly involved as a binding site or indirectly influences the conformation of the receptor to associate with ARNO. Crosslinking assays with the isolated JM domain as well as JM-containing and JM-devoid EGFR ICD constructs show that this receptor part is both required and sufficient for ARNO binding showing that the JM domain represents a direct binding site. However, it cannot be excluded that other structural features of the receptor modulate binding.

It was shown that ARNO induces a conformational change in EGFR (*145*) suggesting that an active conformation is induced. The JM domain indeed is also a crucial element in the negative control of EGFR activity in a cellular environment by association with the plasma membrane, thereby preventing the formation of an asymmetric dimer (*17, 18*). The direct interaction of ARNO with the JM domain suggests a role in facilitating the required reorientation of the JM domains. However, more detailed knowledge of the interaction on a structural level is required to support this hypothesis.

Negative feedback in a cellular system is mediated via the JM domain as well. Phosphorylation of Thr654 and Thr669 by PKC or Erk respectively leads to reduction of EGFR activity (*9, 85*). By blocking access of these regulatory kinases through sterically blocking the JM domain, ARNO could inhibit the negative feedback and thereby sustain the response of EGFR after activation.
However, ARNO Sec7 has a direct effect on the activity of the purified EGFR intracellular domain (*145*) indicating that conformational stabilization of the active conformation also occurs in absence of membranes or other regulatory molecules. Therefore, a potential role of ARNO in EGFR activation can affect several aspects in the cellular context.

5.2.4 ARNO binds to EGFR independent of the activity of both proteins

It was previously shown that the exchange activity of ARNO is not required for its effect on EGFR. A catalytically inactive mutant still increases EGFR phosphorylation levels inside the cell and stimulates autophosphorylation in an *in vitro* assay (*145*). Studies in the presence of the ARNO Sec7 inhibitor SecinH3 support these finding since addition of the inhibitor does not influence crosslinking efficiency (Supplementary Figure 2) while it inhibits EGFR activity in cells (*145*). Neither the known catalytic function nor binding to the receptor alone can explain the effect of ARNO on EGFR signaling. Hence, a so far unknown conformational or catalytic mechanism that is inhibited by SecinH3 but not simply explained by steric hindrance could cause the observed effects.
Moreover the catalytic activity of EGFR is also not required for the interaction with ARNO Sec7. Both the inactive mutant K745M and addition of AMPPNP (Supplementary Figure 3) has no influence in the crosslink assay. This indicates that ARNO binding occurs even to intrinsically inactive receptors, a mechanism that could be important to position the activator at its target to ensure rapid response after external stimulation. Additionally, phosphorylation of the EGFR in the presence of ATP has no effect on the interaction with ARNO (Supplementary Figure 3), further supporting the idea of an association that is not dependent on receptor activation.

5.2.5 The C-terminus of ARNO Sec7 is an important crosslinking site for EGFR

By systematically removing lysine residues in the ARNO Sec7 domain it was possible to deplete the protein of crosslinking sites in certain surface areas. Evaluation of crosslinking efficiency allowed for classification of the residues regarding their importance in the assay. This can be used to obtain indirect information about the binding site in for EGFR on ARNO. Since the reagent employed for crosslinking in this study (Bis[sulfosuccinimidyl]suberate) only tolerates two residues to be separated by 11.4 Å, an important residue has to be close to or at the actual binding site.

Only one single lysine was identified as an important crosslinking site (Lys 244). The mutation of other lysines has no effect on crosslinking. It is important to mention that the evaluation of N-terminal lysine mutations is difficult. They result in proteins that are difficult to purify due to precipitation. Furthermore, crosslinking results with different EGFR constructs are not consistent. While a reduction in crosslinking is observed for ARNO Sec7 and EGFR JM, EGFR intracellular domain crosslinks are not influenced.

Additionally a dramatic increase in homodimerization and a severe reduction of exchange activity (Supplementary Figure 4) indicates that these constructs aggregate and are therefore not suitable for the experiments.

Although the reduction in crosslinking efficiency is modest it is striking that only removing Lys 244 shows an effect while lysines located in the middle or C-terminal part of ARNO Sec7 do not contribute to crosslinking. This indicates that binding of EGFR takes place at the C-terminus of the Sec7 domain.

5.2.6 A preliminary model for the interaction between EGFR and ARNO

ARNO increases the autophosphorylation of EGFR (*145*). Therefore, one can expect that it bind to the receptor while leaving the active conformation intact or even inducing it. Active EGFR is characterized by the formation of an asymmetric dimer that allows one monomer (activator kinase) to stimulate the other (receiver kinase) (*76*). It was further demonstrated that the EGFR JM domain is essential for stabilizing this conformation (*13, 15*). Fig. 5.4 shows an EGFR dimer and illustrates how the JM domain of the receiver kinase makes contact with the C-lobe of the activator. While the binding interface of the JM domain with the other kinase is not available for interaction with ARNO, the opposite site can be engaged.

Modification of the N-terminus of EGFR JM constructs with either fluorescein or biotin results in a reduction of crosslinking (Supplementary Figure 5). Furthermore, the only lysine in this construct is located at position ten of forty amino acids. This locates potential crosslinking sites to the N-terminal region of EGFR JM. In addition to the information from paragraph 5.2.5 one can speculate that the N-terminus of EGFR JM is close to the C-terminus of ARNO Sec7 when crosslinked. However, both JM-A (N-terminal part) and JM-B (C-terminal part) of the juxtamembrane domain are required for efficient crosslinking (Supplementary Figure 6) indicating a larger interaction site with a head-to-tail conformation of ARNO Sec7 and EGFR JM. Taking into account that the isolated JM domain of EGFR influences the nucleotide exchange catalyzed by ARNO Sec7 on Arf1 it is reasonable to assume that the receptor and the GTPase have similar binding sites. The helices F, G and H in ARNO Sec7 create a hydrophobic grove that serves as the binding site for Arf1 (*204*). The C-terminus crosses this grove and Lys 244 is aligned in close proximity to it (Fig. 5.4). If the EGFR JM domain associates in a head-to-tail conformation with ARNO Sec7, it would nicely fit into the hydrophobic grove generated in ARNO Sec7. Therefore, it might compete with Arf1 for binding and explain the observed inhibition of nucleotide exchange. Indeed several hydrophobic residues are located in EGFR JM that are not involved in formation of the asymmetric dimer and can therefore be engaged in association with the hydrophobic grove in ARNO Sec7 (Fig. 5.4). It is important to note that three leucine residues located in the LRRLL-motif close to the C-terminus of JM-A are buried in the plasma membrane in inactive receptors (*17, 18*). This disturbs the formation of an asymmetric dimer and engaging the LRRLL motif in an interaction outside the lipid bilayer could result in release of the inhibition. Indeed NMR studies suggest that the leucines form an antiparallel JM-A helix dimer thereby facilitating the receptor activation by releasing the helices from the plasma membrane (*13, 17*). It is tempting to speculate that ARNO has a similar effect on receptor conformation. Both release of inhibition by membranes and stabilization of the asymmetric dimer via association with the JM domain to cover hydrophobic residues can lead to increased catalytic activity.

This hypothesis needs confirmation by studies performed in a membrane environment. NanoDiscs or liposomes can serve as *in vitro* model systems and allow to gain a more detailed understanding of how lipids and membrane recruitment influence the interaction. Furthermore, structural studies can yield information about the complex between ARNO and EGFR in atomic detail.

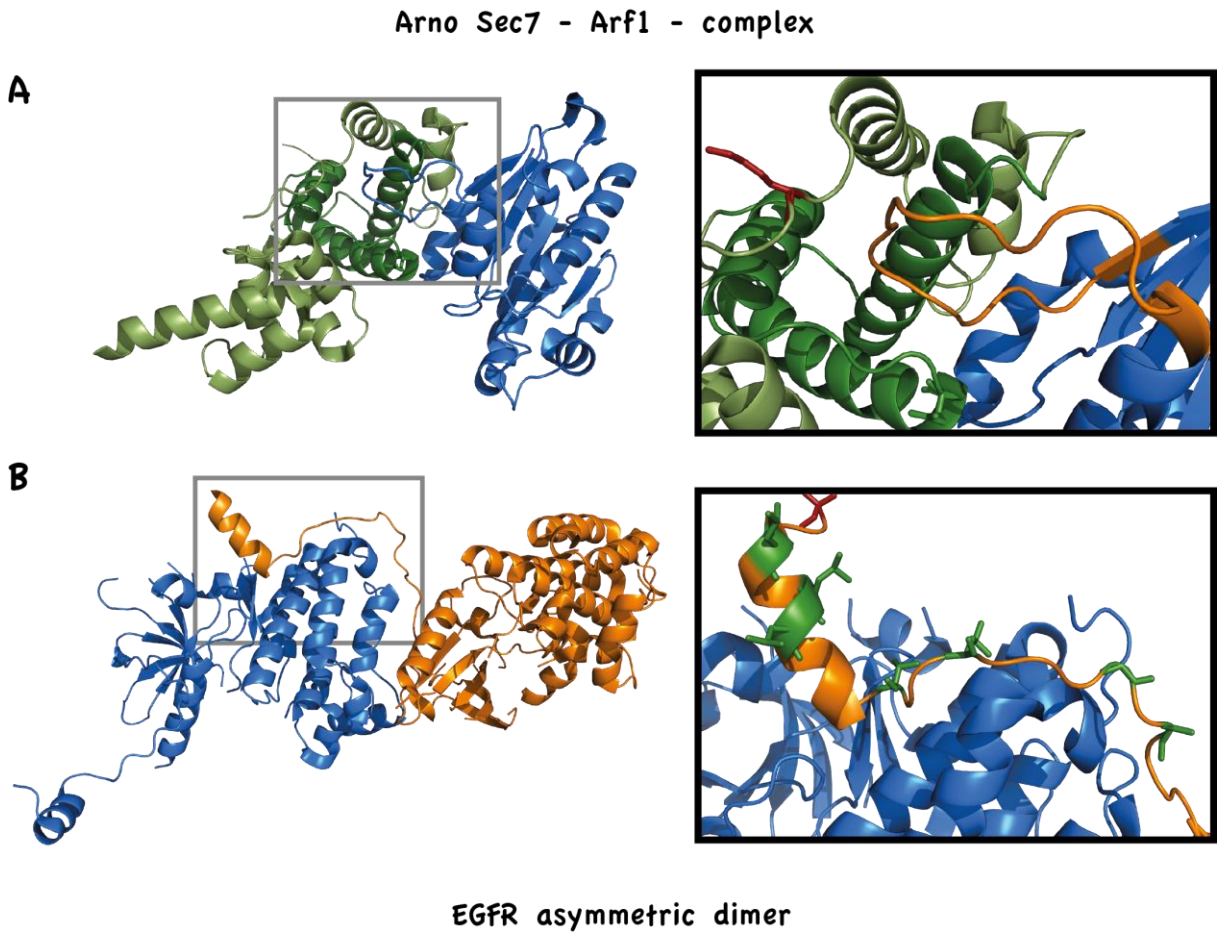

Fig. 5.4 Crystal structures of ARNO Sec7-Arf1 and the EGFR asymmetric dimer. A: A hydrophobic grove formed by the helices F,G and H in ARNO Sec7 (dark green helices in ARNO Sec7 colored in pale green) serves as the binding site for Arf1 (blue). The magnified region (grey box in overview) shows a loop in Arf1 (orange) that interacts with this grove. The important crosslinking site Lys244 in ARNO Sec7 is shown as a red stick representation. PDB 1R8Q (*204*) B: The JM domain of the acceptor kinase (orange) contacts the C-lobe of the donor kinase (blue) in the EGFR asymmetric dimer. The magnified region (grey box in overview) shows hydrophobic residues in the EGFR JM domain (green stick representation) that are not involved in asymmetric dimer formation and could therefore make contact to the hydrophobic grove in ARNO Sec7. The only lysine in EGFR JM is shown as a red stick representation. PDB 3GOP (*15*).

5.2.7 Purification of complexes by size exclusion chromatography and initial crystallization trials

Size exclusion chromatography (SEC) is often employed to separate a complex of two proteins from the monomers for crystallization. This was not successful for ARNO Sec7 and the different EGFR constructs from this study. Interestingly the EGFR construct alone elutes as a monomer, which is in contrast to published data suggesting a stable receptor dimer for proteins containing the JM domain (*13*). Hence, it is not unambiguous to conclude whether a complex between ARNO Sec7 and the intracellular domain of EGFR is formed. However, no separation from the monomers is possible.

Furthermore, the JM domain of EGFR shows no interaction with ARNO Sec7 in a SEC experiment (Supplementary Figure 8). It is important to note that no elution peak was observed for the JM domain alone during the measurement. This indicates an unspecific interaction of the peptide with the size exclusion matrix and makes drawing conclusions regarding the interaction of ARNO Sec7 with EGFR JM difficult.

Nevertheless no complex was purified and crystallization condition screens were performed with solutions containing ARNO Sec7 and EGFR JM in different molar ratios. Up to 20 times excess of EGFR JM was added to drive the equilibrium towards the ARNO Sec7-EGFR JM complex. Unexpectedly depending on the ARNO Sec7 construct, no well diffracting crystals were obtained (ARNO Sec7 61-246) or only ARNO Sec7 was resolved in the electron density (ARNO Sec7 52-256). This implicates two problems: 1) the N-terminal helical part of ARNO Sec7 is important for crystal package and 2) ARNO Sec7 with the N-terminal helix crystallizes readily, thereby potentially prohibiting the formation of a crystal in complex with EGFR JM. Problems for the co-crystal formation arise if the interaction is rather transient and ARNO Sec7 crystallization removes free protein from the solution that in turn can no longer form the desired complex (Fig. 5.5).

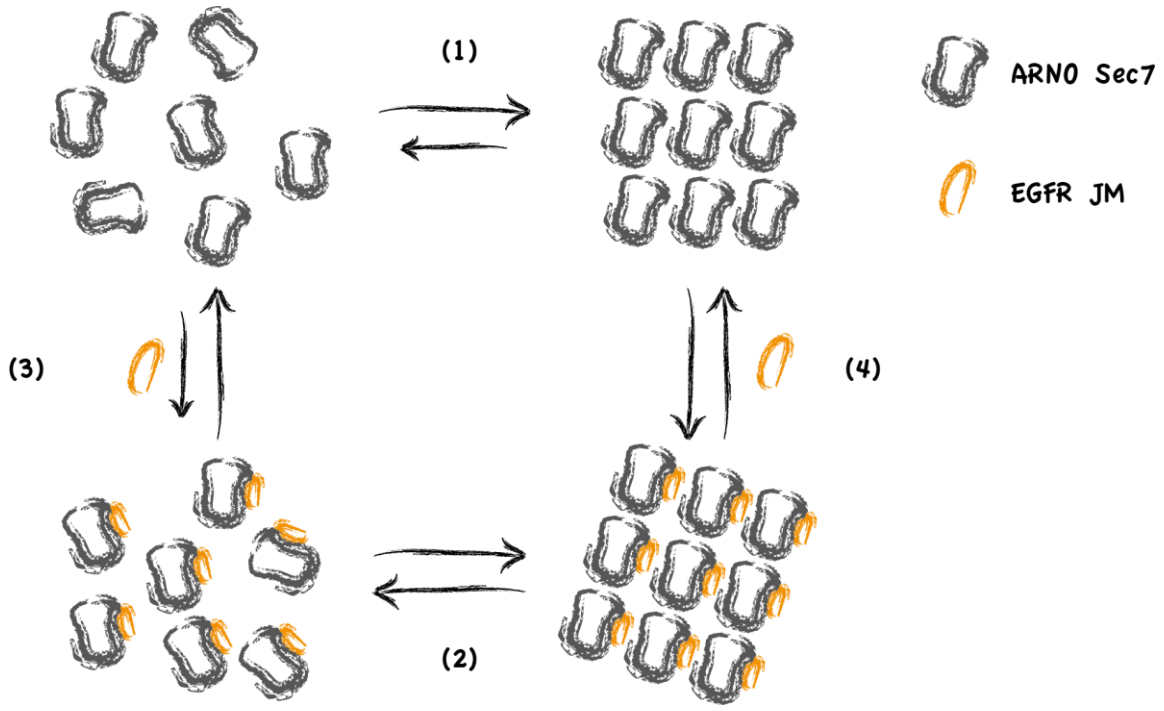

Fig. 5.5 Different equilibria that influence the formation of an ARNO Sec7 EGFR JM co-crystal. ARNO Sec7 alone crystallizes readily (1). Thus, free protein is removed from the solution that can no longer bind to EGFR JM (3). Hence, the chances to obtain a co-crystal (2) are reduced. Shifting the equilibria (1) and (3) by reducing the ability of ARNO Sec7 to crystallize (paragraph 5.2.8) or increasing the local concentration of EGFR JM at ARNO via genetic fusion of the interaction partners (paragraph 5.2.9) could promote the formation of desired crystals. Free EGFR JM can only diffuse into an Apo-crystal of ARNO Sec7 if the binding does not destroy the crystal packing (4).

5.2.8 Crystallization of N-terminal truncated ARNO Sec7 constructs

One option to solve the potential problems illustrated in Fig. 5.5 is to employ ARNO Sec7 constructs that show less efficient crystallization. From the results obtained with ARNO Sec7 61-246 it is clear that the N-terminal part is critical for crystal formation. The intermolecular contacts observed in the ARNO Sec7 crystal explain the contribution of the N-terminus (Fig. 5.6). It is involved in forming contacts with neighboring monomers in the crystal lattice and thereby promotes structured association of single molecules. In order to obtain ARNO Sec7 construct that crystallize less frequently we designed constructs with successive truncation of the N-terminus. Crystallization trials demonstrated that the truncated construct indeed formed crystals less frequently. With a reduced crystallization rate of ARNO Sec7 alone we anticipated that a complex is more likely to form. However, co-crystallization with EGFR JM did not yield crystals that contained both proteins. The resulting structure models show no electron density apart from ARNO Sec7.

It was possible to show that the N-terminal region of ARNO Sec7 (amino acids 52-261) is crucial for crystal formation. Nonetheless shifting the crystallization equilibrium of the protein by N-terminal truncation did not have the desired effect on co-crystallization.

5.2.9 Fusion constructs allow for stabilization of transient complexes

A transient complex is difficult to crystallize since a constant pool of homogenous units (in our case ARNO Sec7-EGFR JM complexes) is required for a crystal lattice to form. Therefore, stabilization of the complex was achieved by genetically linking the interaction partners. This results in a dramatic increase in the local concentration of both proteins and should enhance complex formation. A flexible amino acid linker is found in the transcription factor Oct-1. A detailed study on the function of the linker regions shows that different linker length are suitable to connect two domains and still allow complex conformational rearrangements required for protein function (*181*). Fusion of two low affinity interaction partners via a linker region designed from this example was successfully employed to obtain crystal structures of protein complexes (*182*). Therefore, ARNO Sec7 was genetically fused to EGFR JM both at its N-terminus and C-terminus in order to stabilize the interaction and increase the chance of crystal formation. Using three different linker lengths I tried to balance the flexibility required

for productive interaction of the fused proteins and the negative effects that flexible parts in a protein can have on crystallization.

The purified constructs were active in nucleotide exchange on Arf1 albeit to a lesser extend than wild type ARNO Sec7. Indeed C-terminal fusion of EGFR JM to ARNO resulted in a reduction of activity below 25% (Supplementary Figure 4). This is in accordance with the inhibitory effect of soluble EGFR JM on the exchange reaction (Fig. 4.25) and suggests that the fusion constructs allow normal interaction of ARNO Sec7 with EGFR JM. In contrast the N-terminal fusion of EGFR JM shows a less pronounced exchange inhibition (Supplementary Figure 4). These observations support a binding model, in which the C-terminal part of ARNO Sec7 makes contact with the N-terminus of the JM domain. This conformational rearrangement is facilitated by the tail-to-head orientation in the C-terminal fusion proteins. Simple folding back of EGFR JM towards ARNO Sec7 results in proper orientation of the proteins. In contrast the N-terminal fusion proteins exhibit a larger separation of the potential interaction sites making proper binding less likely. Supported by the crosslinking data that argues for an important contribution of the C-terminus of ARNO Sec7 and the N-terminus of EGFR JM it is possible to speculate that the binding site is actually located near the C-terminus of ARNO Sec7.

5.2.10 How ARNO Sec7 crystallizes in the presence of other proteins

The functional ARNO Sec7 construct fused to EGFR JM was than employed for crystallization. Suitable crystals were obtained for all six constructs (three linker length both N-terminal and C-terminal). However, crystal growth was less efficient for the N-terminal fusion proteins. This further illustrates the importance of the N-terminus in ARNO Sec7 crystallization.

All structural models generated from the analyzed crystals exhibited no electron density that could be attributed to the EGFR JM domain. Indeed the electron density nicely resembled published structures (*129, 179*) and no part of the linker or EGFR JM domain was observed for the C-terminal fusion proteins. Up to two amino acids from the linker region could be modeled into the electron density map from N-terminal fusion proteins. Although this indicates the presence of an N-terminal extension on ARNO Sec7, no information regarding the protein complex structure can be deduced from these results.

The linker region and the EGFR JM domain account for up to 80 amino acids in the fusion constructs (or 140 amino acids for the double JM fusion construct). Thus, they represent 30% (up to 40%) of the proteins molecular weight. How is it possible that such a big part of the protein cannot be found in the electron density map calculated from well diffracting crystals? The parts of a protein that become visible in the electron density of a solved crystal structure need to have the same or a very similar position in the repeating unit cell of the crystal lattice. If a part of the protein is very flexible it can have a different orientation in each unit cell, thereby generating no productive diffraction. This results in a lack of electron density in the structural model. The orientation of monomers in the ARNO Sec7 crystal leaves a big water filled cavity (*129, 179*) and the C-terminus of the protein is pointing towards this "free" space (Fig. 5.6). Therefore, the ARNO Sec7 structure can tolerate a flexible part at its C-terminus by allowing the localization in the cavity. Extensions at the N-terminus are not directly released in the cavity (Fig. 5.6). However, the high flexibility of the employed linker region could account for the possible reorientation leading to a conformation that still allows for ARNO Sec7 crystal formation. The fact that the N-terminal EGFR JM-ARNO Sec7 fusion constructs proved to be more difficult to crystallize supports this hypothesis.

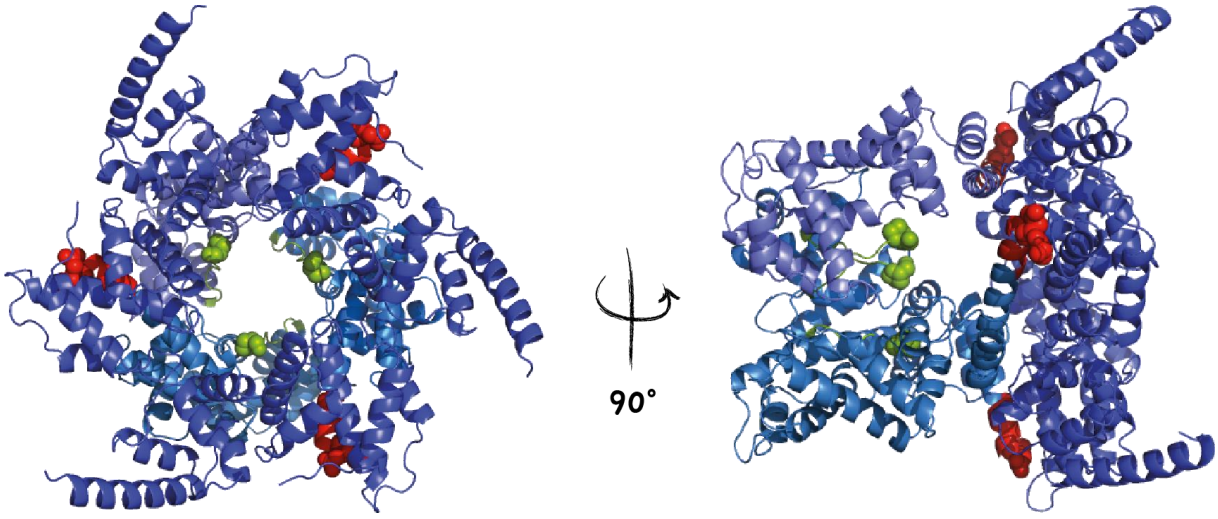

Fig. 5.6 Crystal packing of an ARNO Sec7 crystal. Single ARNO Sec7 molecules are colored in different shades of blue. The left view illustrates that the crystal packing forms a solvent filled cavity. The C-termini of single ARNO Sec7 molecules (green sphere representation) are released into this cavity. EGFR JM domains fused to the C-terminus of ARNO Sec7 can thus be located there without disturbing the crystal packing. The N-termini (red sphere representation) make intermolecular contacts in the crystal packing. Hence, modifications at this position disturb crystal formation. However, a sufficiently long flexible linker sequence can still allow fusion of EGFR JM to the N-terminus of ARNO Sec7. PDB 1PBV (*180*).

Alternative structural biology approaches include nuclear magnetic resonance (NMR) and mass spectrometry (MS) based analysis of crosslinking products. NMR has the advantage of determining macromolecular structures in solution. Hence, it avoids the problem of difficult to crystallize protein complexes as observed for ARNO Sec7 and the EGFR JM domain. Crosslinking of the complex followed by protease digest and MS analysis can also be used to obtain detailed information about a protein-protein-interaction interface (*204, 205*). This technique is convenient to verify the lysine mutagenesis results and obtain a structural picture of the interaction when combined with introducing novel crosslinking sites by mutagenesis.

5.2.11 Summary 2

Although crystallographic studies aiming to solve the structure of an ARNO-EGFR complex were not successful, it was possible to obtain more information about the underlying interaction. The juxtamembrane (JM) domain of EGFR is essential and sufficient for binding to ARNO. Given the importance of the JM domain in regulating EGFR activity it is valid to speculate that ARNO influences conformational rearrangements of this domain and thereby facilitates the formation of an active receptor dimer. Crosslinking results suggest that the C-terminus of the ARNO Sec7 domain is close to the N-terminus of the EGFR JM domain. Together with functional assays this supports a “head-to-tail” interaction, in which the JM domain associates with a hydrophobic grove in ARNO Sec7 that serves as binding site for Arf proteins during nucleotide exchange reactions. Covering of exposed hydrophobic amino acids in the EGFR asymmetric dimer and release of inhibition mediated by plasma membrane interactions are potential mechanisms of ARNO dependent receptor activation.
Structural data about the complex is required to confirm these ideas. Next to crystallographic approaches using other protein constructs, nuclear magnetic resonance (NMR) or mass spectrometry (MS) analysis of crosslinked complexes can be employed for this purpose.

6 Materials and Methods

6.1 Molecular biology

6.1.1 Agarose gel electrophoresis

Analysis of double stranded DNA (PCR products or digested plasmids) was performed by agarose gel electrophoresis. Agarose was dissolved in 0.5x TBE buffer by heating in a microwave until appearance of a homogenous solution. After cooling to approximately 60°C, ethidium bromide was added to the agarose in order to stain the separated DNA. Gels were run at a constant voltage of 100V for 15-30 min and DNA was subsequently visualized by UV irradiation (GelDoc, Bio-Rad). DNA fragment size was compared to the DNA 10kbps ruler (Fermentas).

TBE (1x)
90mM Tris Borate
2mM EDTA

6.1.2 Polymerase chain reaction (PCR)

Polymerase chain reaction was employed for the amplification of DNA fragments and whole plasmids in order to generate expression constructs for protein purification.
The Phusion DNA polymerase (Thermo Fisher Scientific) was used for all PCR reactions and resulting fragments were analyzed on agarose gels to verify the expected size. Purification of DNA fragments was done using the NucleoSpin PCR clean up kit (Macherey-Nagel) according to the manufacturers instructions.

6.1.3 Cloning of ARNO Sec7 EGFR JM fusion constructs and generation of Arf6 mutants

Generation of the JM-Sec7 fusion proteins was done by PCR amplifying both the EGFR JM domain and ARNO Sec7 coding sequences with adjacent restriction sites. The linker region was included in the primer as an overhang of the complementary sequences.

Restriction digest of the resulting fragments and target plasmid (pET28HT) was done using the FastDigest restriction enzymes (Fermentas, Thermo Scientific) for 30' at 37°C (restriction sites from 5' to 3'on pET28 HT: EcoRI, KpnI, HindIII). Subsequently fragments were sequentially ligated to the vector using the Rapid Ligase Kit (Roche Applied Science) for 5 minutes at room temperature. Ligation reactions were transformed into chemically competent DH5α cells.

Arf6 mutants were generated in Arf6 in the plasmid pASK IBA 45+ NΔ13Arf6. Primers were designed to fully amplify the plasmid (two primers for single strand amplification in opposite directions) and one primer contained the respective mutation in the coding sequence. Amplified vectors were 5' phosphorylated using Polynucleotide kinase (PNK, NEB) for 1h at 37°C. Subsequently the phosphorylated vectors were ligated with the Rapid Ligation Kit (Roche) and transformed into DH5α cells (see below). N-terminal truncations of ARNO Sec7 were generated with the same protocol in the plasmid pET15b ARNO Sec7.

6.1.4 Transformation of chemically competent E.coli cells

Competent cells were thawed on ice. Up to 5µl ligation reaction or 1ng to 100ng plasmid DNA was mixed with 50µl of competent cells and incubated on ice for 30min. After a heat shock (42°C) for 45 seconds, 500µl LB medium was added and the resulting mixture was incubated at 37°C for 45min. Subsequently the cells were harvested by centrifugation (1000g for 5 minutes), the pellet was resuspended in a small volume (50µl LB) and distributed on a LB Agar plate containing the appropriate antibiotics. The plates were incubated overnight at 37°C and subsequently stored at 4°C.

6.1.5 Preparation of chemically competent E.coli cells

The desired E.coli strain was grown over night in LB medium. The following day, 100µl of the culture were added to 20ml TYM medium in a 100ml flask. After growth to an OD_{600} of 0.2-0.8 the whole medium was transferred to 2l flask containing additional 100ml of TYM. Growth to an OD_{600}0.5-0.9 was followed by further addition of 300ml TYM. All incubation steps take place at 37°C and medium is heated to 37°C prior to addition.

When the final culture reaches an optical density of 0.6 it is rapidly cooled on ice. Bacterial cells are centrifuged for 15 minutes at 2000g and 4°C. The resulting pellet is resuspended in 100ml ice cold TfBI buffer and spun down for 8 minutes at 2000g and 4°C. Finally the cell pellet is resuspended in 20ml of TfBII buffer, transferred to small reaction vials in appropriate amounts and stored at -80°C after flash freezing in liquid nitrogen.

TYM medium (1l)

20 g bacto trypton
5 g yeast extract
5.84 g NaCl
2.46 g $MgSO_4$

TfBI buffer

30 mM KAc
50 mM $MnCl_2$
100 mM KCl
10 mM $CaCl_2$
15 % (v/v) glycerol

TfBII buffer

10 mM NaMOPS pH 7.0
75 mM $CaCl_2$
10 mM KCl
15 % (v/v) glycerol

6.1.6 DNA preparation and validation of sequences

Plasmids were replicated in E.coli DH5α and isolated using the Macherey-Nagel Plasmid Mini Prep Kit according to the manufacturer's protocol. Pure plasmid DNA was sent for sequencing and results were analyzed with a sequence alignment tool (EMBOSS Needle).

6.2 Protein Expression and purification

6.2.1 Bacterial culture and induction of protein expression

E.coli BL21 DE3 harboring the expression plasmid of choice were grown over night at 37°C in Luria Bertani (LB) medium supplemented with the appropriate antibiotics. The main culture was inoculated with 1% preculture and grown at 37°C until OD600

reached 0.6-0.8. Cells were cooled to 20°C and induced with 0.2mM IPTG (ARNO constructs) or kept at 37°C while adding 200 ng/ml anhydrotetracycline (AHT for Arf6 constructs). Protein expression lasts for 4h at 37°C and over night at 20°C. After expression bacterial cell were harvested via centrifugation at 5000g for 15 minutes at 4°C and the pellets were either immediately used for purification or stored at -80°C for up to 6 months.

6.2.2 Cell lysis for protein purification

Bacterial cells or Sf9 cells were resuspended in specific lysis buffer supplemented with 2mM β-mercaptoethanol and protease inhibitor (inhibitor mix (Serva) or leupetin/aprotinin and 1mM PMSF). Lysis was performed using a french pressure system or a microfluidizer (Microfluidics International Corporation, Newton USA). Subsequently the lysate was cleared of insoluble material by centrifugation (25000 rpm, 4°C, JA 25.50 rotor, Avanti J-20 XP centrifuge from Beckman Coulter Inc.) and filtration through a 0.44µm filter membrane (Sigma Aldrich).

Lysis buffer (ARNO constructs)
50 mM HEPES pH 7.8
500 mM NaCl

Lysis buffer (EGFR constructs)
50 mM Tris pH 8
500 mM NaCl
5 % glycerol

Lysis buffer (Arf6)
50 mM Tris pH 7.4
150 mM NaCl
1 mM $MgCl_2$

6.2.3 Purification of recombinant proteins from cell lysates

Proteins were purified in a multistep procedure either with the help of an ÄKTA liquid chromatography system (GE Healthcare) or with the affinity matrix in solution. Arf6 was purified using StrepTactin High capacity resin (iba technologies). Cleared lysate was incubated for 1h at 4°C with constant mixing. The beads were separated by from the

soluble material by centrifugation (at 2000g and 4°C for 10') and washed twice with lysis buffer. Arf6 was eluted with 2.5mM desthiobiotin and stored in final buffer after gel filtration using Desalting columns (GE Healthcare).

For ARNO and EGFR constructs, the cleared lysate was applied to NiNTA columns (Hi-Trap Chelating HP 5ml, GE Healthcare) using an ÄKTA liquid chromatography system. The column was washed with buffer A and up to 5% buffer B and elution was performed with a gradient to 100% buffer B. The eluate was collected in fractions and analyzed on SDS PAGE gels. The fractions containing the protein of interest were pooled and dialyzed over night in the presence of an appropriate protease to remove the affinity tag (TEV or Thrombin, Sigma Aldrich).

Buffer A (ARNO)

50 mM HEPES pH 7.8
500 mM NaCl

buffer B (ARNO)

50 mM HEPES pH 7.8
50 mM NaCl
500 mM Imidazol

Buffer A (EGFR)

50 mM Tris pH 8
500 mM NaCl
5% glycerol

buffer B (EGFR)

50 mM Tris pH 8
50 mM NaCl
500 mM Imidazol
5 % glycerol

Dialysis buffer (ARNO)

50 mM HEPES pH 7.8
100 mM NaCl
2 mM β mercaptoethanol

dialysis buffer (EGFR)

50 mM Tris pH 8
100 mM NaCl
2 mM β mercaptoethanol

Thrombin concentration for cleavage

2.5 units/ mg of protein (Sigma Aldrich, Munich)

TEV concentration for cleavage

TEV was purified via Ni affinity chromatography (expression plasmid was a gift of A. Itzen, TU Munich; (*160*)). The activity was tested for each batch and the amount of protease required for digest of target protein was determined according to the obtained test results.

After dialysis the protein solution was cleared from precipitates by centrifugation (10', 5000 rpm, 4°C, Eppendorf Centrifuge 5804R, rotor: A-4-44) and the supernatant was applied to the NiNTA column to remove uncleaved protein and His tagged TEV protease. The flowthrough was collected and fractions analyzed on SDS PAGE gels. Fractions containing the desired proteins were pooled and concentrated to a final volume of 2ml before the final purification step via size exclusion chromatography (SEC). The resulting protein solution was concentrated and stored at -80°C in appropriate aliquots.

SEC buffer/storage buffer (ARNO)
20 mM HEPES pH 7.8
100 mM NaCl
1 mM DTT

SEC buffer/storage buffer (EGFR)
20 mM Tris pH 8
100 mM NaCl
1 mM DTT

SEC columns
Superose 12 column
Hi-Load Superdex 75/200 16/60 (GE Healthcare)

Material used for proteins concentration
Vivapore 10/20 Solvent Absorption Concentrators (Sartorius, Göttingen, Germany)
Amicon Ultra Centrifugal filter units (Merck Millipore, Darmstadt, Germany)

6.2.4 Purification of JIP4 LZII

The construct JIP4 LZII (392-462) was expressed as a GST fusion protein (expression plasmid was a kind gift of J. Menetrey). The cleared lysate was incubated with glutathione agarose for 1h at 4°C and washed twice with buffer B1 and B2. Subsequently the resin was resuspended in Buffer C and TEV protease was added to the solution. After

over night cleavage at 4°C the supernatant was collected, concentrated to a final volume 4ml and applied to a SEC column for final purification. Free JIP4 LZII elutes very late and forms a double peak. The first peak contains the desired protein as illustrated in figure 6.1. The final protein was concentrated (molecular weight cutoff (MWCO) of 10kDa is applicable due to dimer formation of JIP4 LZII) and stored at -80°C. The protein Mig6 EBR S1 was purified using the same protocol.

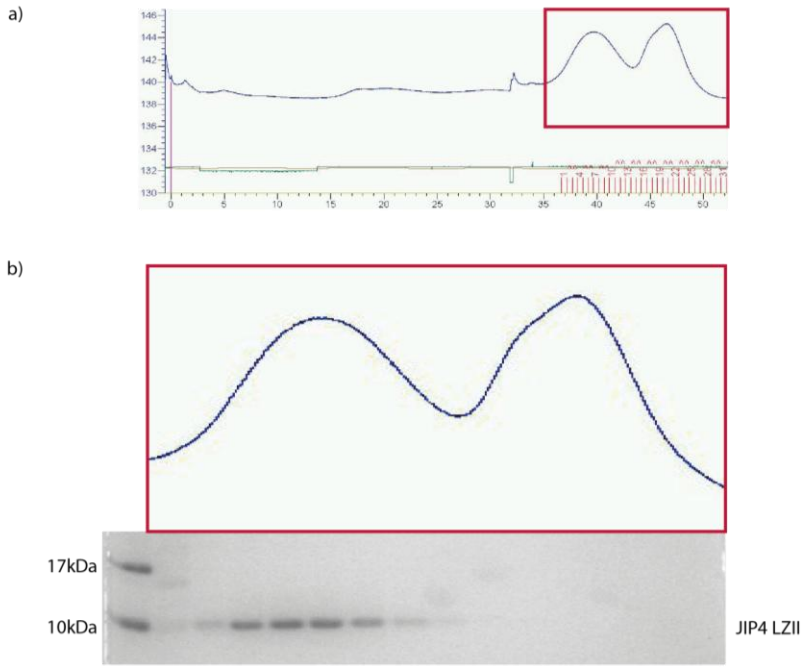

Fig. 6.1 Size exclusion chromatography elution profile of JIP4 LZII. Crude JIP4 LZII after over night digest of the GST tag is injected into a SEC column (Superdex 200 material, column volume: 50ml).The protein elutes very late and a double peak is observed (a). Only the first peak contains JIP4 LZII as shown by analyzing the collected fractions on Coomassie stained SDS PAGE gels (b).

Lysis buffer

50 mM Tris pH 8

250 mM NaCl

10 % glycerol

1 mM $MgCl_2$

storage buffer

20 mM HEPES pH 8

150 mM NaCl

2 mM $MgCl_2$

Buffer B1

50 mM Tris pH 8

300 mM NaCl

5 mM $MgCl_2$

2 mM DTT

Buffer B2

50 mM Tris pH 8

150 mM NaCl

5 mM $MgCl_2$

2 mM DTT

Buffer C

50 mM Tris pH 8

300 mM NaCl

5 mM $MgCl_2$

2 mM β mercaptoethanol

Resin

Glutathione Agarose 4B (Macherey-Nagel)

6.2.5 Purification of other protein constructs

The following other constructs are used in this study and purified according to one of the above described protocols:

The GEF domain of the bacterial protein DrrA (DrrA (340-533)) and the small GTPase Ran were purified like ARNO Sec7 constructs.

MIG6 EBR S1 was purified using the protocol for JIP4 LZII.

PLCγ SH2 GST was purified in a single step GST affinity purification followed by SEC into the final storage buffer.

Erk2 and NΔ17Arf1 were purified using NiNTA resin and SEC.

Lysis/wash buffer (DrrA and Ran)

50 mM Tris pH 7.6

300 mM NaCl

2 mM $MgCl_2$

20 mM Imidazol

lysis/wash buffer (Erk2 and NΔ17Arf1)

20 mM Tris pH 7.8

300 mM NaCl

2 mM $MgCl_2$

20 mM Imidazol

Lysis/wash buffer (MIG6 EBR S1 GST and PLCγSH2 GST)

20 mM HEPES pH 7.8

500 mM NaCl

Proteins were stored in 20mM HEPES (with appropriate pH) + 100mM NaCl and 1mM DTT.

6.2.6 Protein concentration determination and purity control

Concentration of protein solutions was determined with the Bradford reagent (Bio-Rad) according to the manufacturer's instructions. Pure protein was analyzed by measuring the absorbance at 280nm and using their specific extinction coefficient (ε) and the following equation:

$$\mathbf{A = c*\varepsilon*d}$$

A: absorbance of the sample at 280nm
c: concentration of the sample in mol/l
d: path length in cm
ε: molar extinction coefficient in l mol^{-1} cm^{-1}

Purity of proteins was controlled by separation on SDS PAGE gels and staining with Coomassie Brilliant Blue.

6.2.7 SDS Polyacrylamide gel electrophoresis (PAGE)

Analytical separation of proteins was performed according to the protocol by Laemmli (*205*). Separating and stacking gel solutions were independently prepared and sequentially poured between two appropriately spaced glass plates after induction of polymerization with tetramethylethylenediamine (TEMED) and ammonium persulfate (APS). Samples were mixed with SDS loading buffer, heated to 95°C for 5' and loaded on the gel for separation in SDS running buffer.

Stacking gel buffer
0.5 M Tris, pH 6.8

separating gel buffer
1.5 M Tris pH 8.8

SDS loading buffer (5x)
50 mM Tris pH 6.8
30 % glycerol
15 % SDS
600 mM DTT
Bromophenol Blue

Tris-Glycine running buffer (10x)
250 mM Tris
2 M glycine
1 % SDS

Example recipe for a 12% SDS PAGE gel

Acrylamide mix (30%)	2000 µl
Separating buffer	1250 µl
Water	1700 µl
SDS (10% stock)	50 µl
TEMED	2.5 µl
APS (10%)	25 µl

6.2.8 Tricine SDS PAGE

Tricine SDS PAGE was performed according to a published protocol (*206*). In brief an acrylamide-bisacrylamide (AB) solution was prepared and used to cast the gels. Electrophoresis is performed with tricine instead of glycine in the running buffer (only at the cathode). 10 % gels were used for the separation of JIP4 LZII and gels were further treated as described below.

Cathode buffer (10 x)

1 M Tris
1 M Tricine
1 % SDS

Anode buffer (10 x)

1 M Tris
0.225 M HCL

AB solution

48 g Acrylamide
1.5 g Bis Acrylamide
in 100 ml water

Gel buffer (3 x)

3 M Tris
1 M HCl
0.3 % SDS

4 % stacking gel

1 ml AB solution
3 ml Gel buffer
8 ml water

90 µl APS (10%)
9 µl TEMED

10 % separating gel

6 ml AB solution
10 ml Gel buffer
3 ml glycerol
11 ml water

150 µl APS (10%)
15 µl TEMED

6.2.9 Coomassie staining

SDS PAGE gels covered with Coomassie staining solution and stained for 30' at room temperature or heated in a microwave for 1' at 600W. Subsequently the gels were destained over night in Destaining solution. A paper towel was added to the solution to adsorb free dye and improve destaining.

Coomassie staining solution

10 % acetic acid
30 % methanol
700 mg/l Coomassie Brilliant Blue G250

Destaining solution

10 % acetic acid
30 % methanol

6.2.10 Western Blot and immunodetection of proteins

Proteins separated by SDS PAGE were transferred onto nitrocellulose membranes by a semi dry Western Blot. For this purpose the gel and the membrane are equilibrated in transfer buffer and mounted in between four buffer soaked pieces of Whatman paper. Transfer was achieved by applying 1 mA/cm^2 of gel for 45 minutes.
After blotting, the membrane was blocked in 5 % BSA in TBS-T for 30 minutes. Appropriate dilutions of primary antibody in 5 % BSA in TBS-T were subsequently added and incubated at 4°C. Incubation times ranged from 1h to over night. The membrane was thereafter washed three times with TBS-T and incubated with the fluorescently labeled secondary antibody (in 5 % BAS in TBS-T) for 1h. After three more wash steps the membrane was scanned using a Licor Odyssey Gel documentation system.

Transfer buffer

25 mM Tris
200 mM glycine
0.1 % SDS
20 % methanol

TBS-T

100 mM Tris/HCl pH 7.4
150 mM NaCl
0.1 % Tween 20

6.3 Protein modification

6.3.1 Labeling of JIP4 LZII with IAA fluorescein

The purified JIP4 LZII domain contains one cysteine residue that was modified using iodoacetamido fluorescein (IAA fluorescein, Sigma Aldrich). A five times molar excess of labeling reagent was incubated with the protein for 2 h at room temperature. Labeled proteins were desalted using a Desalting column (GE Healthcare) and an Äkta FPLC. Separation on Tricine SDS PAGE gels and visualization using UV irradiation (BioRad GelDoc) was employed to evaluate labeling efficiency and removal of free IAA fluorescein.

6.3.2 Covalent modification of proteins with biotin and detection via DotBlot

Proteins used in biochemical assays that required immobilization on a streptavidin-coupled matrix (pulldowns or ALPHA screen) were modified on free amine groups using NHS-LC-Sulfo-Biotin (Pierce Protein Science). The protein was incubated with 5 times molar excess of reagent in an appropriate buffer (HEPES or phosphate buffered solutions) for 1 h at room temperature. If protein stability was a concern, the reaction was performed on ice for 2 h. The reaction was stopped by the addition of 1 M Tris pH 6.8 to a final concentration of 1 mM Tris. Subsequently the labeled protein was desalted using 5 ml Desalting columns (GE Healthcare) on an Äkta FPLC.
Biotin modification was evaluated by immobilizing the final protein on a nitrocellulose membrane (Whatman) and detection of biotin with FITC coupled biotin reactive antibodies (DotBlot).

6.4 Peptide synthesis and modification

Peptide synthesis was done in a Peptidesynthesizer PS3 (Protein Technologies Inc.) using standard Fmoc chemistry. A Rink amide AM resin was used as a solid phase support and each amino acid coupling included the following steps:

1. Deprotection (2x): 20 % piperidine in dimethylformamide (DMF) for 5 minutes.

2. Activation of amino acids, linker or biotin/fluorescein in 0.4 M morpholine in DMF by adding O-Benzotriazole-N,N,N',N'-tetramethyl-uronium-hexafluoro-phosphate (HBTU) in a 1:1 molar ratio for 1 minute.
3. Coupling for 40 minutes at room temperature.

The coupled reagents were added in a 4 x molar excess to the peptide chains and washing of the resin after coupling and deprotection was done with pure DMF. After the synthesis, the resin is washed with dichlormethane (DCM) and dried over night in a vacuum. The resulting peptides are cleaved from the resin with 95 % trifluoroacetic acid and 2.5 % triisopropylsilane (TIPS) for 2 h at room temperature.
The peptide is precipitated with diethyl ether and dried over night in a vacuum. Purification of the crude material is done using HPLC and peptide mass was validated by mass spectrometry.

6.5 Screening for small molecule inhibitors

The in-house compound library contains approximately 17000 small molecules that are stored as 1 mM stock solutions in DMSO at -80°C. The compounds were thawed and prediluted to 120 µM in dilution buffer before screening.
The assays was performed in black 384 well plates in the presence of 0.01 % Triton X100 and 10 % DMSO. 320 compounds were screened on one plate next to 32 positive and negative control reactions (no compound or no Arf6 respectively). Reagents were added to each well in the following order by the TECAN Evolution pipetting robot:

10 µl Arf6 GTP (2 µM)
5 µl pre-diluted compound solution
5 µl fluorescein-labeled JIP4 LZII (250 nM)

After two hours incubation at room temperature in the dark, the fluorescence polarization (FP) values were measured in a TECAN Ultra plate reader. Robustness of the assay was evaluated by repeating the measurement after over night incubation at room temperature. No difference due to incubation time was observed. Z' values (*170*) were calculated for each plate and hit compounds identified by reduction of the FP values more than five standard deviation below the mean.

Screening buffer	***Dilution buffer***
1.33 x PBS pH 7.4	31.8 % DMSO
2.66 mM $MgCl_2$	0.05 % Triton X100

6.6 Crystallization of proteins and x-ray diffraction analysis

Crystallization of macromolecules and subsequent analysis of x-ray diffraction patterns is an elegant method to obtain information about the structure of a molecule with atomic resolution. In this study, constructs of ARNO Sec7 were crystallized in the presence of 2-20 fold molar excess of the EGFR JM peptide. Furthermore, fusion proteins of ARNO Sec7 with EGFR JM were employed in independent screens for crystallization conditions. All proteins were used in concentrations of 8 – 10 mg/ml in all screens and subsequent refinement of crystallization conditions.

Initial screens were performed using the Qiagen crystallization kits (JCSG Core I-IV Suites, Classics Suite, PACT Suite, PEG I+II Suite, Protein Complex Suite) and the sitting drop vapor diffusion method. Identified conditions that allowed crystal formation were reproduced in a 24-well plate using the hanging drop method. The obtained crystals were picked using a nylon loop and frozen in liquid nitrogen. Initial diffraction was analyzed in an in house x-ray source (MICROSTAR x-ray source, Bruker AXS Inc., Madison USA; Mar345 Image Plate Detector, marresearch, Norderstedt, Germany). Full data sets were obtained at the Swiss Light source (X10SA x-ray source, Paul Scherrer institute, Villigen, Switzerland) and processed using the XDS software package (*207*). The structures were solved using molecular replacement using the ARNO Sec7 structure as a search model (PDB: 1PBV, (*180*)) and the software package Phaser (*208*).

All crystals analyzed belong to the space group $P2_13$ (cubic) and diffracted from 1.8 to 2.6 Å. Unit cell parameters are $\alpha = \beta = \gamma = 90°$, a = b = c = 89 Å.

6.6.1 Microseeding of protein crystals

Crystals of fusion constructs between ARNO Sec7 and EGFR JM, which were to small after initial screening for conditions and refinement of these conditions, were optimized via protein crystal microseeding (*209*). Therefore, the obtained crystals were diluted in 50 µl of mother liquor and vortex heavily to break the macrocrystals into smaller

microseeds. Bigger fragments were removed by centrifugation (5' at room temperature and 6000 rpm in an Eppendorf table top centrifuge). The supernatant was sequentially diluted from 1:10 to 1:10000 and the resulting microseed stock solutions were mixed with fresh protein in a hanging drop. The concentration of added protein was reduced (4 – 8 mg/ml). This facilitates crystal growth and reduces the de novo generation of seeds. Therefore, growing of crystals from the microseed stock is enhanced. Crystals for diffraction analysis appeared after 4 days of growth in a 1:100 dilution of microseeds both with 6 mg/ml and 8 mg/ml fresh protein.

6.7 Cell culture

6.7.1 General handling of mammalian cells and cell lines

Adherent mammalian cells were grown at 37°C in the presence of 5 % CO2 and passaged every 2-3 days to maintain confluence below 90 %. For culture maintenance, the cells were grown in their respective culture medium supplemented with 10% fetal calf serum (FCS). For passage cells were rinsed with PBS and subsequently detached from the surface via the addition of Trypsin-EDTA solution. The cell suspension was appropriately diluted and transferred to new culture flasks.

6.7.2 Stimulation with growth factors or serum

Normal growing cells were transferred to FCS free medium 24 h prior to stimulation. After this starvation the desired growth factor was diluted in fresh serum free medium and added to the cells for 2-4 h. For serum stimulation, medium was exchanged to FCS containing medium.

6.7.3 Preparation of cell lysates

Cells used for western blot or pulldown experiments were harvested as follows. The growth medium was discarded and the cells were put on ice and immediately washed with ice cold PBS. Covered with approximately 1 ml of PBS, cells were removed from the plate surface using a Cell scraper (TPP). The cells were transferred into Falcon tubes and

pelleted by centrifugation (1000g at 4°C for 5' in an Eppendorf Centrifuge 5804-R). Afterwards the cell pellet was resuspended and lysed in lysis buffer for 15 minutes on ice in the presence of a protease inhibitor mix (Serva). Insoluble material was removed by centrifugation for 15 minutes at 12000rpm and 4°C in an Eppendorf table top centrifuge. Protein concentration was determined using the Bradford assay.

Lysis buffer

50 mM Tris pH 7.5
200mM NaCl
10mM $MgCl_2$
1 % Igepal
5% glycerol

6.8 Analytical methods

6.8.1 High performance liquid chromatography (HPLC)

HPLC was employed for the purification of solid phase synthesized peptides. Up to 1 ml of crude peptide solution was loaded onto a Nucleosil 100 – 5C18 reverse phase column and eluted in a gradient from 0 – 60 % buffer B in 40 minutes with a constant flow of 5 ml/minute. The column was rinsed with 100 % buffer B and equilibrated in 100 % buffer A using a rapid gradient. All steps were performed on an Agilent 1200 series HPLC (Agilent Technologies). Peptide containing fractions were collected and the solvent was removed by evaporation in a SpeedVac. The resulting peptide pellet was resuspended in the desired buffer and analyzed using ESI-MS (see below).

Buffer A

0.1 % formic acid
in water

Buffer B

0.1 % formic acid
in acetonitrile

6.8.2 Analytical Size Exclusion Chromatography (SEC)

Proteins were mixed and incubated for 20 minutes at room temperature to allow complex formation (EGFR construct ICD1022 was incubated on ice for 45 minutes due to protein stability). Analysis of complexes was done using a Waters HPLC system (Waters Corporation, Milford, USA) and Superdex 75 10/300 GL or Superdex 200 10/300 GL SEC columns (GE Healthcare, Munich). A total volume of 40 µl was injected and run for 60 minutes at 0.5 ml/min. The BioRad molecular weight standard was employed as a reference.
For SDS PAGE analysis of elution fractions, they were collected with a fraction collector (Waters Corporation, Milford, USA), separated on a 12 % SDS PAGE gel and further analyzed by Coomassie Brilliant Blue staining.

analytical SEC buffer
50 mM Tris pH 7.8
100 mM NaCl

6.8.3 Electrospray Ionization Mass spectrometry (ESI MS)

Recombinantly expressed proteins were separated and desalted on a C4 reverse phase column (Grace Vydac 214TP C4 5µ)by running a gradient from 20 % to 70 % buffer B (see buffers used for HPLC analysis above) in 10 minutes (flow: 200 µl/min). MS analysis was done in a Finnigan LCQ Advantage Max Mass spectrometer. Spectra were analyzed using the software Xcalibur (Thermo Fisher Scientific Inc., Waltham, USA) and MagTran (*210*).
Purified solid phase synthesized peptides were separated on a MultoHigh 100 RP 18 5µ reverse phase column and analyzed in a Bruker Esquire HCT Electron Spray Mass Spectrometer. Obtained spectra were analyzed with the Compass software (Bruker).

6.8.4 Dynamic Light Scattering (DLS)

Buffers used for DLS measurements were filtered and degassed before the experiment. Proteins were diluted to 1 mg/ml in assay buffer (20 mM Tris pH 8, 100 mM NaCl). Measurements were performed in a Quartz cuvette using the DynaProTitan (Wyatt

Technology) DLS detector. The count rate measuring the scattered light intensity should be stable before the actual measurement. All values were obtained with 50 % light laser intensity and analyzed using the DynaProV6 Dynamic software.

6.8.5 Circular dichroism (CD) spectroscopy

Far UV CD spectroscopy was employed to evaluate the secondary structure of the purified proteins. The measurements were performed in a Jasco J-815 CD spectrometer at 25°C. Protein solutions were prepared in 20mM HEPES pH 8, 100mM NaCl, 2mM DTTto a final concentration of 0.5 mg/ml. Spectra were obtained between 178nm and 260nm (50nm/min and 1nm steps). The molar ellipticity was calculated using the following formula:

$$\Theta_{MRW,,\lambda} = \Theta_{\lambda} * MRW / 10 * c * d$$

$\Theta_{MRW,,\lambda}$: molar ellipticity[deg dmol^{-1} cm^{2}]

$\Theta_{\lambda:}$ measured ellipticity [deg]

MRW: average molecular weight of the amino acids in the protein [g mol^{-1}]

c: concentration of protein [g ml^{-1}]

d: path length [cm]

6.9 Biochemical assays

6.9.1 ALPHA screen

Alpha Screen measurements were performed using Streptavidin coupled donor beads and either fluorescein detecting (for the JIP4 LZII Arf6 *in vitro* interaction) or protein A coupled (for the GTPase activation sensor) acceptor beads (Perkin Elmer). The beads were diluted to a final concentration of 100 µg/ml. All pipetting steps were performed under subdued light conditions to avoid bleaching of Alpha Screen beads.
For the Arf6 JIP4 LZII interaction assay the indicated concentrations of proteins were added to the bead mixture in PBS + 3 mM $MgCl_2$ in the presence of 0.1 mg/ml bovine serum albumin (BSA).

Biotinylated effector protein (GGA3 or PAK1) was used in a final concentration of 100 nM and mixed with the indicated amounts of *in vitro* nucleotide preloaded GTPase (Arf1, Arf6 or Rac1) or cell lysate in PBS + 3mM MgCl2.
The reactions were performed in a white 384-well microtiter plate (Proxiplate, Perkin Elmer) and incubated for 2h or over night at room temperature in the dark. All measurements were taken on a plate reader equipped with an Alpha Screen module (LB940 Mithras, Berthold Instruments) and excitation and emission times set to 0.5 s.

6.9.2 Pulldown of Arf GTPases by immobilized effector proteins

Arf GTPases were preloaded with either GDP or GTP (see Nucleotide Exchange assay). 10 µl of Glutathione 4B Agarose (Protino, Macherey-Nagel) was incubated with 4 µM of GST tagged effector protein (JIP4 LZII or GGA3) and 2.5 µM nucleotide preloaded GTPase in Pulldown Buffer. For competition experiments, 20 µM of soluble JIP4 LZII was added. Incubation was done over night at 4 °C and constant shaking of the reaction tubes. The agarose resin was pelleted by centrifugation (2500 rpm, 5', 4°C, Eppendorf table top centrifuge) and washed two times with 500µl wash buffer. Finally the beads were resuspended in SDS loading buffer prior to analyzing the reaction via SDS PAGE and Western Blot or Coomassie stain.

Pulldown buffer
20 mM HEPES pH 7.4
150 mM NaCl
5 mM $MgCl_2$

Wash buffer
20 mM HEPES pH 7.4
300 mM NaCl
5 mM $MgCl_2$
0.02 % Triton X100

6.9.3 Pulldown of Rac1 GTP from cell lysates

Precipitation of GTP bound Rac1 was facilitated with the help of the effector protein Pak1. The Rac binding domain of Pak1 was biotin-modified and immobilized on monomeric avidin agarose (Pierce Protein Science). The desired amount of cell lysate was added to the immobilized effector (20 µg protein on 10 µl agarose beads) and incubated for 1h at 4°C. The beads are separated from the supernatant by centrifugation

(2500 rpm, 5', 4°C, Eppendorf table top centrifuge) and washed three times with wash buffer. The beads were finally resuspended in 20µl SDS loading buffer and further analyzed by SDS PAGE and Western Blot.

Wash buffer	***Antibody***
25 mM Tris pH 8	anti Rac1 (polyclonal, Millipore)
30 mM $MgCl_2$	1:1000
40 mM NaCl	anti-mouse IgG GAM800 (polyclonal, Licor)
1 mM DTT	1:20000

6.9.4 Fluorescence Polarization (FP)

Fluorescein labeled proteins (JIP4 LZII or ARNO Sec7) were incubated with increasing concentrations of interaction partners or control proteins in a black 384 well plate. For JIP4 LZII, a final concentration of 100 nM fluorescein labeled protein was sufficient while 200 nM of ARNO Sec7 fluorescein was used in the assays. 100 mM bovine serum albumin (BSA) was added to the reactions containing ARNO Sec7 fluorescein to reduce unspecific binding. The reactions were incubated at room temperature for 1 h or at 4 °C for 2 h if EGFR ICD constructs were present. Fluorescence polarization was measured in a TECAN Ultra plate reader (TECAN, Crailsheim, Germany).

FP buffer (JIP4 LZII)	***FP buffer (ARNO Sec7)***
PBS pH 7.4	50 mM HEPES pH 7.8
2 mM $MgCl_2$	150 mM NaCl
0.01 % Triton X100	0.01 % Triton X100

6.9.5 Nucleotide Exchange

Arf GTPases were preloaded with GDP. Therefore, the nucleotide binding site was destabilized by the addition of 2 mM ethylenediaminetetraacetic acid (EDTA) for 10 minutes at 37 °C in the presence of 50 µM GDP. Adding 3 mM $MgCl_2$ stabilizes the binding pocket and the excess of GDP in the solution results in predominant GDP associated GTPase. Preloaded Arf (1 µM) was mixed with ARNO Sec7 (from 12.5 nM to

200 nM) in phosphate buffered saline (PBS) supplemented with 2 mM $MgCl_2$. The exchange reaction was started by the addition of 50 µM GTP and followed by measuring the tryptophan fluorescence in an appropriate plate reader (VarioScan, Thermo Electron corporation or Enspire Multimode Reader, Perkin Elmer). This parameter changes dependent on the bound nucleotide and is therefore suitable for the detection of the catalytic activity.
The resulting curves were fit using a linear regression model (software: Graphpad PRISM) for the early parts of the reaction (the first 150-300 s dependent on the GTPase GEF pair).

6.9.6 Thermal Shift

Thermal stability of proteins was evaluated using a fluorescence-based assay that monitors the unfolding of the protein of interest in solution. Therefore, 2 – 10 µM of protein was incubated with 5x SYPRO Orange (Molecular Probes) in a final volume of 100 µl.
A Real Time PCR thermo cycler (Bio-Rad) was used for following the change in fluorescence intensity (mant fluorescence) in a temperature gradient from 20 °C to 75 °C (incremental temperature increase by 1 K). Total intensity (RFU) and change in intensity (ΔRFU) were plotted against the temperature. The melting temperature is easily visible as the local maximum observed in the ΔRFU plot and is a quantitative parameter for evaluating the thermal stability of a protein in the employed buffer conditions.

6.9.7 Crosslinking assay

Proteins were mixed in crosslink buffer to obtain final concentrations of 25 µM for ARNO Sec7 constructs and 10 µM for EGFR constructs. 25µM bovine serum albumine was added to reactions containing EGFR JM peptide variants to reduce unspecific binding. The reactions were incubated for 15 minutes at room temperature to allow complex formation. Subsequently 5 mM Bis(Sulfosuccinimidyl)suberate (BS3, Thermo Scientific) was added and incubated for another 20 minutes at room temperature. The reaction was stopped by the addition of SDS loading buffer. EGFR ICD crosslinks were

separated on 10 % SDS PAGE gels while EGFR JM crosslinks were separated on 15 % SDS PAGE gels. Crosslinks were visualized with Coomassie Brilliant Blue staining and detected in a Licor Odyssey gel scanner (Licor). All shown results are representative gels. Experiments were performed at least 3 times for each analyzed construct.

Crosslink buffer

20 mM HEPES pH 8

150 mM NaCl

5 mM $MgCl_2$

0.005 % Triton X100

6.9.8 Kinase assay for EGFR constructs

For the evaluation of enzymatic activity for EGFR constructs an *in vitro* phosphorylation assay was employed. 0.5 µM EGFR ICD1022 and KC1022 (lacking the JM domain) were incubated with 15 µM of the SH2 domain of PLCγ at 25 °C. ATP was added to a final concentration of 500 µM to start the reaction. Samples were taken after 1, 2 and 5 minutes for ICD1022 and 10, 30 and 60 minutes for KC1022.

Adding SDS loading buffer and boiling the sample stopped the reaction. The samples were separated on a SDS PAGE gel, blotted onto a nitrocellulose membrane and phosphorylation was detected using phospho-tyrosine specific antibodies (pY-99, Santa Cruz).

Kinase reaction buffer

20 mM HEPES pH 7.4

150 mM NaCl

5 mM $MgCl_2$

6.10 Materials

EQUIPMENT, TYPE	MANUFACTURER
Agarose gel chamber	Institue for chemistry, Bonn, Germany
Äkta, FPLC	GE Helathcare
Äkta, Prime plus	GE Helathcare
Analytical balance	Sartorius AG
Avanti J-20 XP centrifuge	Beckman Coulter
Balance	Sartorius AG
Blot chamber, Semi Dry	Bio-Rad
CD spectrophotometer, J-815	Jasco
centrifuge, 5417C	Eppendorf
centrifuge, 5804R	Eppendorf
centrifuge, 5810R	Eppendorf
DynaProTitan	Wyatt Technology
Eppendorf Mastercycler Gradient	Eppendorf
Esi MS, esquire HCT	Bruker Daltonics
Esi MS, Finnigan LCQ Advantage Max	Thermo Scientific
French press	Thermo Scientific
gel documentation system, Odyssey	LICOR
Hi Trap Desalting columns	GE Healthcare
Hi-Load Superdex 200 26/60 prep grade	GE Healthcare
Hi-Trap Chelating HP columns	GE Healthcare
HPLC, 1100 Serie	Agilent
HPLC, 1200 Series	Agilent
Impressa Xr50	Jura
incubator, Hera Cell	Heraeus
Mar345 Image Plate Detector	Marresearch GmbH
Microfluidizer	Microfluidics International Corporaton
MicroMax 007 HF x-ray source	Rigaku
multimode platereader, Enspire	Perkin Elmer
Nanodrop, ND-1000	PeqLab
Peptide synthesizer PS3	Protein Technologies Inc.
pH electrode MP220	Mettler Toledo
Pipetting robot, Freedom Evo	Tecan
Pipetting robot, mosquito	TTP Labtech
platereader infinite M 200	Tecan
platereader TECAN Ultra	Tecan
platereader Varioscan	Thermo electron corporation
real-time PCR Cycler; iCycler iQ5	Bio-Rad
rotors, JLA 8.1000,JA 25.50	Beckman Coulter
Shaker/Incubator innova 4430	New Brunswick Scientific
SpeedVac, Concentrator 5301	Eppendorf
sterile hood, HeraSafe	Heraeus
Superdex 200 10/300 GL	GE Healthcare
Superdex 75 10/300 GL	GE Healthcare
VersaDoc 5000 CCD camera	Bio-Rad
Waters HPLC system	Waters

CHEMICALS AND REAGENTS	MANUFACTURER
Standard chemicals were purchased from Roth or Sigma unless otherwise stated.	
1,4-Dithiothreitol (DTT)	Sigma Aldrich
1000 bp DNA ladder	PeqLab
2-mercaptoethanol	Sigma Aldrich
Agarose	Invitrogen
Ampicillin	Sigma Aldrich
AMPPNP (Adenylyl-imidodiphosphate)	Roche
Bis(Sulfosuccinimidyl)suberate (BS3)	Thermo Scientific
Bradford Reagent	Bio-Rad
BSA (bovine serum albumin)	AppliChem
Chloramphenicol	Sigma Aldrich
Coomassie Brilliant Blue G250	AppliChem
Ethidium Bromide	Roth
EZ-link Sulf- NHS-LC Biotin	Pierce
FITC detection Kit	PerkinElmer
Fluorescein Isothiocyanate (FITC)	Roth
Gel filtration MW standard	Bio-Rad
Glutathione (reduced)	Roth
Iodoacetamido (IAA) fluorescein	Sigma Aldrich
Kanamycin	Sigma Aldrich
LB medium mix	Roth
Low Molecular Weight Protein Marker	GE Healthcare
NHS fluorescein	Sigma Aldrich
PAGE Ruler Prestained Plus	Thermo Scientific
Protease Inhibitor Mix	Serva
Protein A detection kit	PerkinElmer
SYPRO Orange (5000x)	Molecular Probes
TEMED (N-N-N'-N'-tetramethylethylenediamine)	Merck
Triton X-100	Merck

CONSUMABLES	MANUFACTURER
384 well plate, black	Greiner Bio One
96 well plate, black, half area	Greiner Bio One
Amicon concentrators	Millipore
Dialysis tubes	Spectrum Laboratories Inc.
filter membrane, 45 µm	Sigma Aldrich
Glutathione Agarose 4B	Protino, Macherey-Nagel
Nitrocellulose membrane	Schleicher and Schuell
PCR purification kit	Macherey-Nagel
Plasmid mini präp kit	Macherey-Nagel
Proxi Plate, 384 well, white	Perkin Elmer
Strep Tactin Superflow High capacity resin	iba
Whatman filter paper	Schleicher and Schuell

CELL CULTURE	MANUFACTURER
DMEM	PAA
Dulbecco's PBS	PAA
Fetal Calf Serum (FCS)	Lonza
Penicillin/Streptomycin (100x)	PAA
RPMI	Gibco
Trypsin/EDTA (10x)	PAA

SOFTWARE	MANUFACTURER
Adobe Illustrator	Adobe Systems
CCP4	STFC Rutherford Appleton Laboratory
Compass	Bruker Daltonics
DynaPro V6 Dynamic	Wyatt Technology
Empower	Waters
i-control	Tecan
Mac PyMol	Schrödinger, LLC
Rock Maker	Formulatrix
Xcalibur 2.0.7	Thermo Fischer Scientific
XDS	MPI, Heidelberg

ANTIBODIES	MANUFACTURER
Arf1, mouse, monoclonal	Millipore
Arf6, mouse, monoclonal	Santa Cruz (sc-7971)
Bitotin, mouse, monoclonal, FITC coupled	Sigma Aldrich
mouse-IgG, goat, NIRD (800) coupled (GAM800)	Thermo Scientific
phospho-tyrosine, mouse, monoclonal	Santa Cruz (sc-7020)
Rac1, mouse, polyclonal	Millipore
Rac1, rabbit, polyclonal	Santa Cruz (sc-95)

CELL LINES AND BACTERIAL STRAINS	USED FOR:
Hela cells	GTPase activation experiments
NIH 3T3 cells	GTPase activation experiments
E.coli BL21 (DE3)	protein expression
E.coli DH5 α	molecular biology and plasmid propagation

7 Appendix

7.1 Supplementary Figures

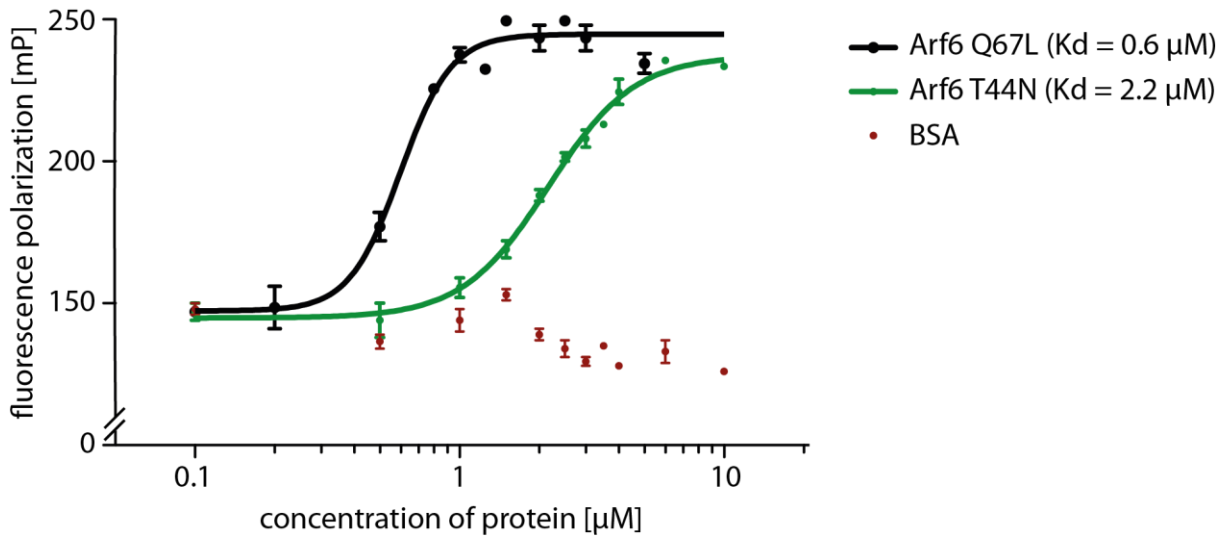

Supplementary Figure 1. Fluorescence polarization assay with Arf6 mutants locking the GTPase in the active or inactive conformation. Fluorescein labeled JIP4 LZII was incubated with increasing concentrations of Arf6 Q67L ("active") or Arf6 T44N ("inactive"). As a negative control, BSA was employed and results in no increase of the FP signal. Results are mean +/- SEM (n=5).

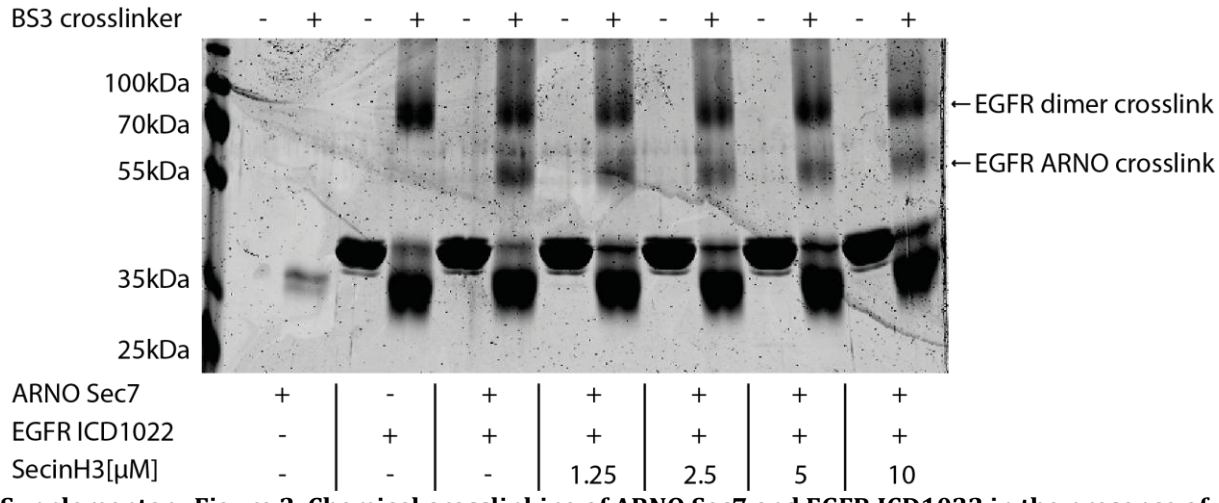

Supplementary Figure 2. Chemical crosslinking of ARNO Sec7 and EGFR ICD1022 in the presence of SecinH3. The indicated proteins were incubated with the chemical crosslinker BS3 in the presence of increasing concentrations of SecinH3 or DMSO. Crosslinks were visualized on SDS PAGE gels stained with Coomassie Brilliant Blue.

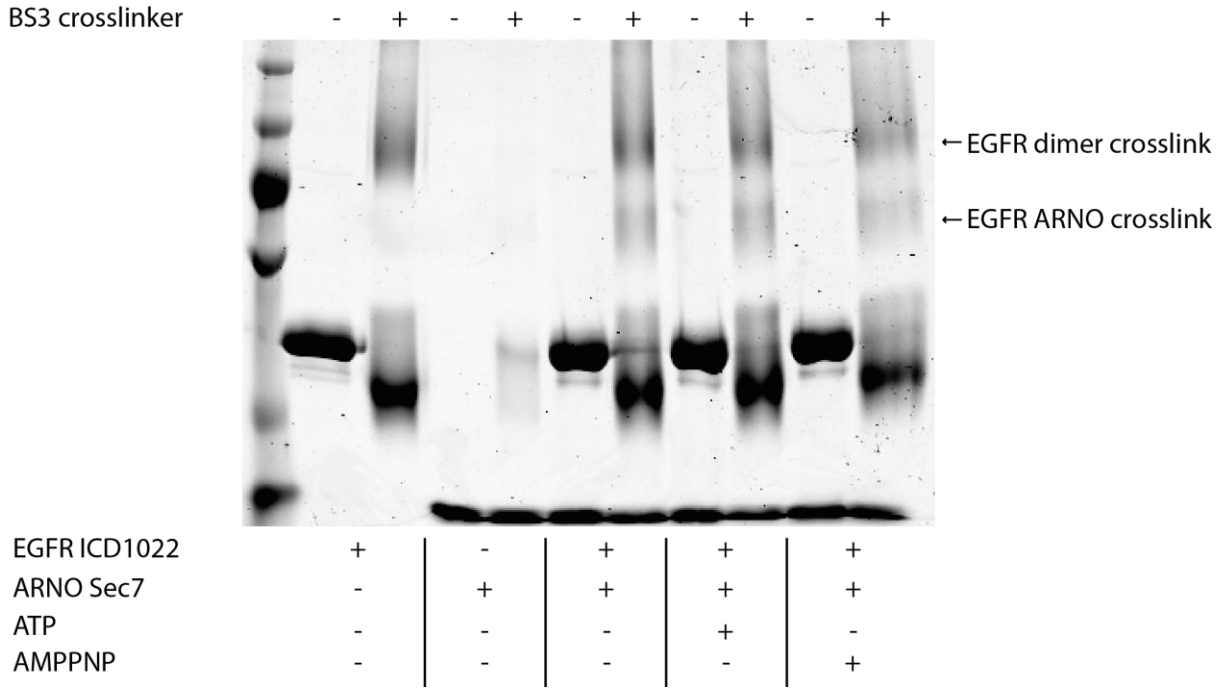

Supplementary Figure 3. Chemical crosslinking of ARNO Sec7 and EGFR ICD1022 in the presence of different adenine nucleotides. The indicated proteins were incubated with the chemical crosslinker BS3 in the presence of ATP or the non-hydrolysable nucleotide AMPPNP. Crosslinks were visualized on SDS PAGE gels stained with Coomassie Brilliant Blue.

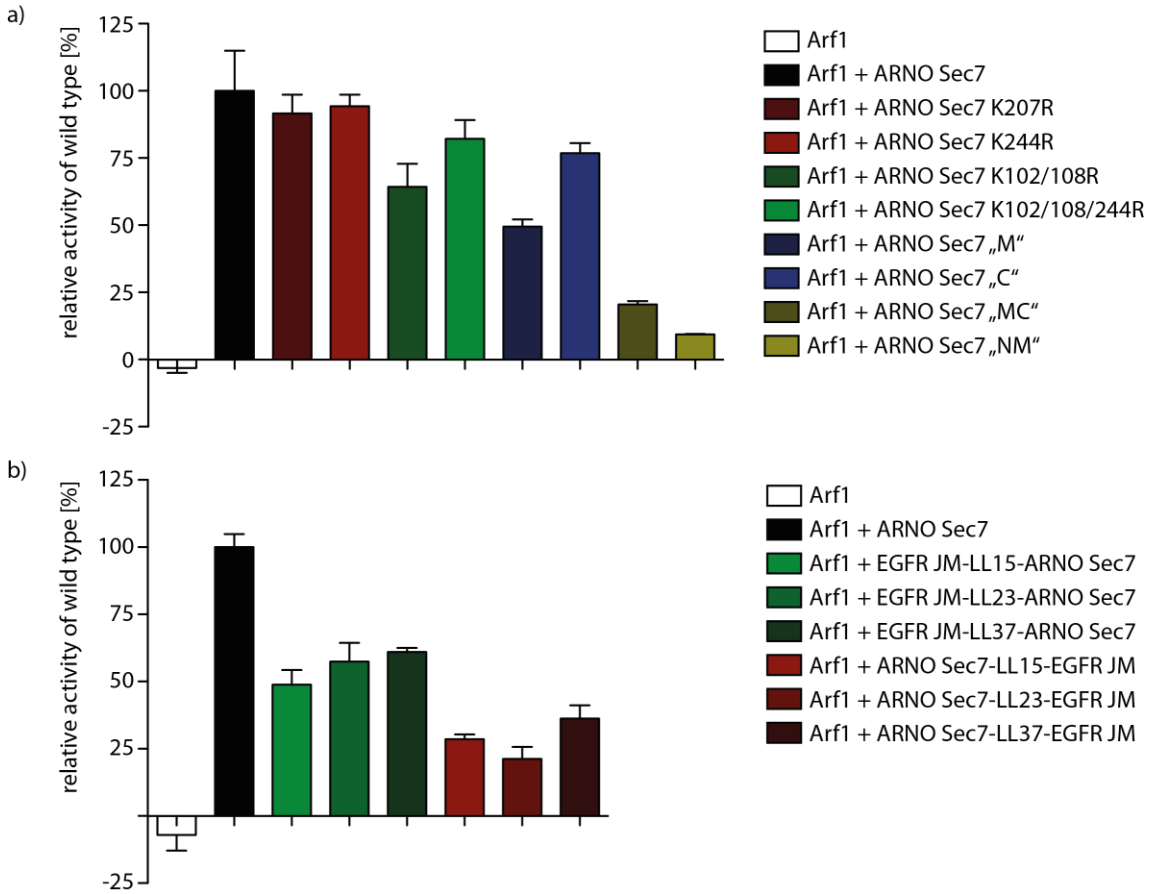

Supplementary Figure 4. Nucleotide exchange activity of ARNO Sec7 constructs employed in this study. Arf1 preloaded with GDP was incubated with the indicated ARNO Sec7 constructs in the presence of excess GTP. The change in tryptophan fluorescence is measured and fitted to a linear regression model. The slope is plotted as mean +/- SEM (n=4).

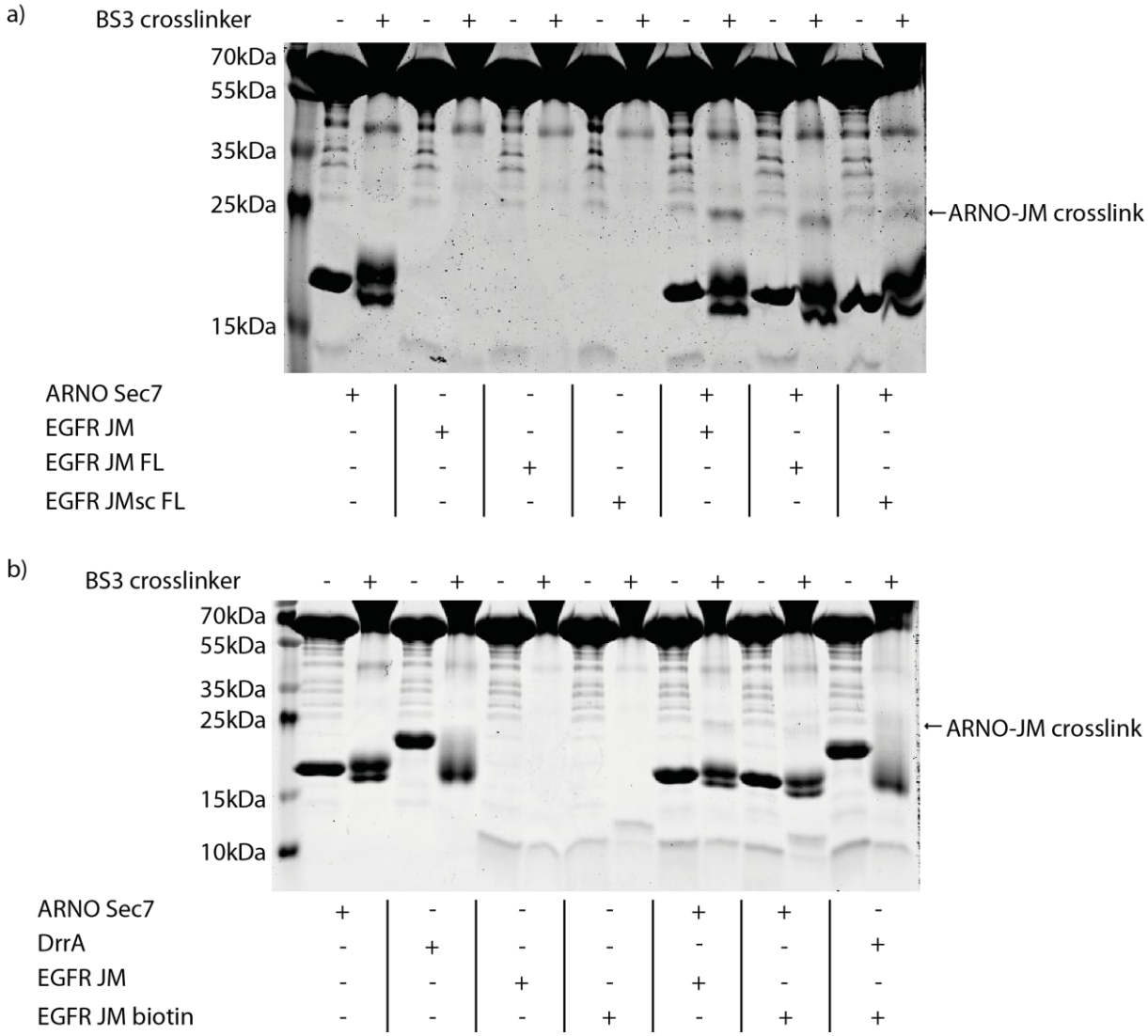

Supplementary Figure 5.Chemical crosslinking of N-terminally modified EGFR JM with ARNO Sec7. The N-terminus of EGFR JM was modified with fluorescein ("FL",a) or biotin (b). Thus, the primary amine was removed as a potential crosslinking site in experiments with lysine reactive crosslinker reagents. The resulting constructs were crosslinked to ARNO Sec7 with BS3. A scrambled version of EGFR JM ("sc") and DrrA were used as controls. Crosslinks were visualized on SDS PAGE gels stained with Coomassie Brilliant Blue.

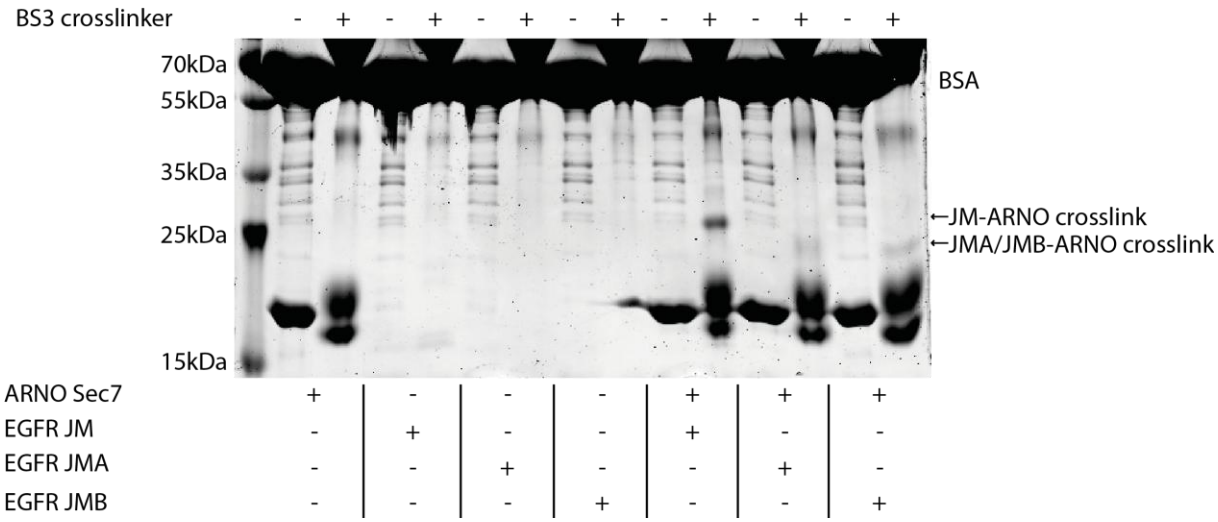

Supplementary Figure 6.Chemical crosslinking of EGFR JM A and EGFR JM B with ARNO Sec7. EGFR JM can be divided into an N-terminal part (JM A) forming a helical structure involved in EGFR dimer formation and a C-terminal part (JM B) that stabilizes the asymmetric dimer. Both JM A and JM B and the full length JM domain were crosslinked to ARNO Sec7 using the chemical crosslinker BS3. Crosslinks were visualized on SDS PAGE gels stained with Coomassie Brilliant Blue..

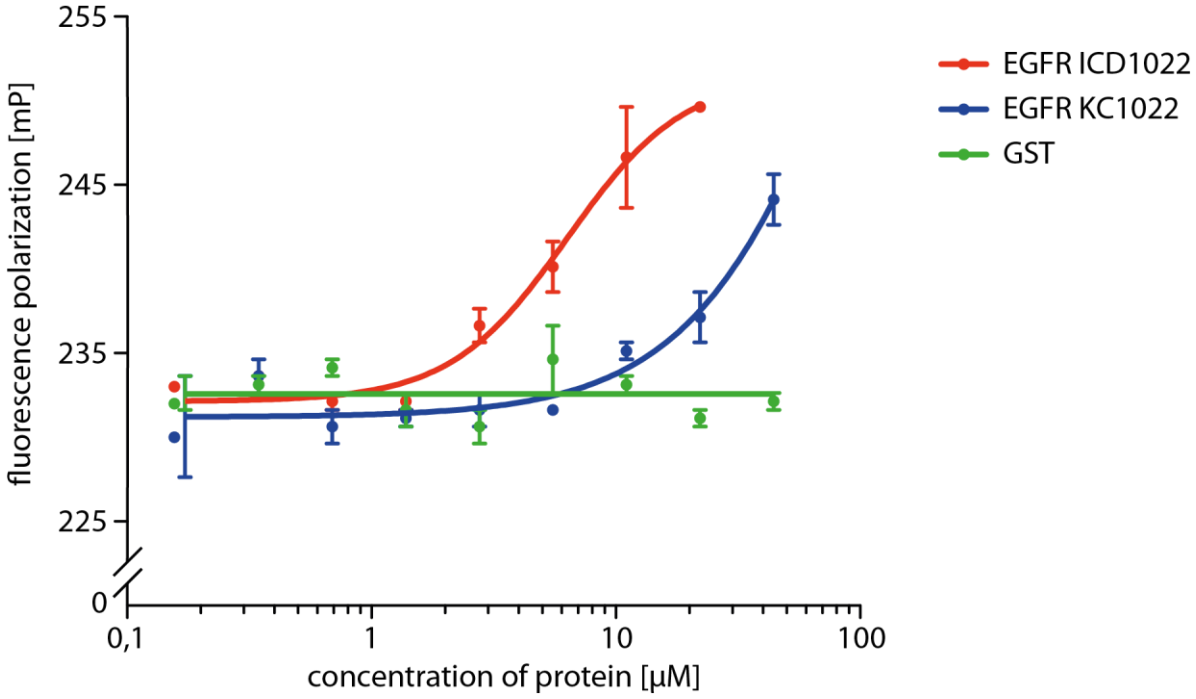

Supplementary Figure 7. Fluorescence polarization assay with fluorescein labeled ARNO Sec7 and EGFR constructs. ARNO Sec7 was labeled with fluorescein and incubated with increasing concentrations of EGFR ICD1022 and EGFR KC1022resulting in an increase in fluorescence polarization. No binding to GST was observed.Values are mean +/- SEM (n=2).

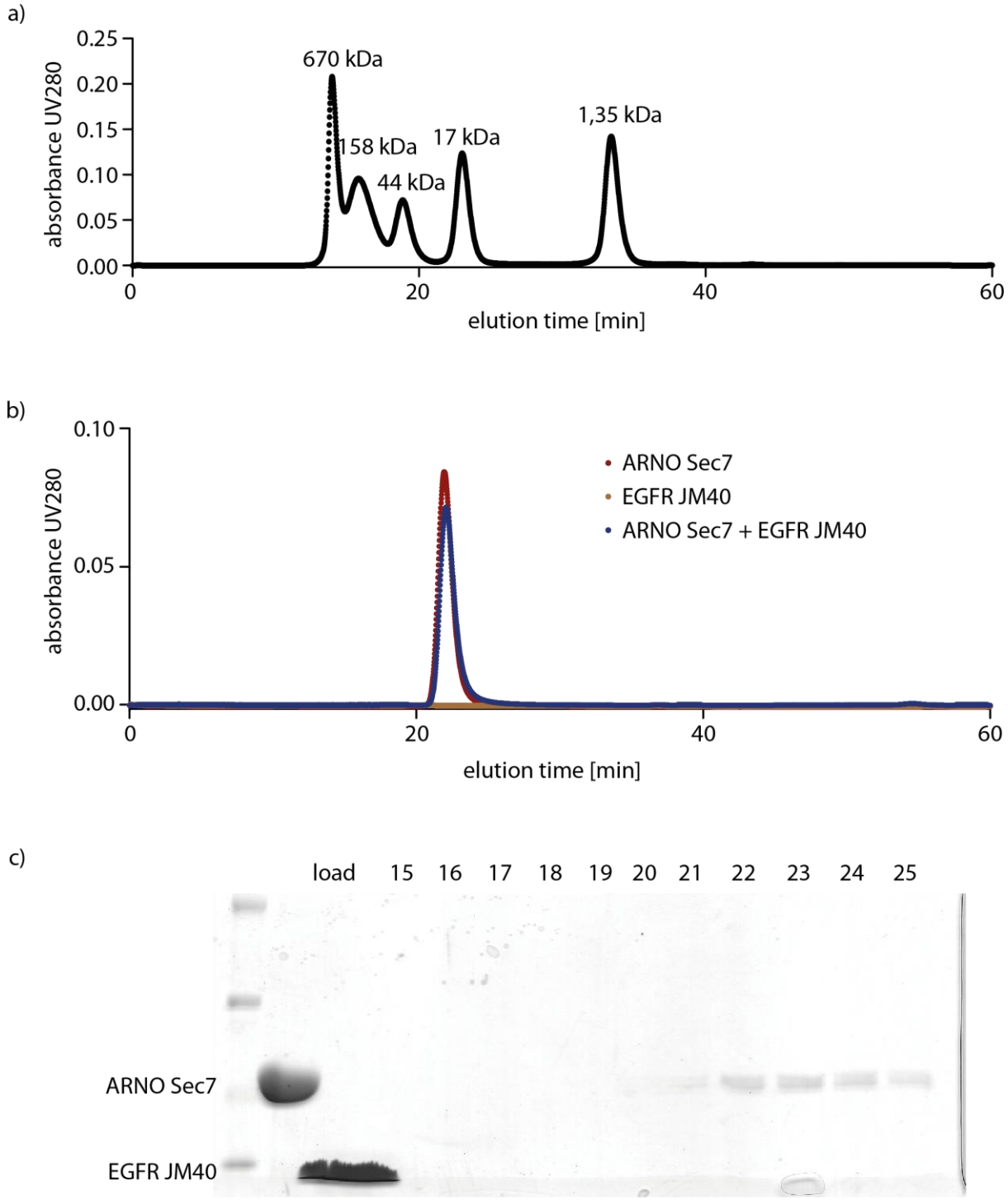

Supplementary Figure 8. Analytical gel filtration analysis of ARNO Sec7 with EGFR JM. ARNO Sec7, EGFR JM40 (40 amino acids of the juxtamembrane domain of EGFR) and a mixture of both proteins incubated for 30 minutes at room temperature were separated on a Superdex 75 size exclusion chromatography column (b). The eluted proteins were analyzed by SDS PAGE and Coomassie Brilliant Blue staining (c). No co-elution of ARNO Sec7 and EGFR JM is observed. A molecular weight standard (Bio-Rad) was used as a size reference (a).

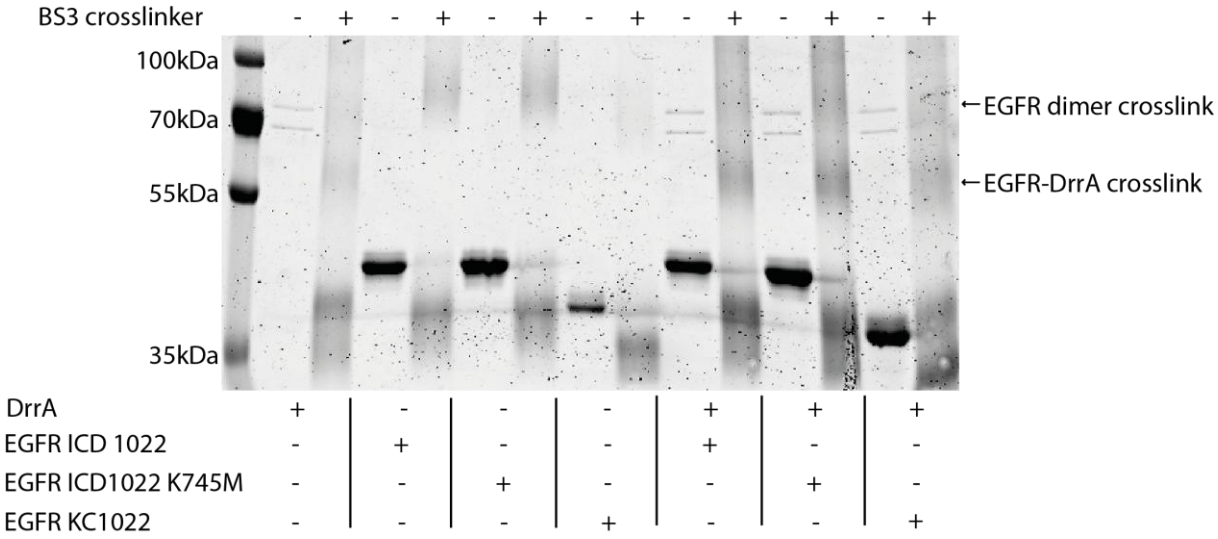

Supplementary Figure 9. Chemical crosslinking of DrrA with different EGFR constructs. The indicated proteins were incubated with the chemical crosslinker BS3. All three EGFR constructs form crosslinks with DrrA independent of the presence of the juxtamembrane domain. Crosslinks were visualized on SDS PAGE gels stained with Coomassie Brilliant Blue.

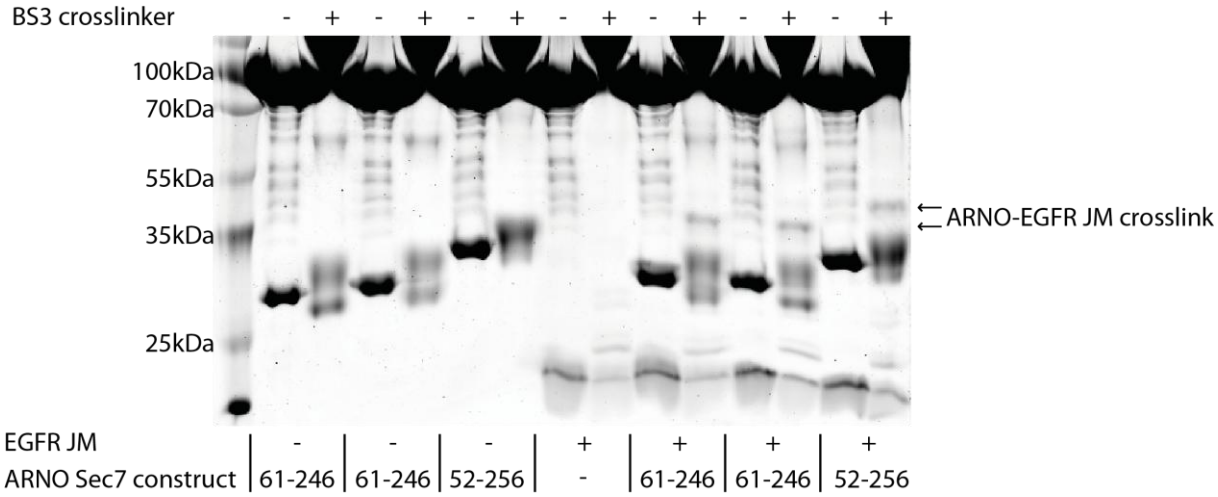

Supplementary Figure 10. Chemical crosslinking of ARNO Sec7 constructs used for crystallization with EGFR JM. The indicated proteins were incubated with the chemical crosslinker BS3. Both ARNO Sec7 constructs crosslink to EGFR JM. Crosslinks were visualized on SDS PAGE gels stained with Coomassie Brilliant Blue.

7.2 Plasmids

vector	constructs
pASK IBA 45+	N delta 13 Arf6 and mutants
pET 15b	ARNO Sec7 52-256 and N-terminal truncations
pET19mod	DrrA (340-533)
pET28 HT	ARNO Sec7 EGFR JM fusion constructs
pGEX_2T_TEV	Rac1
pGST1	JIP4 LZII (392-462)
pIBA 101 HT	ARNO Sec7 61-246

7.3 Primer

primer	sequence	used for:
Arf6 T44N for	5' ACCATTCCCAACGTGGGTTTCAAC 3'	Arf6 mutagenesis
Arf6 T44N rev	5' GGTCACCGACTGGCCCAGCT 3'	Arf6 mutagenesis
Arf6 Q67L for	5' GCGGCCTGGACAAGATCCGG 3'	Arf6 mutagenesis
Arf6 Q67L rev	5' CCACATCCCATACGTTGAACTTGACA 3'	Arf6 mutagenesis
ARNO HT for	5' phosphate CGGAACCGGAAGATGGCAA TGGGC 3'	ARNO Sec7 truncations
ARNO HT+2 for	5' phosphate TTGCAACGGAACCGGAAGA TGGCAATGGGC 3'	ARNO Sec7 truncations
ARNO HT+4 for	5' phosphate AAGACCTTGCAACGGAACC GGAAGATGGCAATGGGC 3'	ARNO Sec7 truncations
ARNO HT+6 for	5' phosphate GGCAGTAAGACCTTGCAAC GGAACCGGAAGATGGCAATGGGC 3'	ARNO Sec7 truncations
ARNO HT+8 for	5' phosphate AATGAGGGCAGTAAGACCT TGCAACGGAACCGGAAGATGGCAATGGGC 3'	ARNO Sec7 truncations
ARNO truncations rev	5' phosphate CGTCTCAGACTGAAAATACA GGTT 3'	ARNO Sec7 truncations
N Sec7 for	5' GTTGTTGAATTCGCCAATGAGGGCAGTA AGACCTTG 3'	JM-Sec7-fusion
N Sec7 rev	5' GTTGTTGGTACCGGAGTGGGTCACGTCA TTCCCGTC 3'	JM-Sec7-fusion
N JM LL 15 for	5' GTTGTTGGTACCAACCTGTCTTCCGACTC TAACTCCCCGGGTATCGAAGGTCTGTCTACG CGACGCCACATCGTCCGGAAGCGCACT 3'	JM-Sec7-fusion
N JM LL 23 for	5' GTTGTTGGTACCAACCTGTCTTCCGACT CTTCCCTGTCTTCCCCGTCCGCTCTGAACT CCCCGGGTATCGAAGGTCTGTCTACGCGAC GCCACATCGTCCGGAAGCGCACT 3'	JM-Sec7-fusion
N JM rev	5' GTTGTTAAGCTTTTAGATCCGCAGCAGAG CTTGGTTCGG 3'	JM-Sec7-fusion

C JM for	5' GTTGTTGAATTCCGACGACGCCACATCGT CCGGAAGCGC 3'	Sec7-JM-fusion
C JM LL 15 rev	5' GTTGTTGGTACCAGACAGACCTTCGATAC CCGGGGAGTTAGAGTCGGAAGACAGGTTG ATCCGCAGAGCTTGGTTCGGAGCTTC 3'	Sec7-JM-fusion
C JM LL 23 rev	5' GTTGTTGGTACCAGACAGACCTTCGATAC CCGGGGAGTTCAGAGCGGACGGGGAAGAC AGGGAAGAGTCGGAAGACAGGTTGATCCG CAGAGCTTGGTTCGGAGCTTC 3'	Sec7-JM-fusion
C Sec7 for	5' GTTGTTGGTACCGCCAATGAGGGCAGTAA GACCTTG 3'	Sec7-JM-fusion
C Sec7 rev	5' GTTGTTAAGCTTTTAGGAGTGGGTCACGT CATTCCC 3'	Sec7-JM-fusion
LL37 extend for	5' phosphate TCCACTGCTTCTAACTCCCCG GGTATCGAAGGTCTGTCT 3'	linker extension fusion proteins
LL37 extend rev	5' phosphate GTTCAGAGCGGACGGAGAGG ACAGGGAGTTCAGAGCGGACGGGGA 3'	linker extension fusion proteins
N Vec for	5' phosphate TCCGCTCTGAACTCCCCGGGT ATCGAAGGTCTGTCTCGACGACGCCACATC GTCCGGAAG 3'	double JM fusion proteins
N Vec rev	5' GAAGAAGAGCTCGAATTCCATGGCGCCC TGAAAATA 3'	double JM fusion proteins
N JM for	5' GAAGAAGAGCTCCGACGACGCCACATCG TCCGGAAG 3'	double JM fusion proteins
N JM rev	5' phosphate CGGGGAAGACAGGGAGAGG TCGGAAGACAGGTTGATCCGCAGCAGAGC TTGGTTCGG 3'	double JM fusion proteins
C Vec for	5' GAAGAAGAGCTCTAAAAGCTTCTCGAGC ACCACCAC 3'	double JM fusion proteins
C Vec rev	5' phosphate CGGGGAAGACAGGGAAGAG TCGGAAGACAGGTTGATCCGCAGCAGAGC TTGGTTCGG 3'	double JM fusion proteins
C JM for	5' phosphate TCCGCTCTGAACTCCCCGGG TATCGAAGGTCTGTCTCGACGACGCCACAT CGTCCGGAAG 3'	double JM fusion proteins
C JM rev	5' GAAGAAGAGCTCGATCCGCAGCAGAGC TTGGTTCGG 3'	double JM fusion proteins

APPENDIX

8 References

1. Chan, Y. M., and Jan, Y. N. (1998) Roles for proteolysis and trafficking in notch maturation and signal transduction, *Cell94*, 423-426.
2. Hlsken, J., and Behrens, J. (2000) The Wnt signalling pathway, *J Cell Sci113 (Pt 20)*, 3545.
3. Collins, S., Caron, M. G., and Lefkowitz, R. J. (1992) From ligand binding to gene expression: new insights into the regulation of G-protein-coupled receptors, *Trends Biochem Sci17*, 37-39.
4. Baylor, D. (1996) How photons start vision, *Proc Natl Acad Sci U S A93*, 560-565.
5. Buck, L. B. (2000) The molecular architecture of odor and pheromone sensing in mammals, *Cell100*, 611-618.
6. Betz, H. (1990) Ligand-gated ion channels in the brain: the amino acid receptor superfamily, *Neuron5*, 383-392.
7. Doyle, D. A., Morais Cabral, J., Pfuetzner, R. A., Kuo, A., Gulbis, J. M., Cohen, S. L., Chait, B. T., and MacKinnon, R. (1998) The structure of the potassium channel: molecular basis of K+ conduction and selectivity, *Science280*, 69-77.
8. Perozo, E., Cortes, D. M., and Cuello, L. G. (1999) Structural rearrangements underlying K+-channel activation gating, *Science285*, 73-78.
9. Ullrich, A., and Schlessinger, J. (1990) Signal transduction by receptors with tyrosine kinase activity, *Cell61*, 203-212.
10. Lemmon, M. A., and Schlessinger, J. (2010) Cell signaling by receptor tyrosine kinases, *Cell141*, 1117-1134.
11. Gajiwala, K. S. (2013) EGFR: tale of the C-terminal tail, *Protein Sci22*, 995-999.
12. Mustafa, M., Mirza, A., and Kannan, N. (2011) Conformational regulation of the EGFR kinase core by the juxtamembrane and C-terminal tail: a molecular dynamics study, *Proteins79*, 99-114.
13. Jura, N., Endres, N. F., Engel, K., Deindl, S., Das, R., Lamers, M. H., Wemmer, D. E., Zhang, X., and Kuriyan, J. (2009) Mechanism for activation of the EGF receptor catalytic domain by the juxtamembrane segment, *Cell137*, 1293-1307.
14. Wybenga-Groot, L. E., Baskin, B., Ong, S. H., Tong, J., Pawson, T., and Sicheri, F. (2001) Structural basis for autoinhibition of the Ephb2 receptor tyrosine kinase by the unphosphorylated juxtamembrane region, *Cell106*, 745-757.
15. Red Brewer, M., Choi, S. H., Alvarado, D., Moravcevic, K., Pozzi, A., Lemmon, M. A., and Carpenter, G. (2009) The juxtamembrane region of the EGF receptor functions as an activation domain, *Mol Cell34*, 641-651.
16. Li, E., and Hristova, K. (2010) Receptor tyrosine kinase transmembrane domains: Function, dimer structure and dimerization energetics, *Cell Adh Migr4*, 249-254.
17. Endres, N. F., Das, R., Smith, A. W., Arkhipov, A., Kovacs, E., Huang, Y., Pelton, J. G., Shan, Y., Shaw, D. E., Wemmer, D. E., Groves, J. T., and Kuriyan, J. (2013) Conformational coupling across the plasma membrane in activation of the EGF receptor, *Cell152*, 543-556.
18. Arkhipov, A., Shan, Y., Das, R., Endres, N. F., Eastwood, M. P., Wemmer, D. E., Kuriyan, J., and Shaw, D. E. (2013) Architecture and membrane interactions of the EGF receptor, *Cell152*, 557-569.
19. Waterfield, M. D., Scrace, G. T., Whittle, N., Stroobant, P., Johnsson, A., Wasteson, A., Westermark, B., Heldin, C. H., Huang, J. S., and Deuel, T. F. (1983) Platelet-

derived growth factor is structurally related to the putative transforming protein p28sis of simian sarcoma virus, *Nature304*, 35-39.
20. Downward, J., Yarden, Y., Mayes, E., Scrace, G., Totty, N., Stockwell, P., Ullrich, A., Schlessinger, J., and Waterfield, M. D. (1984) Close similarity of epidermal growth factor receptor and v-erb-B oncogene protein sequences, *Nature307*, 521-527.
21. Doolittle, R. F., Hunkapiller, M. W., Hood, L. E., Devare, S. G., Robbins, K. C., Aaronson, S. A., and Antoniades, H. N. (1983) Simian sarcoma virus onc gene, v-sis, is derived from the gene (or genes) encoding a platelet-derived growth factor, *Science221*, 275-277.
22. Libermann, T. A., Nusbaum, H. R., Razon, N., Kris, R., Lax, I., Soreq, H., Whittle, N., Waterfield, M. D., Ullrich, A., and Schlessinger, J. (1985) Amplification, enhanced expression and possible rearrangement of EGF receptor gene in primary human brain tumours of glial origin, *Nature313*, 144-147.
23. Taylor, S. I., Kadowaki, T., Kadowaki, H., Accili, D., Cama, A., and McKeon, C. (1990) Mutations in insulin-receptor gene in insulin-resistant patients, *Diabetes Care13*, 257-279.
24. Rohmann, E., Brunner, H. G., Kayserili, H., Uyguner, O., Nurnberg, G., Lew, E. D., Dobbie, A., Eswarakumar, V. P., Uzumcu, A., Ulubil-Emeroglu, M., Leroy, J. G., Li, Y., Becker, C., Lehnerdt, K., Cremers, C. W., Yuksel-Apak, M., Nurnberg, P., Kubisch, C., Schlessinger, J., van Bokhoven, H., and Wollnik, B. (2006) Mutations in different components of FGF signaling in LADD syndrome, *Nat Genet38*, 414-417.
25. Liu, H., Chen, X., Focia, P. J., and He, X. (2007) Structural basis for stem cell factor-KIT signaling and activation of class III receptor tyrosine kinases, *EMBO J26*, 891-901.
26. Leppanen, V. M., Prota, A. E., Jeltsch, M., Anisimov, A., Kalkkinen, N., Strandin, T., Lankinen, H., Goldman, A., Ballmer-Hofer, K., and Alitalo, K. (2010) Structural determinants of growth factor binding and specificity by VEGF receptor 2, *Proc Natl Acad Sci U S A107*, 2425-2430.
27. Clayton, A. H., Walker, F., Orchard, S. G., Henderson, C., Fuchs, D., Rothacker, J., Nice, E. C., and Burgess, A. W. (2005) Ligand-induced dimer-tetramer transition during the activation of the cell surface epidermal growth factor receptor-A multidimensional microscopy analysis, *J Biol Chem280*, 30392-30399.
28. Barton, W. A., Tzvetkova-Robev, D., Miranda, E. P., Kolev, M. V., Rajashankar, K. R., Himanen, J. P., and Nikolov, D. B. (2006) Crystal structures of the Tie2 receptor ectodomain and the angiopoietin-2-Tie2 complex, *Nat Struct Mol Biol13*, 524-532.
29. Ward, C. W., Lawrence, M. C., Streltsov, V. A., Adams, T. E., and McKern, N. M. (2007) The insulin and EGF receptor structures: new insights into ligand-induced receptor activation, *Trends Biochem Sci32*, 129-137.
30. Menting, J. G., Whittaker, J., Margetts, M. B., Whittaker, L. J., Kong, G. K., Smith, B. J., Watson, C. J., Zakova, L., Kletvikova, E., Jiracek, J., Chan, S. J., Steiner, D. F., Dodson, G. G., Brzozowski, A. M., Weiss, M. A., Ward, C. W., and Lawrence, M. C. (2013) How insulin engages its primary binding site on the insulin receptor, *Nature493*, 241-245.
31. Huse, M., and Kuriyan, J. (2002) The conformational plasticity of protein kinases, *Cell109*, 275-282.
32. Jura, N., Zhang, X., Endres, N. F., Seeliger, M. A., Schindler, T., and Kuriyan, J. (2011) Catalytic control in the EGF receptor and its connection to general kinase regulatory mechanisms, *Mol Cell42*, 9-22.

33. Nolen, B., Taylor, S., and Ghosh, G. (2004) Regulation of protein kinases; controlling activity through activation segment conformation, *Mol Cell15*, 661-675.
34. Robinson, M. J., Harkins, P. C., Zhang, J., Baer, R., Haycock, J. W., Cobb, M. H., and Goldsmith, E. J. (1996) Mutation of position 52 in ERK2 creates a nonproductive binding mode for adenosine 5'-triphosphate, *Biochemistry35*, 5641-5646.
35. Xu, W., Doshi, A., Lei, M., Eck, M. J., and Harrison, S. C. (1999) Crystal structures of c-Src reveal features of its autoinhibitory mechanism, *Mol Cell3*, 629-638.
36. Schindler, T., Sicheri, F., Pico, A., Gazit, A., Levitzki, A., and Kuriyan, J. (1999) Crystal structure of Hck in complex with a Src family-selective tyrosine kinase inhibitor, *Mol Cell3*, 639-648.
37. Sicheri, F., and Kuriyan, J. (1997) Structures of Src-family tyrosine kinases, *Curr Opin Struct Biol7*, 777-785.
38. Xu, W., Harrison, S. C., and Eck, M. J. (1997) Three-dimensional structure of the tyrosine kinase c-Src, *Nature385*, 595-602.
39. Martin, G. S. (2004) The road to Src, *Oncogene23*, 7910-7917.
40. De Bondt, H. L., Rosenblatt, J., Jancarik, J., Jones, H. D., Morgan, D. O., and Kim, S. H. (1993) Crystal structure of cyclin-dependent kinase 2, *Nature363*, 595-602.
41. Mol, C. D., Dougan, D. R., Schneider, T. R., Skene, R. J., Kraus, M. L., Scheibe, D. N., Snell, G. P., Zou, H., Sang, B. C., and Wilson, K. P. (2004) Structural basis for the autoinhibition and STI-571 inhibition of c-Kit tyrosine kinase, *J Biol Chem279*, 31655-31663.
42. Nagar, B., Bornmann, W. G., Pellicena, P., Schindler, T., Veach, D. R., Miller, W. T., Clarkson, B., and Kuriyan, J. (2002) Crystal structures of the kinase domain of c-Abl in complex with the small molecule inhibitors PD173955 and imatinib (STI-571), *Cancer Res62*, 4236-4243.
43. Chen, H., Ma, J., Li, W., Eliseenkova, A. V., Xu, C., Neubert, T. A., Miller, W. T., and Mohammadi, M. (2007) A molecular brake in the kinase hinge region regulates the activity of receptor tyrosine kinases, *Mol Cell27*, 717-730.
44. Hubbard, S. R. (2004) Juxtamembrane autoinhibition in receptor tyrosine kinases, *Nat Rev Mol Cell Biol5*, 464-471.
45. Niu, X. L., Peters, K. G., and Kontos, C. D. (2002) Deletion of the carboxyl terminus of Tie2 enhances kinase activity, signaling, and function. Evidence for an autoinhibitory mechanism, *J Biol Chem277*, 31768-31773.
46. Favelyukis, S., Till, J. H., Hubbard, S. R., and Miller, W. T. (2001) Structure and autoregulation of the insulin-like growth factor 1 receptor kinase, *Nat Struct Biol8*, 1058-1063.
47. Furdui, C. M., Lew, E. D., Schlessinger, J., and Anderson, K. S. (2006) Autophosphorylation of FGFR1 kinase is mediated by a sequential and precisely ordered reaction, *Mol Cell21*, 711-717.
48. Pawson, T. (2004) Specificity in signal transduction: from phosphotyrosine-SH2 domain interactions to complex cellular systems, *Cell116*, 191-203.
49. Pelech, S. L., and Sanghera, J. S. (1992) Mitogen-activated protein kinases: versatile transducers for cell signaling, *Trends Biochem Sci17*, 233-238.
50. Pawson, T. (2007) Dynamic control of signaling by modular adaptor proteins, *Curr Opin Cell Biol19*, 112-116.
51. Ladbury, J. E., and Arold, S. (2000) Searching for specificity in SH domains, *Chem Biol7*, R3-8.
52. Rhee, S. G., and Choi, K. D. (1992) Regulation of inositol phospholipid-specific phospholipase C isozymes, *J Biol Chem267*, 12393-12396.

53. Cantley, L. C., Auger, K. R., Carpenter, C., Duckworth, B., Graziani, A., Kapeller, R., and Soltoff, S. (1991) Oncogenes and signal transduction, *Cell64*, 281-302.
54. Jallal, B., Schlessinger, J., and Ullrich, A. (1992) Tyrosine phosphatase inhibition permits analysis of signal transduction complexes in p185HER2/neu-overexpressing human tumor cells, *J Biol Chem267*, 4357-4363.
55. Ostman, A., Hellberg, C., and Bohmer, F. D. (2006) Protein-tyrosine phosphatases and cancer, *Nat Rev Cancer6*, 307-320.
56. Ostman, A., and Bohmer, F. D. (2001) Regulation of receptor tyrosine kinase signaling by protein tyrosine phosphatases, *Trends Cell Biol11*, 258-266.
57. Haglund, K., and Dikic, I. (2012) The role of ubiquitylation in receptor endocytosis and endosomal sorting, *J Cell Sci125*, 265-275.
58. Lill, N. L., and Sever, N. I. (2012) Where EGF receptors transmit their signals, *Sci Signal5*, pe41.
59. Sorkin, A., and von Zastrow, M. (2009) Endocytosis and signalling: intertwining molecular networks, *Nat Rev Mol Cell Biol10*, 609-622.
60. Brankatschk, B., Wichert, S. P., Johnson, S. D., Schaad, O., Rossner, M. J., and Gruenberg, J. (2012) Regulation of the EGF transcriptional response by endocytic sorting, *Sci Signal5*, ra21.
61. Sousa, L. P., Lax, I., Shen, H., Ferguson, S. M., De Camilli, P., and Schlessinger, J. (2012) Suppression of EGFR endocytosis by dynamin depletion reveals that EGFR signaling occurs primarily at the plasma membrane, *Proc Natl Acad Sci U S A109*, 4419-4424.
62. Miettinen, P. J., Berger, J. E., Meneses, J., Phung, Y., Pedersen, R. A., Werb, Z., and Derynck, R. (1995) Epithelial immaturity and multiorgan failure in mice lacking epidermal growth factor receptor, *Nature376*, 337-341.
63. Zhang, H., Berezov, A., Wang, Q., Zhang, G., Drebin, J., Murali, R., and Greene, M. I. (2007) ErbB receptors: from oncogenes to targeted cancer therapies, *J Clin Invest117*, 2051-2058.
64. Olayioye, M. A., Neve, R. M., Lane, H. A., and Hynes, N. E. (2000) The ErbB signaling network: receptor heterodimerization in development and cancer, *EMBO J19*, 3159-3167.
65. Guy, P. M., Platko, J. V., Cantley, L. C., Cerione, R. A., and Carraway, K. L., 3rd. (1994) Insect cell-expressed p180erbB3 possesses an impaired tyrosine kinase activity, *Proc Natl Acad Sci U S A91*, 8132-8136.
66. Klapper, L. N., Glathe, S., Vaisman, N., Hynes, N. E., Andrews, G. C., Sela, M., and Yarden, Y. (1999) The ErbB-2/HER2 oncoprotein of human carcinomas may function solely as a shared coreceptor for multiple stroma-derived growth factors, *Proc Natl Acad Sci U S A96*, 4995-5000.
67. Yarden, Y., and Sliwkowski, M. X. (2001) Untangling the ErbB signalling network, *Nat Rev Mol Cell Biol2*, 127-137.
68. Garrett, T. P., McKern, N. M., Lou, M., Elleman, T. C., Adams, T. E., Lovrecz, G. O., Zhu, H. J., Walker, F., Frenkel, M. J., Hoyne, P. A., Jorissen, R. N., Nice, E. C., Burgess, A. W., and Ward, C. W. (2002) Crystal structure of a truncated epidermal growth factor receptor extracellular domain bound to transforming growth factor alpha, *Cell110*, 763-773.
69. Ogiso, H., Ishitani, R., Nureki, O., Fukai, S., Yamanaka, M., Kim, J. H., Saito, K., Sakamoto, A., Inoue, M., Shirouzu, M., and Yokoyama, S. (2002) Crystal structure of the complex of human epidermal growth factor and receptor extracellular domains, *Cell110*, 775-787.

70. Cho, H. S., and Leahy, D. J. (2002) Structure of the extracellular region of HER3 reveals an interdomain tether, *Science297*, 1330-1333.
71. Ferguson, K. M., Berger, M. B., Mendrola, J. M., Cho, H. S., Leahy, D. J., and Lemmon, M. A. (2003) EGF activates its receptor by removing interactions that autoinhibit ectodomain dimerization, *Mol Cell11*, 507-517.
72. Burgess, A. W., Cho, H. S., Eigenbrot, C., Ferguson, K. M., Garrett, T. P., Leahy, D. J., Lemmon, M. A., Sliwkowski, M. X., Ward, C. W., and Yokoyama, S. (2003) An open-and-shut case? Recent insights into the activation of EGF/ErbB receptors, *Mol Cell12*, 541-552.
73. Garrett, T. P., McKern, N. M., Lou, M., Elleman, T. C., Adams, T. E., Lovrecz, G. O., Kofler, M., Jorissen, R. N., Nice, E. C., Burgess, A. W., and Ward, C. W. (2003) The crystal structure of a truncated ErbB2 ectodomain reveals an active conformation, poised to interact with other ErbB receptors, *Mol Cell11*, 495-505.
74. Gotoh, N., Tojo, A., Hino, M., Yazaki, Y., and Shibuya, M. (1992) A highly conserved tyrosine residue at codon 845 within the kinase domain is not required for the transforming activity of human epidermal growth factor receptor, *Biochem Biophys Res Commun186*, 768-774.
75. Tice, D. A., Biscardi, J. S., Nickles, A. L., and Parsons, S. J. (1999) Mechanism of biological synergy between cellular Src and epidermal growth factor receptor, *Proc Natl Acad Sci U S A96*, 1415-1420.
76. Wood, E. R., Shewchuk, L. M., Ellis, B., Brignola, P., Brashear, R. L., Caferro, T. R., Dickerson, S. H., Dickson, H. D., Donaldson, K. H., Gaul, M., Griffin, R. J., Hassell, A. M., Keith, B., Mullin, R., Petrov, K. G., Reno, M. J., Rusnak, D. W., Tadepalli, S. M., Ulrich, J. C., Wagner, C. D., Vanderwall, D. E., Waterson, A. G., Williams, J. D., White, W. L., and Uehling, D. E. (2008) 6-Ethynylthieno[3,2-d]- and 6-ethynylthieno[2,3-d]pyrimidin-4-anilines as tunable covalent modifiers of ErbB kinases, *Proc Natl Acad Sci U S A105*, 2773-2778.
77. Zhang, X., Gureasko, J., Shen, K., Cole, P. A., and Kuriyan, J. (2006) An allosteric mechanism for activation of the kinase domain of epidermal growth factor receptor, *Cell125*, 1137-1149.
78. Stamos, J., Sliwkowski, M. X., and Eigenbrot, C. (2002) Structure of the epidermal growth factor receptor kinase domain alone and in complex with a 4-anilinoquinazoline inhibitor, *J Biol Chem277*, 46265-46272.
79. Jura, N., Shan, Y., Cao, X., Shaw, D. E., and Kuriyan, J. (2009) Structural analysis of the catalytically inactive kinase domain of the human EGF receptor 3, *Proc Natl Acad Sci U S A106*, 21608-21613.
80. Qiu, C., Tarrant, M. K., Choi, S. H., Sathyamurthy, A., Bose, R., Banjade, S., Pal, A., Bornmann, W. G., Lemmon, M. A., Cole, P. A., and Leahy, D. J. (2008) Mechanism of activation and inhibition of the HER4/ErbB4 kinase, *Structure16*, 460-467.
81. Thiel, K. W., and Carpenter, G. (2007) Epidermal growth factor receptor juxtamembrane region regulates allosteric tyrosine kinase activation, *Proc Natl Acad Sci U S A104*, 19238-19243.
82. Bublil, E. M., Pines, G., Patel, G., Fruhwirth, G., Ng, T., and Yarden, Y. (2010) Kinase-mediated quasi-dimers of EGFR, *FASEB J24*, 4744-4755.
83. Pines, G., Huang, P. H., Zwang, Y., White, F. M., and Yarden, Y. (2010) EGFRvIV: a previously uncharacterized oncogenic mutant reveals a kinase autoinhibitory mechanism, *Oncogene29*, 5850-5860.
84. Aifa, S., Aydin, J., Nordvall, G., Lundstrom, I., Svensson, S. P., and Hermanson, O. (2005) A basic peptide within the juxtamembrane region is required for EGF receptor dimerization, *Exp Cell Res302*, 108-114.

85. McLaughlin, S., Smith, S. O., Hayman, M. J., and Murray, D. (2005) An electrostatic engine model for autoinhibition and activation of the epidermal growth factor receptor (EGFR/ErbB) family, *J Gen Physiol126*, 41-53.
86. Li, X., Huang, Y., Jiang, J., and Frank, S. J. (2008) ERK-dependent threonine phosphorylation of EGF receptor modulates receptor downregulation and signaling, *Cell Signal20*, 2145-2155.
87. Zhang, X., Pickin, K. A., Bose, R., Jura, N., Cole, P. A., and Kuriyan, J. (2007) Inhibition of the EGF receptor by binding of MIG6 to an activating kinase domain interface, *Nature450*, 741-744.
88. Hynes, N. E., and Schlange, T. (2006) Targeting ADAMS and ERBBs in lung cancer, *Cancer Cell10*, 7-11.
89. Bae, Y. S., Kang, S. W., Seo, M. S., Baines, I. C., Tekle, E., Chock, P. B., and Rhee, S. G. (1997) Epidermal growth factor (EGF)-induced generation of hydrogen peroxide. Role in EGF receptor-mediated tyrosine phosphorylation, *J Biol Chem272*, 217-221.
90. Reynolds, A. R., Tischer, C., Verveer, P. J., Rocks, O., and Bastiaens, P. I. (2003) EGFR activation coupled to inhibition of tyrosine phosphatases causes lateral signal propagation, *Nat Cell Biol5*, 447-453.
91. Wennerberg, K., Rossman, K. L., and Der, C. J. (2005) The Ras superfamily at a glance, *J Cell Sci118*, 843-846.
92. Shaw, R. J., and Cantley, L. C. (2006) Ras, PI(3)K and mTOR signalling controls tumour cell growth, *Nature441*, 424-430.
93. Karnoub, A. E., and Weinberg, R. A. (2008) Ras oncogenes: split personalities, *Nat Rev Mol Cell Biol9*, 517-531.
94. Heasman, S. J., and Ridley, A. J. (2008) Mammalian Rho GTPases: new insights into their functions from in vivo studies, *Nat Rev Mol Cell Biol9*, 690-701.
95. Donaldson, J. G., and Honda, A. (2005) Localization and function of Arf family GTPases, *Biochem Soc Trans33*, 639-642.
96. D'Souza-Schorey, C., and Chavrier, P. (2006) ARF proteins: roles in membrane traffic and beyond, *Nat Rev Mol Cell Biol7*, 347-358.
97. Zerial, M., and McBride, H. (2001) Rab proteins as membrane organizers, *Nat Rev Mol Cell Biol2*, 107-117.
98. Clarke, P. R., and Zhang, C. (2008) Spatial and temporal coordination of mitosis by Ran GTPase, *Nat Rev Mol Cell Biol9*, 464-477.
99. Vetter, I. R., and Wittinghofer, A. (2001) The guanine nucleotide-binding switch in three dimensions, *Science294*, 1299-1304.
100. Itzen, A., Pylypenko, O., Goody, R. S., Alexandrov, K., and Rak, A. (2006) Nucleotide exchange via local protein unfolding--structure of Rab8 in complex with MSS4, *EMBO J25*, 1445-1455.
101. Goldberg, J. (1998) Structural basis for activation of ARF GTPase: mechanisms of guanine nucleotide exchange and GTP-myristoyl switching, *Cell95*, 237-248.
102. Worthylake, D. K., Rossman, K. L., and Sondek, J. (2000) Crystal structure of Rac1 in complex with the guanine nucleotide exchange region of Tiam1, *Nature408*, 682-688.
103. Bos, J. L., Rehmann, H., and Wittinghofer, A. (2007) GEFs and GAPs: critical elements in the control of small G proteins, *Cell129*, 865-877.
104. Sondermann, H., Soisson, S. M., Boykevisch, S., Yang, S. S., Bar-Sagi, D., and Kuriyan, J. (2004) Structural analysis of autoinhibition in the Ras activator Son of sevenless, *Cell119*, 393-405.

105. Margarit, S. M., Sondermann, H., Hall, B. E., Nagar, B., Hoelz, A., Pirruccello, M., Bar-Sagi, D., and Kuriyan, J. (2003) Structural evidence for feedback activation by Ras.GTP of the Ras-specific nucleotide exchange factor SOS, *Cell112*, 685-695.
106. Scheffzek, K., Ahmadian, M. R., Kabsch, W., Wiesmuller, L., Lautwein, A., Schmitz, F., and Wittinghofer, A. (1997) The Ras-RasGAP complex: structural basis for GTPase activation and its loss in oncogenic Ras mutants, *Science277*, 333-338.
107. Kahn, R. A., and Gilman, A. G. (1986) The protein cofactor necessary for ADP-ribosylation of Gs by cholera toxin is itself a GTP binding protein, *J Biol Chem261*, 7906-7911.
108. Kahn, R. A., Cherfils, J., Elias, M., Lovering, R. C., Munro, S., and Schurmann, A. (2006) Nomenclature for the human Arf family of GTP-binding proteins: ARF, ARL, and SAR proteins, *J Cell Biol172*, 645-650.
109. Fucini, R. V., Navarrete, A., Vadakkan, C., Lacomis, L., Erdjument-Bromage, H., Tempst, P., and Stamnes, M. (2000) Activated ADP-ribosylation factor assembles distinct pools of actin on golgi membranes, *J Biol Chem275*, 18824-18829.
110. Volpicelli-Daley, L. A., Li, Y., Zhang, C. J., and Kahn, R. A. (2005) Isoform-selective effects of the depletion of ADP-ribosylation factors 1-5 on membrane traffic, *Mol Biol Cell16*, 4495-4508.
111. Burd, C. G., Strochlic, T. I., and Gangi Setty, S. R. (2004) Arf-like GTPases: not so Arf-like after all, *Trends Cell Biol14*, 687-694.
112. Wenk, M. R., and De Camilli, P. (2004) Protein-lipid interactions and phosphoinositide metabolism in membrane traffic: insights from vesicle recycling in nerve terminals, *Proc Natl Acad Sci U S A101*, 8262-8269.
113. Donaldson, J. G. (2003) Multiple roles for Arf6: sorting, structuring, and signaling at the plasma membrane, *J Biol Chem278*, 41573-41576.
114. Brown, F. D., Rozelle, A. L., Yin, H. L., Balla, T., and Donaldson, J. G. (2001) Phosphatidylinositol 4,5-bisphosphate and Arf6-regulated membrane traffic, *J Cell Biol154*, 1007-1017.
115. Palacios, F., Price, L., Schweitzer, J., Collard, J. G., and D'Souza-Schorey, C. (2001) An essential role for ARF6-regulated membrane traffic in adherens junction turnover and epithelial cell migration, *EMBO J20*, 4973-4986.
116. Houndolo, T., Boulay, P. L., and Claing, A. (2005) G protein-coupled receptor endocytosis in ADP-ribosylation factor 6-depleted cells, *J Biol Chem280*, 5598-5604.
117. Maxfield, F. R., and McGraw, T. E. (2004) Endocytic recycling, *Nat Rev Mol Cell Biol5*, 121-132.
118. Jovanovic, O. A., Brown, F. D., and Donaldson, J. G. (2006) An effector domain mutant of Arf6 implicates phospholipase D in endosomal membrane recycling, *Mol Biol Cell17*, 327-335.
119. Prigent, M., Dubois, T., Raposo, G., Derrien, V., Tenza, D., Rosse, C., Camonis, J., and Chavrier, P. (2003) ARF6 controls post-endocytic recycling through its downstream exocyst complex effector, *J Cell Biol163*, 1111-1121.
120. Dai, J., Li, J., Bos, E., Porcionatto, M., Premont, R. T., Bourgoin, S., Peters, P. J., and Hsu, V. W. (2004) ACAP1 promotes endocytic recycling by recognizing recycling sorting signals, *Dev Cell7*, 771-776.
121. Mayor, S., Presley, J. F., and Maxfield, F. R. (1993) Sorting of membrane components from endosomes and subsequent recycling to the cell surface occurs by a bulk flow process, *J Cell Biol121*, 1257-1269.

122. Radhakrishna, H., Klausner, R. D., and Donaldson, J. G. (1996) Aluminum fluoride stimulates surface protrusions in cells overexpressing the ARF6 GTPase, *J Cell Biol134*, 935-947.
123. Santy, L. C., and Casanova, J. E. (2001) Activation of ARF6 by ARNO stimulates epithelial cell migration through downstream activation of both Rac1 and phospholipase D, *J Cell Biol154*, 599-610.
124. D'Souza-Schorey, C. (2005) Disassembling adherens junctions: breaking up is hard to do, *Trends Cell Biol15*, 19-26.
125. Hashimoto, S., Onodera, Y., Hashimoto, A., Tanaka, M., Hamaguchi, M., Yamada, A., and Sabe, H. (2004) Requirement for Arf6 in breast cancer invasive activities, *Proc Natl Acad Sci U S A101*, 6647-6652.
126. Achstetter, T., Franzusoff, A., Field, C., and Schekman, R. (1988) SEC7 encodes an unusual, high molecular weight protein required for membrane traffic from the yeast Golgi apparatus, *J Biol Chem263*, 11711-11717.
127. Jackson, C. L., and Casanova, J. E. (2000) Turning on ARF: the Sec7 family of guanine-nucleotide-exchange factors, *Trends Cell Biol10*, 60-67.
128. Peyroche, A., Antonny, B., Robineau, S., Acker, J., Cherfils, J., and Jackson, C. L. (1999) Brefeldin A acts to stabilize an abortive ARF-GDP-Sec7 domain protein complex: involvement of specific residues of the Sec7 domain, *Mol Cell3*, 275-285.
129. Donaldson, J. G., Finazzi, D., and Klausner, R. D. (1992) Brefeldin A inhibits Golgi membrane-catalysed exchange of guanine nucleotide onto ARF protein, *Nature360*, 350-352.
130. Mossessova, E., Gulbis, J. M., and Goldberg, J. (1998) Structure of the guanine nucleotide exchange factor Sec7 domain of human arno and analysis of the interaction with ARF GTPase, *Cell92*, 415-423.
131. Beraud-Dufour, S., Robineau, S., Chardin, P., Paris, S., Chabre, M., Cherfils, J., and Antonny, B. (1998) A glutamic finger in the guanine nucleotide exchange factor ARNO displaces Mg2+ and the beta-phosphate to destabilize GDP on ARF1, *EMBO J17*, 3651-3659.
132. Beraud-Dufour, S., Paris, S., Chabre, M., and Antonny, B. (1999) Dual interaction of ADP ribosylation factor 1 with Sec7 domain and with lipid membranes during catalysis of guanine nucleotide exchange, *J Biol Chem274*, 37629-37636.
133. Franco, M., Chardin, P., Chabre, M., and Paris, S. (1996) Myristoylation-facilitated binding of the G protein ARF1GDP to membrane phospholipids is required for its activation by a soluble nucleotide exchange factor, *J Biol Chem271*, 1573-1578.
134. Kolanus, W. (2007) Guanine nucleotide exchange factors of the cytohesin family and their roles in signal transduction, *Immunol Rev218*, 102-113.
135. Cohen, L. A., Honda, A., Varnai, P., Brown, F. D., Balla, T., and Donaldson, J. G. (2007) Active Arf6 recruits ARNO/cytohesin GEFs to the PM by binding their PH domains, *Mol Biol Cell18*, 2244-2253.
136. Macia, E., Chabre, M., and Franco, M. (2001) Specificities for the small G proteins ARF1 and ARF6 of the guanine nucleotide exchange factors ARNO and EFA6, *J Biol Chem276*, 24925-24930.
137. Peters, P. J., Hsu, V. W., Ooi, C. E., Finazzi, D., Teal, S. B., Oorschot, V., Donaldson, J. G., and Klausner, R. D. (1995) Overexpression of wild-type and mutant ARF1 and ARF6: distinct perturbations of nonoverlapping membrane compartments, *J Cell Biol128*, 1003-1017.
138. Hafner, M., Schmitz, A., Grune, I., Srivatsan, S. G., Paul, B., Kolanus, W., Quast, T., Kremmer, E., Bauer, I., and Famulok, M. (2006) Inhibition of cytohesins by SecinH3 leads to hepatic insulin resistance, *Nature444*, 941-944.

139. Orci, L., Tagaya, M., Amherdt, M., Perrelet, A., Donaldson, J. G., Lippincott-Schwartz, J., Klausner, R. D., and Rothman, J. E. (1991) Brefeldin A, a drug that blocks secretion, prevents the assembly of non-clathrin-coated buds on Golgi cisternae, *Cell64*, 1183-1195.
140. Klausner, R. D., Donaldson, J. G., and Lippincott-Schwartz, J. (1992) Brefeldin A: insights into the control of membrane traffic and organelle structure, *J Cell Biol116*, 1071-1080.
141. Viaud, J., Zeghouf, M., Barelli, H., Zeeh, J. C., Padilla, A., Guibert, B., Chardin, P., Royer, C. A., Cherfils, J., and Chavanieu, A. (2007) Structure-based discovery of an inhibitor of Arf activation by Sec7 domains through targeting of protein-protein complexes, *Proc Natl Acad Sci U S A104*, 10370-10375.
142. Zhu, W., London, N. R., Gibson, C. C., Davis, C. T., Tong, Z., Sorensen, L. K., Shi, D. S., Guo, J., Smith, M. C., Grossmann, A. H., Thomas, K. R., and Li, D. Y. (2012) Interleukin receptor activates a MYD88-ARNO-ARF6 cascade to disrupt vascular stability, *Nature492*, 252-255.
143. Jones, C. A., Nishiya, N., London, N. R., Zhu, W., Sorensen, L. K., Chan, A. C., Lim, C. J., Chen, H., Zhang, Q., Schultz, P. G., Hayallah, A. M., Thomas, K. R., Famulok, M., Zhang, K., Ginsberg, M. H., and Li, D. Y. (2009) Slit2-Robo4 signalling promotes vascular stability by blocking Arf6 activity, *Nat Cell Biol11*, 1325-1331.
144. Fuss, B., Becker, T., Zinke, I., and Hoch, M. (2006) The cytohesin Steppke is essential for insulin signalling in Drosophila, *Nature444*, 945-948.
145. Lim, J., Zhou, M., Veenstra, T. D., and Morrison, D. K. (2010) The CNK1 scaffold binds cytohesins and promotes insulin pathway signaling, *Genes Dev24*, 1496-1506.
146. Bill, A., Schmitz, A., Albertoni, B., Song, J. N., Heukamp, L. C., Walrafen, D., Thorwirth, F., Verveer, P. J., Zimmer, S., Meffert, L., Schreiber, A., Chatterjee, S., Thomas, R. K., Ullrich, R. T., Lang, T., and Famulok, M. (2010) Cytohesins are cytoplasmic ErbB receptor activators, *Cell143*, 201-211.
147. Mannell, H. K., Pircher, J., Chaudhry, D. I., Alig, S. K., Koch, E. G., Mettler, R., Pohl, U., and Krotz, F. (2012) ARNO regulates VEGF-dependent tissue responses by stabilizing endothelial VEGFR-2 surface expression, *Cardiovasc Res93*, 111-119.
148. Pan, T., Sun, J., Zhou, J., Fu, Z., Hu, Y., Zheng, S., and Zhang, S. (2013) Function and mode of action of cytohesins in the epidermal growth factor pathway in colorectal cancer cells, *Oncol Lett5*, 521-526.
149. Bill, A., Schmitz, A., Konig, K., Heukamp, L. C., Hannam, J. S., and Famulok, M. (2012) Anti-proliferative effect of cytohesin inhibition in gefitinib-resistant lung cancer cells, *PLoS One7*, e41179.
150. Tai, Y., Janas, J. A., Wang, C. L., and Van Aelst, L. (2014) Regulation of chandelier cell cartridge and bouton development via DOCK7-mediated ErbB4 activation, *Cell Rep6*, 254-263.
151. Pasqualato, S., Menetrey, J., Franco, M., and Cherfils, J. (2001) The structural GDP/GTP cycle of human Arf6, *EMBO Rep2*, 234-238.
152. Menetrey, J., Macia, E., Pasqualato, S., Franco, M., and Cherfils, J. (2000) Structure of Arf6-GDP suggests a basis for guanine nucleotide exchange factors specificity, *Nat Struct Biol7*, 466-469.
153. Bowman, A. B., Kamal, A., Ritchings, B. W., Philp, A. V., McGrail, M., Gindhart, J. G., and Goldstein, L. S. (2000) Kinesin-dependent axonal transport is mediated by the sunday driver (SYD) protein, *Cell103*, 583-594.
154. Cavalli, V., Kujala, P., Klumperman, J., and Goldstein, L. S. (2005) Sunday Driver links axonal transport to damage signaling, *J Cell Biol168*, 775-787.

155. Montagnac, G., Sibarita, J. B., Loubery, S., Daviet, L., Romao, M., Raposo, G., and Chavrier, P. (2009) ARF6 Interacts with JIP4 to control a motor switch mechanism regulating endosome traffic in cytokinesis, *Curr Biol19*, 184-195.
156. Isabet, T., Montagnac, G., Regazzoni, K., Raynal, B., El Khadali, F., England, P., Franco, M., Chavrier, P., Houdusse, A., and Menetrey, J. (2009) The structural basis of Arf effector specificity: the crystal structure of ARF6 in a complex with JIP4, *EMBO J28*, 2835-2845.
157. Amor, J. C., Harrison, D. H., Kahn, R. A., and Ringe, D. (1994) Structure of the human ADP-ribosylation factor 1 complexed with GDP, *Nature372*, 704-708.
158. Hussein, M., Bettio, M., Schmitz, A., Hannam, J. S., Theis, J., Mayer, G., Dosa, S., Gutschow, M., and Famulok, M. (2013) Cyplecksins are covalent inhibitors of the pleckstrin homology domain of cytohesin, *Angew Chem Int Ed Engl52*, 9529-9533.
159. Hafner, M., Vianini, E., Albertoni, B., Marchetti, L., Grune, I., Gloeckner, C., and Famulok, M. (2008) Displacement of protein-bound aptamers with small molecules screened by fluorescence polarization, *Nat Protoc3*, 579-587.
160. Kapust, R. B., Tozser, J., Fox, J. D., Anderson, D. E., Cherry, S., Copeland, T. D., and Waugh, D. S. (2001) Tobacco etch virus protease: mechanism of autolysis and rational design of stable mutants with wild-type catalytic proficiency, *Protein Eng14*, 993-1000.
161. Frank, S., Upender, S., Hansen, S. H., and Casanova, J. E. (1998) ARNO is a guanine nucleotide exchange factor for ADP-ribosylation factor 6, *J Biol Chem273*, 23-27.
162. Ullman, E. F., Kirakossian, H., Singh, S., Wu, Z. P., Irvin, B. R., Pease, J. S., Switchenko, A. C., Irvine, J. D., Dafforn, A., Skold, C. N., and et al. (1994) Luminescent oxygen channeling immunoassay: measurement of particle binding kinetics by chemiluminescence, *Proc Natl Acad Sci U S A91*, 5426-5430.
163. Puertollano, R., Randazzo, P. A., Presley, J. F., Hartnell, L. M., and Bonifacino, J. S. (2001) The GGAs promote ARF-dependent recruitment of clathrin to the TGN, *Cell105*, 93-102.
164. Zhang, S., Han, J., Sells, M. A., Chernoff, J., Knaus, U. G., Ulevitch, R. J., and Bokoch, G. M. (1995) Rho family GTPases regulate p38 mitogen-activated protein kinase through the downstream mediator Pak1, *J Biol Chem270*, 23934-23936.
165. Hall, B., McLean, M. A., Davis, K., Casanova, J. E., Sligar, S. G., and Schwartz, M. A. (2008) A fluorescence resonance energy transfer activation sensor for Arf6, *Anal Biochem374*, 243-249.
166. Takatsu, H., Yoshino, K., Toda, K., and Nakayama, K. (2002) GGA proteins associate with Golgi membranes through interaction between their GGAH domains and ADP-ribosylation factors, *Biochem J365*, 369-378.
167. Niebel, B., Weiche, B., Mueller, A. L., Li, D. Y., Karnowski, N., and Famulok, M. (2011) A luminescent oxygen channeling biosensor that measures small GTPase activation, *Chem Commun (Camb)47*, 7521-7523.
168. Lacowicz, J. R. (2006) *Principles of fluorescence spectroscopy*, 3rd ed.
169. Feng, B. Y., Shelat, A., Doman, T. N., Guy, R. K., and Shoichet, B. K. (2005) High-throughput assays for promiscuous inhibitors, *Nat Chem Biol1*, 146-148.
170. Zhang, J. H., Chung, T. D., and Oldenburg, K. R. (1999) A Simple Statistical Parameter for Use in Evaluation and Validation of High Throughput Screening Assays, *J Biomol Screen4*, 67-73.
171. D'Amato, R. J., Loughnan, M. S., Flynn, E., and Folkman, J. (1994) Thalidomide is an inhibitor of angiogenesis, *Proc Natl Acad Sci U S A91*, 4082-4085.

172. Therapontos, C., Erskine, L., Gardner, E. R., Figg, W. D., and Vargesson, N. (2009) Thalidomide induces limb defects by preventing angiogenic outgrowth during early limb formation, *Proc Natl Acad Sci U S A106*, 8573-8578.
173. Christ, W. (1998) *Medizinische Embryologie*, Ullstein Medical.
174. Wosnitza, C. (2013) Chemical modulation of guanine nucleotide exchange factor activity.
175. Nettleship, J. E., Brown, J., Groves, M. R., and Geerlof, A. (2008) Methods for protein characterization by mass spectrometry, thermal shift (ThermoFluor) assay, and multiangle or static light scattering, *Methods Mol Biol426*, 299-318.
176. Mossessova, E., Corpina, R. A., and Goldberg, J. (2003) Crystal structure of ARF1*Sec7 complexed with Brefeldin A and its implications for the guanine nucleotide exchange mechanism, *Mol Cell12*, 1403-1411.
177. Paris, S., Beraud-Dufour, S., Robineau, S., Bigay, J., Antonny, B., Chabre, M., and Chardin, P. (1997) Role of protein-phospholipid interactions in the activation of ARF1 by the guanine nucleotide exchange factor Arno, *J Biol Chem272*, 22221-22226.
178. Hackel, P. O., Gishizky, M., and Ullrich, A. (2001) Mig-6 is a negative regulator of the epidermal growth factor receptor signal, *Biol Chem382*, 1649-1662.
179. Wheeler, D. L., Dunn, E. F., and Harari, P. M. (2010) Understanding resistance to EGFR inhibitors-impact on future treatment strategies, *Nat Rev Clin Oncol7*, 493-507.
180. Cherfils, J., Menetrey, J., Mathieu, M., Le Bras, G., Robineau, S., Beraud-Dufour, S., Antonny, B., and Chardin, P. (1998) Structure of the Sec7 domain of the Arf exchange factor ARNO, *Nature392*, 101-105.
181. van Leeuwen, H. C., Strating, M. J., Rensen, M., de Laat, W., and van der Vliet, P. C. (1997) Linker length and composition influence the flexibility of Oct-1 DNA binding, *EMBO J16*, 2043-2053.
182. Ismail, S. A., Vetter, I. R., Sot, B., and Wittinghofer, A. (2010) The structure of an Arf-ArfGAP complex reveals a Ca2+ regulatory mechanism, *Cell141*, 812-821.
183. Parker, M. W., Lo Bello, M., and Federici, G. (1990) Crystallization of glutathione S-transferase from human placenta, *J Mol Biol213*, 221-222.
184. Ji, X., Zhang, P., Armstrong, R. N., and Gilliland, G. L. (1992) The three-dimensional structure of a glutathione S-transferase from the mu gene class. Structural analysis of the binary complex of isoenzyme 3-3 and glutathione at 2.2-A resolution, *Biochemistry31*, 10169-10184.
185. Losonczi, J. A., Tian, F., and Prestegard, J. H. (2000) Nuclear magnetic resonance studies of the N-terminal fragment of adenosine diphosphate ribosylation factor 1 in micelles and bicelles: influence of N-myristoylation, *Biochemistry39*, 3804-3816.
186. Biou, V., Aizel, K., Roblin, P., Thureau, A., Jacquet, E., Hansson, S., Guibert, B., Guittet, E., van Heijenoort, C., Zeghouf, M., Perez, J., and Cherfils, J. (2010) SAXS and X-ray crystallography suggest an unfolding model for the GDP/GTP conformational switch of the small GTPase Arf6, *J Mol Biol402*, 696-707.
187. Herrmann, C., Martin, G. A., and Wittinghofer, A. (1995) Quantitative analysis of the complex between p21ras and the Ras-binding domain of the human Raf-1 protein kinase, *J Biol Chem270*, 2901-2905.
188. Chavrier, P., and Goud, B. (1999) The role of ARF and Rab GTPases in membrane transport, *Curr Opin Cell Biol11*, 466-475.
189. Shiba, T., Kawasaki, M., Takatsu, H., Nogi, T., Matsugaki, N., Igarashi, N., Suzuki, M., Kato, R., Nakayama, K., and Wakatsuki, S. (2003) Molecular mechanism of

membrane recruitment of GGA by ARF in lysosomal protein transport, *Nat Struct Biol10*, 386-393.
190. Sukuru, S. C. K., Jenkins, J. L., Beckwith, R. E. J., Scheiber, J., Bender, A., Mikhailov, D., Davies, J. W., and Glick, M. (2009) Plate-Based Diversity Selection Based on Empirical HTS Data to Enhance the Number of Hits and Their Chemical Diversity, *Journal of Biomolecular Screening14*.
191. Wells, J. A., and McClendon, C. L. (2007) Reaching for high-hanging fruit in drug discovery at protein-protein interfaces, *Nature450*, 1001-1009.
192. Lipinski, C. A., Lombardo, F., Dominy, B. W., and Feeney, P. J. (2001) Experimental and computational approaches to estimate solubility and permeability in drug discovery and development settings, *Adv Drug Deliv Rev46*, 3-26.
193. Keiser, M. J., Roth, B. L., Armbruster, B. N., Ernsberger, P., Irwin, J. J., and Shoichet, B. K. (2007) Relating protein pharmacology by ligand chemistry, *Nat Biotechnol25*, 197-206.
194. Vassilev, L. T., Vu, B. T., Graves, B., Carvajal, D., Podlaski, F., Filipovic, Z., Kong, N., Kammlott, U., Lukacs, C., Klein, C., Fotouhi, N., and Liu, E. A. (2004) In vivo activation of the p53 pathway by small-molecule antagonists of MDM2, *Science303*, 844-848.
195. Oltersdorf, T., Elmore, S. W., Shoemaker, A. R., Armstrong, R. C., Augeri, D. J., Belli, B. A., Bruncko, M., Deckwerth, T. L., Dinges, J., Hajduk, P. J., Joseph, M. K., Kitada, S., Korsmeyer, S. J., Kunzer, A. R., Letai, A., Li, C., Mitten, M. J., Nettesheim, D. G., Ng, S., Nimmer, P. M., O'Connor, J. M., Oleksijew, A., Petros, A. M., Reed, J. C., Shen, W., Tahir, S. K., Thompson, C. B., Tomaselli, K. J., Wang, B., Wendt, M. D., Zhang, H., Fesik, S. W., and Rosenberg, S. H. (2005) An inhibitor of Bcl-2 family proteins induces regression of solid tumours, *Nature435*, 677-681.
196. Moreira, I. S., Fernandes, P. A., and Ramos, M. J. (2007) Hot spots--a review of the protein-protein interface determinant amino-acid residues, *Proteins68*, 803-812.
197. Bullock, B. N., Jochim, A. L., and Arora, P. S. (2011) Assessing helical protein interfaces for inhibitor design, *J Am Chem Soc133*, 14220-14223.
198. Moellering, R. E., Cornejo, M., Davis, T. N., Del Bianco, C., Aster, J. C., Blacklow, S. C., Kung, A. L., Gilliland, D. G., Verdine, G. L., and Bradner, J. E. (2009) Direct inhibition of the NOTCH transcription factor complex, *Nature462*, 182-188.
199. Patgiri, A., Yadav, K. K., Arora, P. S., and Bar-Sagi, D. (2011) An orthosteric inhibitor of the Ras-Sos interaction, *Nat Chem Biol7*, 585-587.
200. Patgiri, A., Jochim, A. L., and Arora, P. S. (2008) A hydrogen bond surrogate approach for stabilization of short peptide sequences in alpha-helical conformation, *Acc Chem Res41*, 1289-1300.
201. Wang, D., Chen, K., Kulp Iii, J. L., and Arora, P. S. (2006) Evaluation of biologically relevant short alpha-helices stabilized by a main-chain hydrogen-bond surrogate, *J Am Chem Soc128*, 9248-9256.
202. Schafmeister, C. E., Po, J., and Verdine, G. L. (2000) An all-hydrocarbon cross-linking system for enhancing the helicity and metabolic stability of peptides., *Journal of the American Chemical Society*, 5891-5892.
203. Patgiri, A., Menzenski, M. Z., Mahon, A. B., and Arora, P. S. (2010) Solid-phase synthesis of short alpha-helices stabilized by the hydrogen bond surrogate approach, *Nat Protoc5*, 1857-1865.
204. Renault, L., Guibert, B., and Cherfils, J. (2003) Structural snapshots of the mechanism and inhibition of a guanine nucleotide exchange factor, *Nature426*, 525-530.

205. Laemmli, U. K. (1970) Cleavage of structural proteins during the assembly of the head of bacteriophage T4, *Nature227*, 680-685.
206. Schagger, H. (2006) Tricine-SDS-PAGE, *Nat Protoc1*, 16-22.
207. Kabsch, W. Automatic processing of rotation diffraction data from crystals of initially unknown symmetry and cell constants.
208. McCoy, A. J., Grosse-Kunstleve, R. W., Adams, P. D., Winn, M. D., Storoni, L. C., and Read, R. J. (2007) Phaser crystallographic software, *J Appl Crystallogr40*, 658-674.
209. Bergfors, T. (2003) Seeds to crystals, *J Struct Biol142*, 66-76.
210. Zhang, Z., and Marshall, A. G. (1998) A universal algorithm for fast and automated charge state deconvolution of electrospray mass-to-charge ratio spectra, *J Am Soc Mass Spectrom9*, 225-233.

APPENDIX